CHANNEL MODELING FOR LAND MOBILE SATELLITE COMMUNICATIONS

Sayantan Hazra

CHANNEL MODELING FOR LAND MOBILE SATELLITE COMMUNICATIONS

A

Thesis Submitted

in Partial Fulfilment of the Requirements

for the Degree of

DOCTOR OF PHILOSOPHY

by

Sayantan Hazra

Department of Electronics and Electrical Engineering
Indian Institute of Technology Guwahati
Guwahati - 781 039, INDIA.

May, 2014

Certificate

This is to certify that the thesis entitled "**CHANNEL MODELING FOR LAND MOBILE SATELLITE COMMUNICATIONS**", submitted by Sayantan Hazra (roll no: 09610205), a research scholar in the *Department of Electronics & Electrical Engineering, Indian Institute of Technology Guwahati*, for the award of the degree of **Doctor of Philosophy**, has been carried out by him in the Department of EEE, IIT Guwahati. The initial works were carried out under the supervision of Dr. A. Mitra, erstwhile faculty member of EEE department and from December 2011, the thesis work was carried out fully under my supervision. The thesis has fulfilled all requirements as per the regulations of the institute and in my opinion has reached the standard needed for submission. The results embodied in this thesis have not been submitted to any other University or Institute for the award of any degree or diploma.

Prof. Ratnajit Bhattacharjee
Deptt. of Electronics & Electrical Engg.
Indian Institute of Technology Guwahati
Guwahati - 781039, Assam, India.

Acknowledgements

First and foremost, I feel it as a great privilege in expressing my deepest and most sincere gratitude to my supervisors Prof. Ratnajit Bhattacharjee and Dr. A. Mitra, for their excellent guidance throughout my study. Their kindness, dedication, hard work and attention to detail have been a great inspiration to me. My heartfelt thanks to both of them for the unlimited support and patience shown to me. I would particularly like to thank them for all their help in patiently and carefully correcting my manuscripts. I have no doubts that finishing my degree in a proper and timely manner was impossible without their assists, suggestions and advices.

I am also very thankful to my doctoral committee members Dr. P. R. Sahu, Dr. K. Kathik, Dr. M.K. Bhyuan, and Dr. B. K. Rai for sparing their precious time to evaluate the progress of my work. I express my heartfelt thanks to Dr. P. R. Sahu for providing valuable suggestions and study materials required to complete some works in this thesis. I am also thankful to Dr. T. Jacob for the guidance and support given to me in this work.

I have no words to express my thanks to some important friends especially, Rajib Jana, Mandar Maitra, Sanjoy Mondal, Surajit Malik, Om Prakash Singh. My work in this place definitely would not be possible without their love and care that helped me to enjoy my stay in IIT Guwahati, the place where I lived for almost seven long years and the place which I love and call my second home.

My special thanks to Rajib Jana for his witty suggestions in all aspects especially in numerical analysis. My deepest gratitude to Ramesh chandra Mishra for making my life easier by extending his timely help on several occasions. I thank all my fellow research scholars for their cooperation. During these years at IITG I have had several friends that have helped me in several ways, I would like to say a big thank you to all of them for their friendship and support.

My deepest gratitude goes to my parents for their continuous love and support throughout my studies. The opportunities that they have given me and their unlimited sacrifices are the reasons where I am and what I have accomplished so far.

I thank the unspeakable Almighty for giving me strength, courage, and confidence for each and every challenge I faced in my life including this work.

Finally, I believe this research experience will greatly benefit my career in the future.

(Sayantan Hazra)

Abstract

This research deals with various aspects of channel modeling in land mobile satellite (LMS) communications. In this work, we investigate on the effect of propagation phenomena specific to different propagation scenarios on signal received by an LMS receiver.

We sort out the propagation scenarios usually encountered by an LMS receiver and analyze the chain of mechanisms that contribute to the fading effects in that particular scenario. From this analysis, we conclude what type of mathematical formulation and what statistical distributions are appropriate to take into account the effect of the actual propagation phenomena which occur for pertaining to certain scenario. The complex envelope processes proposed this way are used for narrowband and wideband LMS channel modeling.

We include the effect of directivity of LMS antenna systems in the three-dimensional (3D) scattering models available in literature. This significantly modifies the expression of autocovariance function and second order moments useful for calculation of some important second order statistics.

We propose two narrowband models based on complex envelope processes with additive and multiplicative interaction of shadow fading and small-scale fading with 3D scattering mechanism. By comparing with measurement results of second order statistics available in literature, we show that the additive model can be used to depict a wide variety of fading situations for flat urban and suburban areas while the model based on multiplicative process is applicable to areas shadowed by irregular terrain and trees.

For calculation of statistics in multipath frequency-selective wideband channel we propose a new mathematical framework which is also used for state-based models. We also compute channel capacity for all kind of channel models dealt throughout the thesis.

Contents

List of Figures

List of Tables

Glossary

LMS	Land Mobile Satellite
LMSC	Land Mobile Satellite Communications
GMSC	Global Mobile Satellite Communications
GEO	Geostationary Earth Orbit
INMARSAT	International Maritime Satellite
MSAT	Mobile Satellite
AMSC	American Mobile Satellite Corporation
AUSSAT	Australian domestic Satellite operator
CRL	Canadian Research Laboratories
GPS	Global Positioning System
MoBISAT	Mobile Broadband Interactive Satellite Access Technology
QoS	Quality of Service
GTD	Geometrical Theory of Diffraction
CDF	Cumulative Distribution Function
LCR	mean Level Crossing Rate
AFD	Average Fade Duration
AoA	Azimuth angle of Arrival
EoA	Elevation angle of Arrival
PSD	Power Spectral Density
CCIR	Consultative Committee of International Radio
ISI	Inter-Symbol Interference
pdf	Probability Density Function
ITU-R	Radiocommunication sector of International Telecommunications Union
RMS	Root Mean Square

CIR	Channel Impulse Response
MARECS	Maritime European Communication Satellite
RHCP	Right Handed Circular Polarization
LOS	Line-of-Sight
NLOS	Non-Line-of-Sight
SNR	Signal-to-Noise Ratio

List of Publications

Journal Publications:

1. S. Hazra and A. Mitra, "Additive statistical modelling of land mobile satellite channels in three-dimensional scattering environment," *IET Commun.*, vol. 6, no. 15, pp. 2361-2370, Oct. 2012.

2. S. Hazra and A. Mitra, "LMS channel modeling with a multiplicative process under 3D scattering effect," under review, *IET Communications Journal.*

3. S. Hazra and R. Bhattacharjee, "Wideband Modeling for Land Mobile Satellite Channel: statistics and capacity issues" under review, *Physical Communication.*

Conference Publications:

1. S. Hazra and A. Mitra, "A new land mobile satellite channel model with Nakagami-q distribution," in *National Conference on Communication*, Kharagpur, India, Feb. 2012.

2. S. Hazra and R. Bhattacharjee, "A new technique for derivation of LCR and AFD in wideband wireless channel," in *National Conference on Communication*, Delhi, India, Feb. 2013.

1

Introduction

Contents

Land mobile satellite communications (LMSC) are part of Global Mobile Satellite Communications (GMSC), which provides global communication service to end users from a GEO (Geostationary Earth Orbit) or non-GEO satellite. The INMARSAT system was the first to provide international maritime satellite communication services and later expanded its services to aircraft and land mobiles. Other systems like MSAT in Canada, American Mobile Satellite Corporation (AMSC) in USA, and AUSSAT in Australia provide LMSC services for voice communication. Since mid-1970s, many research groups and space research organizations are active on research, testing and small-scale deployment of mobile satellite communications. Examples include Canadian research Laboratories (CRL) with MSAT, MSAT-X in USA, ETS-V in Japan, and PROSAT in Europe.

The purpose of first generation satellite communications was to provide telecommunication services to fixed earth station receiver like television broadcasting, navigation services for maritime etc. Later in second generation systems, satellite services to mobile terminals started with the aim of navigation services like Global Positioning System (GPS), aeronautical and personal communication services. Generally, L- (1-2 GHz) and S-bands (2-4 GHz) were being used for those services. Recently, higher satellite bands – Ku (11-18 GHz), K (18-30 GHz), and Ka (30-40 GHz), are also being exploited for multimedia services. Recent examples of deployments and studies are satellite-based Internet and multimedia services to high-speed trains [2] and the hybrid Ku/Ka band MoBISAT (Mobile Broadband Interactive Satellite Access Technology) system [3]. The later one aims at providing dual services to high speed trains and other land mobile terminals – television broadcasting in Ku-band and high speed Internet service in Ka band based on DVB-S/DVB-RCS standard [4]. There is also attempt at convergence of mobile satellite and terrestrial networks.

The potential of high speed internet and multimedia service of LMS systems has recently drawn enough attention towards the modeling of LMS channels [5–10]. Majority of the LMS channel models available in literature deals with propagation channel which can be defined as the physical medium through which electromagnetic wave propagate between transmitter and receiver antennas [11]. Propagation channel modeling is the method of establishing a mathematical relation between received signal attributes and channel parameters which roughly depicts the different propagation phenomena. If the effect of the antennas are included, the channel under consideration is called as radio channel [11].

1.1 Issues in LMS Channel Modeling

Propagation or radio channel modeling is the prerequisite for the design, testing, and deployment of any wireless communication system. The underlying reasons are elaborated below.

- For better quality of service (QoS) which is target of any communication service, proper communication system design is required with the purpose to control the transmission and reception techniques in a predetermined way to mitigate the channel impairments.
- Towards that, the sources of these impairments have to be thoroughly investigated [11] which demands rigorous study of the propagation phenomena and sufficient information about dependence of signal attributes (power, amplitude, phase, frequency deviation, fluctuation rate, duration of outage etc.) on propagation characteristics.
- Through channel modeling, mathematical expressions are derived which represents the effect of various channel parameters (transmission frequency and bandwidth, elevation angle of satellite or base station, spatial density and distribution of physical objects around the receiver, relative velocity between satellite or base station and receiver, and other mobile objects in vicinity of the receiver etc.) on the signal attributes. These expressions are useful in devising proactive measures for transmission and reception techniques and are reliable up to considerable extent if these expressions yield values of signal attributes close to the ones acquired through measurement campaigns. Once an expression is proved to be reliable, it can be used again and again thus saving the cost and time needed for a measurement campaign. These expressions also work as reference for performance evaluation and comparison of different receiver systems.
- In wireless communication like LMS, the behavior of the channel is more unpredictable leading to difficulty in estimation of the dependence of the signal attributes upon some of the aforementioned parameters. There lies the actual challenge of channel modeling.

Like any wireless communication systems, propagation channel in LMS system can be modeled using methods which may be empirical, analytical or statistical [12]. For deployment and planning of network, the most useful is the empirical approach which yields fast results for attenuation losses and link budget due its simplicity (chapter 4 of [13]). But these models too are site dependent,

providing little option for universal design and performance evaluation of a system let alone the performance comparison of different systems. On the other hand, analytical models can supply enough information about link budget by calculating average received power in a location by using geometrical theory of diffraction (GTD). Moreover, small-scale variations (termed as small-scale fading) around the average power of received electric field is taken into account by summing up the reflected and scattered replicas of the transmitted wave. Using these field equations, one can derive the autocovariance function and power spectral density, caused due to Doppler shift (Doppler PSD), of the received signal, and the crosscorrelation between the signals received on two different antennas in a multi-antenna system; the last quantity being very useful for design of spatial diversity [1]. However, due to inability of capturing the effects of slow temporal or spatial variation of shadow fading, analytical models may not be considered completely site independent. Apart from that, analytical models based on ray-tracing techniques are incapable of capturing the effects of multipath delays which are both random and time-varying [14]. If the number, location, speed and other characteristics of the reflectors and scatterers are not deterministic, statistical models are essential. Statistical channel modeling provides sufficient information about some very important attributes of the received signal like the probability of received envelope or power being under a certain level, fluctuation rate, duration of deep fades etc. in the form of respective statistical quantities – cumulative distribution function (CDF), mean level crossing rate (LCR) and average fade duration (AFD). LCR and AFD provide the a-priori information about burst error statistics [15] required for the design of communication systems, mainly the diversity schemes, error control coding and other techniques used for signal quality improvement. For a newly proposed system, these statistics also stand for figure of merit and thus can be used as a platform for performance comparison of different systems in different propagation scenarios. Thus, it is very important to compare these quantities calculated from expressions derived in a channel model with the same obtained from measured data to ensure the credibility of that channel model. However, to calculate the power spectral density and autocorrelation function of received signal, expression for the autocorrelation of the envelope with certain statistical distribution have to be related with the expression formulated in some analytical model. One popular example is [16], where autocovariance of Nakagami-m distributed envelope has been related with the same of received signal envelope formulated in [17–19].

Though both being variants of wireless communications, LMS and cellular systems differ a lot and so does the respective channel modeling approaches. In cellular communications, the base station is elevated at a very small angle. The scattering models, therefore, assume a two-dimensional (2D) scattering geometry. Even if a 3D geometry is considered, the elevation angle of wave arrivals are assumed with a mean of 0° and biased heavily towards small angles [1]. The scenario can be quite different in case of LMS with higher elevation angle of satellite. The mean cannot be zero as antennas are adjusted to have more directivity towards a positive angle close to satellite elevation angle [20, 21]. Instead of linear polarization, the transmitted signal and receiver antenna are circularly polarized which might have a different impact on received signal characteristics. For satellite communication systems, scattering needs to be considered only for the mobile units.

1.2 Relevant Works in LMS Channel Modeling

The majority of the LMS channel models are narrowband statistical models though there have been few works done in wideband modeling. The narrowband models with a single statistical distribution are summarized in Table 1.1. More elaborate discussions on these models is provided in section 2.3.2.3.

Table 1.1: Comparison of Single Distribution LMS Channel Models

Proposed by	Scattering model	Comments on complex envelope process
Loo [22]	2D with uniformly distributed azimuth angle of arrival (AoA)	Shadow fading only affects the line-of-sight (LOS) component which is additive to the multipath fading process representing the scattered components collectively.
Pätzold *et al.* [23]	Asymmetrical Doppler PSD; provides another modification to 2nd order statistics	Like [22]; but the LOS component is Doppler shifted, providing extra degree of freedom by modifying 2nd order statistics.
Corazza-Vatalaro [24]	2D with uniformly distributed AoA	Both LOS component and scattered components are under the effect of shadow fading which is multiplicative to the process which collectively represents the said components.
Vatalaro [25]	2D with uniformly distributed AoA	An extra additive scattered component is included to [24]. This model is a compromise between the extreme cases of [22] and [24].
Hwang *et al.* [26]	2D with uniformly distributed AoA	Both LOS and scattered components undergo shadow fading, but independently.

These single distribution models cannot properly represent diverse fading situations in different geographical locations covered by LMS communication. To overcome this problem, models utilizing more than one distribution have been proposed. The different propagation scenarios are considered as different states with a single distribution assigned to each. The states are combined with a Markov chain to yield what is called state-oriented modeling. Some important examples of these models are provided in Table 1.2.

Table 1.2: Comparison of State-oriented LMS Channel Models

Proposed by	Structure of the model	Shadow fading
Lutz *et al.* [27]	two-state: unshadowed + shadowed	Multiplicative
Karasawa *et al.* [21]	three-state: unshadowed + shadowed + blocked	LOS, additive
Fontán *et al.* [28]	three-state: unshadowed + moderately shadowed + deeply shadowed	LOS, additive
Scalise *et al.* [10]	three-state: unshadowed + shadowed + blocked	Multiplicative
Milojević *et al.* [9]	dynamic state model in contrast to a fixed state model with shadowing at each state	LOS, additive

Wideband effects are usually studied via delay profile of multipaths or impulse response of the channel. The underlying assumption is that a discrete number of scatterers are around the receiver or in another way the receiver is able to detect only a finite number of discretely located scatterers or resolve multipaths originated from them. The channel impulse response usually gives a quantitative perspective of how the mean power and delay of arrival of individual multipaths affect the quality of signal received. The effect of the channel impulse response is generally represented by a tapped delay line structure. Each impulse or tap stands for a resolvable multipath. Most of the researchers have aimed to propose distribution of tap gains, delay times and Doppler spectra of each tap [29–31]. In [32] and [10], a narrowband approximation of the original wideband model has been done and LCR and AFD has been computed from this approximated narrowband model in [32]. Also in [10], an approach has been given to calculate LMS channel capacity based on capacity-versus-outage approach given in [33].

1.3 Motivation of the Present Work

As shown in preceding section, there is a wide range of variety among the available LMS channel models which are based on different assumptions. One of the assumptions is how the shadow fading affects the received signal components. This leads to mainly two types of mathematical form of the complex envelope process – additive and multiplicative. The main difference between these two cases is whether the scattered components are under the effect of shadow fading or not. But there is no detailed justification available in literature about exactly what kind of propagation phenomena can result these two or any other cases. To the best of our understanding, whether these different envelope processes are result of different sets of propagational interactions (reflection, diffraction, scattering, attenuation etc.) where each set is a unique sequence corresponding to different propagation scenarios are not specified clearly in literature. This needs to be investigated with utmost care so that diverse type of locations with variation in fading situations are identified and the related fading process are assigned a mathematical form that captures the particular set and sequence of propagation phenomena specific to that situation. This has also to be associated with logical choice of statistical distribution so that good match between numerical and measured results are achieved. In this thesis, we will make use of the measurement data available in literature. However, it may be mentioned that this good match with a particular data set does not ensure good representation of all kind of fading situations in the corresponding scenario. So, our objective is to propose channel models which can yield results (CDF, LCR, AFD) representing worst to best possible situations in a propagation scenario including the specific case of measurement site.

Another drawback of the LMS models available in literature is that these models are based upon the assumption of two-dimensional (2D) scattering which does not effectively reflect the scattering mechanism in an LMS link. As pointed out in Section 1.1, antenna radiation patterns have to be considered while assuming the statistics of azimuth angle of arrival (AoA) and elevation angle of arrival (EoA). In addition, to the best of our knowledge, any investigation on the effect of circular polarization, used in LMS, on signal correlation and PSD has not been reported in literature. In connection with this, one of the objectives of this thesis is to include the effects of the LMS antenna system along with the propagation modeling.

To the best of the authors' knowledge, no method has been proposed to calculate important statistics like CDF, LCR, and AFD of a wideband channel by exploiting the power-delay statistics

from the channel impulse response model. Taking costly and time-consuming measurement in different places is the only way to calculate these quantities. Investigation of the characteristics of the received wideband signal at different excess delays might provide some conclusive ideas about formulation of the same.

Without the knowledge of channel capacity, channel modeling is often considered to be incomplete as capacity is the upper limit of information rate that can be transmitted over the channel with negligible error. It is a fair assumption that the LMS channel is ergodic due to the large transmission time. The ergodic capacity notion has to be used and its a challenging job in frequency-selective fading situations.

1.4 Thesis Contribution

The main contributions of the thesis are summarized below:

- Proposed various narrowband complex envelope processes which effectively represent fading effects in different propagation scenarios. Some of these take other existing LMS channel models as special cases.
- Investigated the effect of circular polarization and antenna directivity, specific for LMS systems, in small-scale fading and introduced significant modification for the expression of autocovariance function and second order moments useful for calculation of some important second order statistics.
- Proposed a narrowband model which includes the effect of 3D scattering, with an additive complex envelope process. It is shown that, this model is applicable in flat (without irregular terrain or hills) urban and suburban areas by comparing the second order statistics acquired from this model and from measurement data available in literature.
- Proposed a narrowband model with a multiplicative complex process in a 3D scattering propagation scenario. Through comparison of analytically derived LCR and AFD with the same obtained from available measurement data, this model is recommended for use in tree-shadowed areas.
- An analytical technique based upon statistical modeling for calculation of CDF, LCR, and AFD in multipath frequency-selective wideband channel.

- Computation of channel capacity in the LMS channel of our concern for both flat fading and frequency-selective fading cases.

1.5 Organization of the Thesis

The rest of this thesis is organized as follows:

Chapter-2 provides a brief description of LMS communication systems, and presents the propagation characteristics of LMS channel and the research works available in literature in the area of LMS channel modeling.

Chapter-3 presents the overview of our approach towards LMS channel modeling. We consider different propagation scenarios and analyze their effect on the propagation phenomena. Based on these analysis, we represent the fading effects in different scenarios with various complex envelope process. These complex processes along with a three-dimensional geometrical scattering model lays the foundation of different narrowband models; some of which we propose and elaborate in subsequent chapters. We also employ some modifications to 3D scattering models based upon antenna properties.

In Chapter-4, we present a narrowband model with additive complex envelope process with a Doppler PSD generated from a 3D scattering model. By comparison with measurement results of LCR and AFD, we show that this model can be used in flat urban and suburban area to depict a wide variety of fading situations including the marginal cases covered by some other models.

Chapter-5 presents another narrowband model with the multiplicative interaction of Nakagami-m distributed small-scale fading and lognormal distributed shadow fading. This model is shown to be applicable to urban or suburban streets shadowed by irregular terrain and areas shadowed by trees.

Chapter-6 provides modeling approaches in wideband cases. In this chapter, a new technique is proposed to derive CDF, LCR, and AFD in a wideband channel. We also model the propagation scenarios considered in Chapter-3 with different channel impulse response and calculate CDF, LCR, and AFD for these.

In Chapter-7, we compute the channel capacity for the narrowband and wideband channels considered in earlier chapters. We also give examples to compute the overall channel capacity for the Markov chain used in combining the channels respective to specific propagation scenario, so

that cut-offs for transmission rate in different satellite bands can be recommended.

Finally, Chapter-8 concludes the thesis giving a summary of the works done in previous chapters and shows some future directions for extending this research.

2

LMS Channel Modeling: Review of Related Work

Contents

In this chapter, first, we elaborate on the problems encountered in LMS system caused by various propagation phenomena which we describe along with their effects on received signal properties. We then come up with various channel modeling approaches, which in general applies to a wireless communication system, and the related works available in literature specifically for LMS channel modeling.

2.1 Problem in Signal Reception in LMS Systems

Like any communication system, LMS systems also suffer problems in proper signal reception or more specifically in extraction of useful information without any error. The major problems encountered are summarized below.

- Satellite unavailability: a single satellite may not be sufficient to maintain the minimum received signal power required for reliable communication most of the time. Especially the situation can be severe for low elevation angles in non-GEO systems where satellite to receiver path is heavily shadowed by obstacles. However, to improve system availability and coverage reliability, constellations of satellites can be exploited allowing the implementation of satellite diversity.

- Low signal power: Even with the availability of multiple satellites, communication cannot be completely reliable or information extraction can be erroneous. It is possible due to several reasons covering huge distances of the available satellites, shadowing of receiver at all directions (e.g. urban streets with high-rise buildings, areas with mountains, tree-covered streets etc.), transmission bandwidth being larger than propagation channel bandwidth, polarization mismatch between antenna and received electromagnetic waves etc.

- Fluctuation in signal amplitude and phase: while shadowing by big obstacles is responsible for low received power, scattered reflection from objects in the close vicinity of the receiver causes reception of numerous electromagnetic waves attenuated and phase shifted to uncertain amount. Consequentially, both constructive and destructive interference happens among the waves yielding great fluctuation in amplitude and phase resulting detection of information very critical.

- Long duration outage or fades: another crucial effect of the aforementioned constructive and

destructive interference is that the received signal power remains below the minimum level required for reliable communication for some duration and this phenomenon is termed as fade or outage. A very short duration fade is acceptable as interruption of communication is unlikely. But if received signal is in outage for a long duration, termination of a voice/video call or interruption of data communication is highly possible. This link failure is an inevitable outcome of loss of synchronization between local reference signal at the receiver and the transmitted signal.

2.2 Propagation Effects in Land Mobile Satellite Channel

The long propagation path between satellite and a mobile receiver on earth comprises layers of atmosphere with widely diverse effects, unique to a particular layer, on transmitted electromagnetic waves. In addition to that are the effects of propagation phenomena introduced by obstacles in proximity of receiver – obstruction, diffraction, specular and scattered reflection etc. The later ones, though being present in terrestrial mobile communications, are considerably different in LMS communications mainly due to higher elevation angles which changes over time due to movement of both satellite and mobile receiver. Several attempts have been made by different aerospace research organizations and researchers in academia and corporate organizations to study and analyze all these propagation phenomena and the consequent effects. In this section, we are going to elaborate those studies and analysis in perspective of the problems mentioned in Section 2.1.

2.2.1 Propagation Characteristics of Land Mobile Satellite (LMS) Channel

The propagation of the received signal is affected by free space attenuation, Faraday rotation, ionospheric scintillation, tropospheric attenuation and depolarization, small-scale fading due scattered components, and shadowing.

Free space attenuation causes the received signal power to decrease with the distance between transmitter and receiver. The free space power received by a receiver antenna at a distance d from the transmitter antenna is given by the Friis free space equation,

$$P_r(d) = \frac{P_t G_t G_r \lambda^2}{(4\pi)^2 d^2} \tag{2.1}$$

where d is the transmitter-receiver (T-R) separation distance in meters, P_t is the transmitted power, $P_r(d)$ is the received power which is a function of d, G_t is the transmitter antenna gain, G_r is the

receiver antenna gain, and λ is the wavelength in meters.

Faraday rotation is defined as the rotation of the polarization axis of a non-circularly polarized wave caused by the ionosphere. It can be expressed as

$$\Omega = \frac{2.36}{f^2} \int_S N(l)\mathbf{B}_0(l).\mathbf{dl} \tag{2.2}$$

where $\mathbf{B}_0$, in Gauss, is the component of the earth's magnetic field along the direct path, N is the electron density of the ionosphere in electrons per meter cubed, and f is frequency in Hz. The integration is performed along the direct path S. The loss due to polarization rotation can be eliminated by using circular polarization of the carriers.

Ionospheric scintillation is produced by irregularities in the electron density in the ionosphere. Nonhomogeneous ionized layers cause scattered reflection of radio waves, yielding fluctuations in amplitude and phase of the received signal. According to CCIR (Consultative Committee of International Radio) data on ionosphere scintillation, its effect on transmission in L band can be ignored [34]. Even more negligible are effects at Ku, K, Ka bands, because these effects are inversely proportional to the transmission frequency.

The tropospheric effects at the higher satellite bands are much more significant. The signal is attenuated mainly due to hydrometeors (rain, ice crystals, clouds) and atmospheric gases (oxygen, water vapor) by two different mechanisms. First, a rotation of the plane of polarization of the signal is caused owing to scattering by hydrometeors and water vapor and secondly, the transformation of electrical energy into thermal energy due to the induction of currents in the rain and ice crystals (which are electrically conductive). These effects can be neglected at L and S bands as they increase with frequency.

Small-scale fading, also known as multipath fading, is small-scale variation or fading of amplitude and phase of the received signal over a short interval of time or travel distance. This is caused by the interference of scattered electromagnetic waves originated by reflections and scattering from obstacles around the receiver, more specifically from the outside of the first Fresnel zone. Its power depends on the spatial distribution of the scattering objects around the receiver. Besides small-scale fluctuation of amplitude and phase, other effects include random variation of instantaneous frequency or frequency modulation caused by time varying Doppler effects and inter-symbol interference (ISI) caused by echoes and consequent time spreading. Time varying Doppler effects

happen not only due to the movement of mobile receiver but also due to speed of surrounding objects like vehicles which causes variation of doppler shifts in different multipath waves. Transmission bandwidth also plays an important role, to be explained in Section , behind the fluctuation and ISI.

Although the mean signal level or power seems to be constant over few meters of travel distance, a slow but random variation of the mean is observed over larger distance. This slow and random attenuation of received signal amplitude or power is termed as shadowing or shadow fading. The reason for this spatial variation is that, the distribution of the obstacles and scattering objects around the receiver may be vastly different at two different locations having the same Transmitter-Receiver separation. Measured signals in these cases vary vastly around the average value of received power predicted by equation (2.1) or by some other link budget equations (like large-scale path loss models with GTD) [35]. This variation may be temporal also due to random attenuation through foliage or change of satellite elevation angle over time even when the receiver is not moving large distance. In [36], assuming a forward scattering model, the reason behind the variation of local mean power is explained to be caused by slow changes in the scattering cross-section of the last scattering object. Its effect depends on the signal path length through the obstacle, type of obstacle, elevation angle, direction of travel, and carrier frequency. The shadowing is more severe at low elevation angles, where the obstacle projected shadow is high.

So, it may be concluded that for most of the satellite bands, shadow fading and small-scale fading are the dominant propagation phenomena which affect the received signal in a land mobile satellite channel.

2.3 Modeling Approaches for Land Mobile Satellite Channel

Several directions have been shown by researchers to deal with the unpredictable nature of channel via different ways of channel modeling. Though there are numerous models in literature, the approaches can be broadly classified according to the relation between transmission bandwidth and propagation channel bandwidth as – narrowband and wideband. The narrowband models deal with the situation of frequency-flat fading (simply called as flat fading) where different frequency components of transmitted signal experience same channel gain. Wideband models try to take care of the case when channel shows frequency-selective nature and these models usually comprise several

narrowband models as components. While the narrowband models available in literature can be classified into three broad categories: empirical models, analytical models and statistical models; the available wideband models mainly comprise narrowband analytical and statistical models. In this section, first we illustrate the impulse response model which provides the basis for the discrimination between narrowband and wideband channel, then elaborate the several approaches of channel modeling, focusing mainly on LMS.

2.3.1 Impulse Response Model of Wireless Multipath Channel

Due to the relative movement between surrounding objects and the receiver, the arrival delay and Doppler shift of multipaths are time varying while the amplitude and arrival delays are random too due to random type and spatial distribution of the surrounding objects which causes random variation in amplitude and phase of waves reflected in a particular direction. In perspective of signal processing, this multipath effect can be well described by a linear time-varying filter with a impulse response denoted by $h(t,\tau)$. Here, τ denotes the delay in arrival of multipaths while t denotes the variation of the impulse response observed in different time. The received signal can be expressed as the convolution of transmitted signal and $h(t,\tau)$. For baseband representation, $h(t,\tau)$ can be expressed as

$$h(t,\tau) = \sum_{i=0}^{N-1} A_i(t) e^{j\theta_i(t)} \delta(t - \tau_i(t)). \tag{2.3}$$

where $A_i(t)$, $\theta_i(t)$ and $\tau_i(t)$ are time-varying random amplitude, phase, and delay in arrival, respectively, of ith multipath component at time t. N is the maximum possible number of multipaths. $\delta(\cdot)$ is the dirac delta function pinpointing the exact time of arrival of a multipath.

When more than one multipath signal arrive within a symbol period, the signal waves combine vectorially at the receiver to yield the small-scale fluctuation of received signal amplitude and phase. These multipaths are called unresolvable. However, if symbol period is so small that only one multipath signal arrives within a symbol period, then small-scale fading does not happen as multipaths are resolvable. So, the time resolution of multipath detection depends on the transmission bandwidth and multipath delay structure in a local area. To measure $h(t,\tau)$ in baseband, a very narrow wideband pulse (called probing pulse) is transmitted so that all possible multipaths are resolved uniquely and accurately. Temporal and spatial averaging of $|h(t,\tau)|^2$ over a local area gives the power delay profile of the multipath propagation channel.

In case of narrowband transmission, almost all multipaths are unresolvable and arrive within a symbol period. The advantage of this is very little spreading of a symbol. On the other hand, wideband signals are prone to this time spreading and consequent ISI due to arrival of one or more echoes at the end of a symbol. The time spread caused in a local area is quantified by RMS delay spread which is given by the power delay profile of that area. In frequency domain, this effect is described as the distortion caused by unequal channel gain at different frequencies of a wideband signal. This frequency domain effect of multipath channel is called as frequency-selective fading and is quantified by coherence bandwidth. Coherence bandwidth is the separation in frequency for which two different frequency components of a signal are strongly correlated and experience same multipath fading gain. If transmission bandwidth is higher than the coherence bandwidth, then equalization is needed to remove the distortion caused by the frequency-selective fading and the channel is called wideband. The opposite case is the narrowband channel characterized by non-frequency-selective or frequency-flat fading for which no equalization is needed as distortion due to symbol spreading is negligible. Coherence bandwidth is inversely proportional to the RMS delay spread.

To represent the time-varying nature of the channel impulse response, another quantity named coherence time is used. It provides the time gap within which correlation between two multipath signals is high. It is inversely proportional to the maximum Doppler frequency. If the symbol period is higher than this coherence time, then the channel impulse response changes within a symbol period and the multipath channel is called a fast fading channel (slow fading in opposite case).

2.3.2 Narrowband modeling

2.3.2.1 Empirical models

Empirical channel models provide a mathematical expression for mean attenuation or path loss and link margin in terms of some physical parameters (path length through vegetation, satellite elevation angle and frequency) with the sole purpose of yielding a curve closely fitted (by regression methods) to some measured data set. Due to simplicity, these expressions are very useful in the specific location where the measurement was taken. But for other areas with different kind of vegetation or obstacles, these expressions are unlikely to work. The underlying reason for this shortcoming is that these models do not represent the effects of different propagation phenomena

(reflection, diffraction, scattering etc.) on received signal properties.

2.3.2.1.1 Vegetative attenuation models: These models provides an estimate of the signal attenuation through vegetation for different link frequency or satellite elevation angles.

Modified Exponential Delay (MED):

Introduced by Wiessberger [37], later simplified by CCIR [38], and modified by Smith, Stutzman, and Barts [39, 40], this model allows prediction of mean path loss due to vegetative attenuation. The expression involving path parameters and frequency is given by

$$L_v = \alpha_v D_v \tag{2.4}$$

where L_v is the attenuation in dB, D_v is the path length through vegetation in meters, and α_v is termed as the specific attenuation of the vegetation in dB/m. 'Specific attenuation' is a contradictory term as α_v is dependent upon vegetative path length D_v. α_v is expressed as function of D_v and frequency with different equations by Wiessberger, CCIR, and Barts and Stutzman. All these equations work for path length up to 400 m and the attenuation increases with frequency at each model. According to CCIR,

$$\alpha_v = 0.2 f^{0.3} D_v^{-0.4}, \qquad 200\text{MHz} < f < 95000\text{MHz} \tag{2.5}$$

Vogel and Goldhirsh model [41–44]:

This model was proposed to predict tree attenuation for different elevation angles and is valid for small elevation angles ranging from 15° to 40°. The mathematical formula is

$$\text{Full Foliage} \quad : \quad L_1(\theta) = -0.48 \cdot \theta + 26.2 \tag{2.6}$$

$$\text{Bare tree} \quad : \quad L_2(\theta) = -0.35 \cdot \theta + 19.2 \tag{2.7}$$

where L is the foliage attenuation in dB and θ is the elevation angle in degrees.

2.3.2.1.2 Models for estimation of link margin: The following models were proposed to estimate the required link margin, which were also expressed as function of frequency and elevation angle, for a specified link outage probability.

CCIR model [45]:

According to this model, the required link margin for an urban area can be estimated as

$$M = 17.8 + 1.93 \cdot f - 0.052 \cdot \theta + K \cdot (7.6 + 0.053 \cdot f + 0.04 \cdot \theta) \tag{2.8}$$

and the same for a suburban or rural area is

$$M = 12.5 + 0.17 \cdot f - 0.17 \cdot \theta + K \cdot (6.4 - 1.19 \cdot f + 0.05 \cdot \theta) \tag{2.9}$$

where M is the link margin in dB, f is the link frequency in GHz, θ is the satellite elevation angle varied from 19° to 43°, and K is a factor relating the percentage of locations where the specified carrier power will be exceeded. These equations were proposed to fit the measurement data taken at 860 MHz and 1550 MHz.

Models directly relating link margin and outage probability [46–48]:
All the models of this kind tend to propose an empirical expression relating the link margin and link outage probability. This expression is usually of the form:

$$M = -A \ln(P) + B \tag{2.10}$$

where M is the link margin in dB, P is the specified probability ranging from 1% to 20%, and A and B are first or second order polynomials of the elevation angle.

In all these empirical models, their is increase in attenuation with link frequency. Besides, the required link margin is high at increased elevation angle due to less shadowing by vegetation and other obstacles.

2.3.2.2 Analytical models

Most of the available analytical models try to represent the effect of small-scale fading by formulating the received electric field usually based on an assumption about the spatial angles of arrival of incoming waves and by providing Doppler power spectral density, autocovariance function, and a statistical distribution for the envelope and phase. The effectiveness of some statistical distributions (Rayleigh, Rician) have been given proper analytical justification by these models e.g. Clarke's model [18]. Doppler PSD is the PSD of received small-scale fading envelope. However, analytical models does not provide prediction of signal fluctuation rate, fade durations, and shadow fading which plays a role in long-term variation of average received signal power. Statistical distributions (Rayleigh, Rician) yielded from these models does not provide good match

with the statistics of measured data in all kind of propagational situations.

The received signal is the vector sum of a number of components which have traveled via different paths. Ossanna's work [49] on this was first where the received resultant wave is assumed to be a vector sum of a LOS component and one or more reflected components. Presence of LOS component means this model is applicable only in open areas outside of cities and forests. Gilbert [17] was the first to work on scattering mechanism. Based on the assumption that a large number of scatterers are uniformly located on the horizontal plane containing the mobile receiver, Clarke has given a two-dimensional (2D) scattering model leading to Rayleigh distribution of signal envelope and a symmetric Doppler power spectral density (PSD) [18]. This kind of 2D scattering model does not effectively reflect the scattering mechanism in an LMS link.

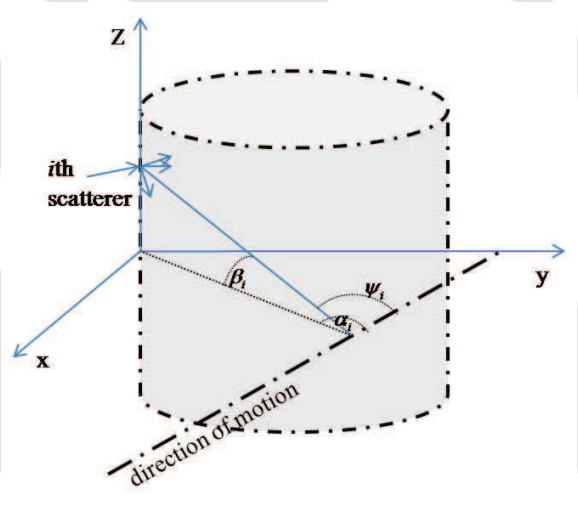

Figure 2.1: 3D scattering geometry [1].

Aulin was the first to propose a 3D scattering model [19] for propagation in land mobile communication. Its modified version proposed by Parsons [1] is widely accepted in literature. The scattering geometry is shown in Fig. 2.1. It shows one of the many scatterers surrounding the receiver. Due to movement of receiver and surrounding objects, the individual components will be subject to a Doppler shift related to the spatial angle of arrival ψ relative to the direction of motion. With reference to Fig. 2.1, the resultant complex signal can be expressed as

$$r(t) = A \sum_{i=0}^{N} \exp j[2\pi(f_c + f_m \cos\psi_i)t + \phi_i]. \tag{2.11}$$

where f_m is maximum Doppler frequency shift, f_c is carrier frequency, ϕ_i is the random phase of ith

multipath, A is the random envelope of the resultant complex signal $r(t)$ and can be represented by some statistical distribution (e.g. Rayleigh distribution in Clarke's model [18]).

The normalized autocovariance function of the received signal $r(t)$ is given by

$$\rho(\tau) = \left| \int_{\psi} \exp[j(2\pi f_{\mathrm{m}} \tau \cos\psi)] p(\psi) d\psi \right|. \tag{2.12}$$

In Fig. 2.1, the angle of arrival of a wave from the ith scatterer, ψ_i, is the angle formed between the line joining the scatterer to the mobile and the direction of motion (assumed to be in the X-Y plane). It is made up of two components, β_i the vertical or elevation angle of arrival (EoA) and α_i the horizontal or azimuth angle of arrival (AoA). It is shown in [1] that in general

$$\cos\psi = \cos\alpha \cos\beta. \tag{2.13}$$

The autocovariance and PSD can only be evaluated if specific probability density functions (pdf) are assumed for the spatial angles α and β. Like [18], a uniform pdf has been assumed for AoA α in [1],

$$p_{\alpha}(\alpha) = \frac{1}{2\pi} \qquad 0 \leq \alpha \leq 2\pi. \tag{2.14}$$

As in a land mobile scenario, majority of incoming waves travel in a nearly horizontal direction, some criteria has been specified in [1] to seek a pdf for EoA β. The criteria are that β has a mean value of 0°, is heavily biased towards small angles, does not extend to infinity and has no discontinuities. The pdf is expressed as

$$p_{\beta}(\beta) = \frac{\pi}{4\beta_{\mathrm{m}}} \cos\left(\frac{\pi}{2}\frac{\beta}{\beta_{\mathrm{m}}}\right) \tag{2.15}$$

This pdf is limited to β_{m}, which is dependent upon the local surroundings. A suitable value for β_{m}, can be estimated from experimental measurements.

By using equations (2.12), (2.13), (2.14) and (2.15) the autocovariance function can be written as

$$\rho(\tau) = \frac{\pi}{4\beta_{\mathrm{m}}} \int_{-\beta_{\mathrm{m}}}^{+\beta_{\mathrm{m}}} J_0(2\pi f_{\mathrm{m}} \tau \cos\beta) \cos\left(\frac{\pi}{2}\frac{\beta}{\beta_{\mathrm{m}}}\right) d\beta \tag{2.16}$$

The Doppler PSD can be evaluated by taking Fourier transform of the autocovariance function and in [1], it is shown to have no discontinuity like the Doppler PSD calculated in [19].

2.3.2.3 Statistical models

Unlike analytical models, statistical models do not provide field equations by summing up the fields of incoming waves. Rather, statistical distributions are assigned for envelope and phase of the received signal with the target of proper match with the statistics of measured data collected in a particular or several locations. These models offer an insight into the effect of different propagation phenomena on the signal attributes (mainly power, envelope, phase, fluctuation rate, fade duration) by proper representation of small-scale fading and shadow fading effects on received signal. However, Doppler PSD and autocorrelation function cannot be calculated by statistical modeling as it does not include the spatial angles of arrival. In the statistical models available in literature, most of the researchers used the expression of autocovariance function provided by some analytical model to derive the second order moments as a function of the first order moments and maximum Doppler frequency. This helps to normalize LCR and AFD with respect to maximum Doppler frequency so that these quantities become independent of transmission carrier frequency and velocity of the mobile receiver and surrounding objects.

After the initial works of Young [50], many researchers have tried to find out what statistical distribution describes best the channel conditions. It has been concluded in this paper that Rayleigh distribution is effective for representation of signal amplitude variations over small areas. The conclusion is drawn upon measurements taken at frequencies ranging from 150 to 3700 MHz in New York City. Clarke's model explained this observation well analytically. Through several measurement campaigns around the world, it has been established that Rayleigh distribution is good to represent small-scale variations of signal envelope when LOS or any dominant signal component is not available which happens in dense urban areas. When these components are available, Rician distribution [51] has been proved good though their are other distributions proven to be better in certain situations. Nakagami-m distribution [52] has been employed in different terrestrial channel models to describe a wide variety of fading situations including those covered by Rayleigh and Rician, by simply changing the parameter $m \in [0.5, \infty)$. For $m \gg 1$, it represents the LOS availability condition described by Rician distribution; for $m = 1$, it stands for the non-LOS condition of Rayleigh, and for $m > 1$ but not very big, it describes the fading situations in between these two extreme cases. For $0.5 < m \leq 1$, this distribution is known as Nakagami-q which is mathematically same as the Hoyt distribution [53] and is the only distribution to represent

fading situations worse than the one represented by Rayleigh. However, a completely different kind of distribution is needed to depict the slow variation of shadow fading. Through comparison with measurement data, empirical evidence has been given that shadow fading is best fitted by lognormal distribution [43,54,55]. In [36], an additive model has been proposed to give a theoretical justification for this log-normal shadow fading.

Two different approaches namely global or single distribution modeling and state-oriented modeling have been taken in the existing statistical models. The first one describes the channel by the use of a single distribution, usually a mixture of aforementioned distributions, with the target of representing both small-scale fading and shadow fading effects in all kind of propagation scenario. In the state-oriented approach, different propagation scenarios with wide variety are considered as separate states of fading and each of these discrete states are modeled separately by a single distribution. The transitions of channel to different propagation scenarios or states are modeled with discrete-time Markov chain.

2.3.2.3.1 Global or Single Distribution Modeling: Approaches by various researchers for statistical channel modeling mainly differ in the distribution assumed for the representation of small-scale and shadow fading and in the consideration of how the shadow fading affects the line-of-sight (LOS) and scattered components. Some of these approaches are briefed in Table 2.1.

As can be seen from the table, some models take the association of the two processes as additive [22, 23] or multiplicative [24].

Main problem with global or single distribution model is it is not valid for stationary conditions. Different propagation conditions due to frequent changes in the elevation angle of the satellite cannot be modeled with a single distribution as the mobile receiver travels from one propagation scenario to another (e.g. urban to rural). This inability of a single pdf, though it may be a mixture pdf to realize diverse propagation conditions, to describe this non-stationary nature of the propagation channel effectively led to the state-oriented channel modeling.

2.3.2.3.2 State-oriented Modeling When large area is covered by mobile receiver, the channel model become non-stationary. It can be divided into different small areas with constant environment with stationary channel model. In this approach a Markov process is used to model long-term variations of the channel and its transitions to different states whereas short-term varia-

Table 2.1: List of Channel Models Available in Literature

Multipath fading	Shadow fading	Complex Channel Model	Comments
Rayleigh	lognormal (LOS, additive)	$r = Se^{j\phi_0} + Re^{j\phi}$; S: log-normal, R: Rayleigh, ϕ_0, ϕ: uniform [22]	Here envelope and phase of shadow faded LOS component and multipath faded scattered components are assumed independent to each other.
Rayleigh	lognormal (LOS, additive)	$r = S\,e^{j(2\pi f_{\mathrm{d}} t + \theta_{\mathrm{d}})} + x_1 + jy_1$; S: lognormal, x_1, y_1: Gaussian, f_{d} and θ_{d}: constant [23]	Like [22]; but the LOS component is Doppler shifted, providing extra degree of freedom by modifying fade statistics.
Rician	lognormal (Multiplicative)	$r = RSe^{j\theta}$; S: lognormal, R: Rician, θ: uniform [24]	Envelope and phase of LOS component and scattered components are not independent to each other, both components are taken care of by a single process R which is under the effect of shadow fading.
Rician and Rayleigh	lognormal (Multiplicative)	$r = RSe^{j\theta} + x_1 + jy_1$; S: lognormal, R: Rician, x_1, y_1: Gaussian [25]	An extra additive scattered component is included to [24]. Envelope and phase of this extra scattered component is independent to the same of R which incorporates the LOS and another part of the scattered components. This model is a compromise between the extreme cases of [22] and [24].
Rayleigh	lognormal	$r = A_c S_1 e^{j\phi} + RS_2 e^{j(\theta+\phi)}$; S_1, S_2: lognormal, R: Rayleigh, A_c: constant [26]	Both LOS and scattered components undergo shadow fading, but independently.

tions corresponding to each individual discrete state are described by one of the above mentioned pdfs with appropriate parameters.

A Markov process is a stochastic process in which a system can take on discrete states in such a way that the probability of taking on a given state depends only on the previous state. For State-oriented statistical modeling, transition between different states are generally modeled with first-order M-state discrete-time Markov chain. The chain is a random process taking on only discrete values satisfying the condition

$$P[(s[n] = s_n)|(s[n-1] = s_{n-1}), (s[n-2] = s_{n-2}), \ldots]$$

$$= P[(s[n] = s_n)|(s[n-1] = s_{n-1})]. \tag{2.17}$$

Table 2.2: List of State-oriented Models available in Literature

Proposed by	Structure of the model
Lutz *et al.* [27]	two-state: Ricean (unshadowed) + Suzuki (shadowed)
Karasawa *et al.* [21]	three-state: Ricean (unshadowed) + Loo (shadowed) + Rayleigh (blocked)
Milojević *et al.* [9]	dynamic state model in contrast to a fixed state model with Loo pdf at each state

When $s[n] = s_i$, the Markov chain is said to be in state i. The conditional probabilities $P_{i|j}[n] = P[(s[n] = s_j)|(s[n-1] = s_i)]$ are known as the state-transition probabilities. The switching process between states is described by the transition probability matrix

$$[P] = \begin{bmatrix} P_{11} & P_{12} & \cdots & P_{1M} \\ P_{21} & P_{22} & \cdots & P_{2M} \\ \vdots & \vdots & \cdots & \vdots \\ P_{M1} & P_{M2} & \cdots & P_{MM} \end{bmatrix}. \tag{2.18}$$

The matrix of the absolute state probabilities, the probability of the system being in state i, is defined as

$$[W] = [W_1, W_2, \cdots, W_M]. \tag{2.19}$$

The convergence property of the Markov chain is defined by the equation

$$[P][W(n-1)] = [W(n)]. \tag{2.20}$$

The probability that the model stays in state i for n samples is

$$P_i(N = n) = P_{i/i}^{n-1} \cdot (1 - P_{i/i}), \qquad n = 1, 2 \ldots. \tag{2.21}$$

The cumulative distribution for the duration of each state is

$$P_i(N \leq n) = (1 - P_{i/i}) \cdot \sum_{j=1}^{n} P_{i/i}^{j-1}, \qquad n = 1, 2 \ldots. \tag{2.22}$$

The number of states of the Markov chain as well as the statistics describing each of these states differ from model to model and from researcher to researcher. Some of these models are briefed in Table 2.2.

In Markov chain, the state durations have to follow an exponential distribution (equation (2.22)). But, Hase *et al.* [56] has shown that the CDF of nonfade and fade durations calculated from measured data were best fitted by curves following power-law and log-normal distribution, respectively. The nonfade duration distribution given by Hase *et al.* and later recommended by the ITU-R (Radiocommunication Sector of International Telecommunications Union) [57] is

$$P(D \leq d) = 1 - \beta d^{-\gamma} \qquad d > \beta^{1/\gamma} \tag{2.23}$$

where the parameters β and γ depend on the degree of optical shadowing. The recommended fade duration distribution is a log-normal model given by

$$P(D \leq d) = \frac{1}{2}\left\{1 + \text{erf}\left(\frac{\ln(d) - \ln(\alpha)}{\sqrt{2}\sigma}\right)\right\} \tag{2.24}$$

where $\ln(\alpha)$ and σ is the mean and standard deviation of $\ln(d)$ respectively.

Bråten *et al.* [58] proved (using measured data) that state durations follow equation (2.23) and (2.24) if a semi-Markov model is used. In a semi-Markov chain, transitions between the states are described by the transition probabilities P_{ij} where $i \neq j$.

2.3.3 Wideband Modeling

With the advent of third and fourth generation LMS communication systems capable of providing multimedia services [2,3], enough attention had been drawn towards the modeling of wideband LMS channels [10]. In the perspective of the theory of multipath fading channels, a channel is considered to be wideband when signal bandwidth is higher than the coherence bandwidth signifying that different frequency components of received signal are not strongly correlated i.e. they are experiencing different channel gains. Coherence bandwidth is inversely proportional to the RMS delay spread which is dependent upon the spatial distribution of the obstacles around the mobile receiver. RMS delay spread is high in urban streets due to presence of numerous scatterers in contrast to open or rural areas with a few number of scatterers. So, it is usual in cellular communications that coherence bandwidth is low in urban scenario leading to frequency-selective fading while it is flat fading in open or rural areas for the same transmission bandwidth. On the other hand, for LMS communications, the channel can be considered wideband with frequency-selective in nature even in open or rural areas with high coherence bandwidth which might be exceeded at higher satellite bands like Ku- and Ka-band.

As already stated, the channel for a particular propagation scenario can be modeled either as narrowband or wideband depending upon the transmission rate. In narrowband channels, the receiver cannot separately process or resolve the several group of replica waves of transmitted signal or multipaths. For statistical analysis, all the dominant and non-dominant components of the received signal are combined into a random complex envelope process with a single mixture distribution to describe all kind of fading experienced by the different components. When the transmission bandwidth W is very high, multipaths that are separated by at least $1/W$ in delay are resolvable. The relative power and the delays of the resolvable groups of received multipaths are described by channel impulse response. For a particular propagation scenario, the single distribution already used in a narrowband model will be replaced by simpler distributions assigned for different multipaths in the channel impulse response. For example, if the distribution was Rician in the narrowband model, the first path in the wideband model will be deterministic representing the LOS component while the other paths will have complex Gaussian envelope. So it can be said that, the complex envelope process of a narrowband model will be spread over time in case of higher transmission bandwidth in a particular propagation scenario. In other words, if a narrowband model is already proved to be applicable in a particular propagation scenario, one can get the distribution of the paths in the channel impulse response (CIR) by simply splitting the narrowband complex envelope process into resolvable groups of dominant and non-dominant components and assigning the corresponding simpler distributions. Doppler power spectral density (PSD), another important quantity in narrowband modeling, of the non-dominant scattered components are usually kept the same for paths representing resolvable groups of non-dominant components in the CIR.

The effect of the channel impulse response is generally represented by a tapped delay line structure. Each impulse or tap stands for a resolvable multipath. Most of the researchers have aimed to propose distribution of tap gains, delay times and Doppler spectra of each tap [29–31]. In [29], the multipaths have been considered to be divided into two groups – 'near echo' and 'far echo'. Excess delay and power of the taps, and number of multipaths both in case of near and far echoes are modeled with various statistics. Model parameters were provided to fit the measured data. In [30], measurements are reported at five different propagation environments at $15° - 40°$ elevation angles at L-band and S-band. The authors derived empirical expressions for the delay spread extracted from those data. The average delay spread was found to be 120-150 ns, smaller

than the same reported in case of terrestrial channel. Rician distribution was taken to represent the amplitude of the first two taps of the six tap structure while the other four were described by Rayleigh distribution. The distribution parameters were optimized to match the measurement results with the purpose of applicability in variety of elevation angles and propagational situations. In [31], the channel is analyzed by dividing it into two parts: the free space propagation (satellite-to-local cluster) and the local cluster which is responsible for the multipath fading effects. A Doppler shift and an attenuation factor epitomized the space propagation. The multipath components are modeled by tapped delay line while the line-of-sight (LOS) was modeled separately.

2.4 Summary

A detailed description of the channel modeling approaches in the context of LMS communication along with underlying theory and literature survey has been provided in this chapter. Keeping in mind the main objective of this thesis work, our target in next chapters will be narrowband and wideband statistical LMS channel modeling with the help of a 3D scattering model. However, before working on statistical modeling, we must include the antenna effects into the 3D scattering model, to be dealt with in next chapter.

3

Overview of the Narrowband Modeling Approach: representation of fading effects and scattering mechanism

Contents

This chapter presents the overview of our approach towards LMS channel modeling. We consider different propagation scenarios and analyze their effect on the propagation phenomena like availability of LOS or some dominant component, scattering, and most importantly shadowing, whether it affects the power of only LOS and/or scattered components of received signal. Working towards one of the motivations of this thesis work, we also give the justification for the use of additive or multiplicative interaction of the small-scale fading and shadow fading process in connection with the actual propagation phenomena. Based on these analysis, we represent the fading effects in different scenarios with various complex envelope process. These complex processes along with a three-dimensional geometrical scattering model lay the foundation for different narrowband models; some of which we propose and elaborate in subsequent chapters. These narrowband models, specific to a particular type of area or propagation environment, can be combined into a Markov or semi-Markov chain to ensure vast geographical applicability. We also formulate the effect of circular polarization on the correlation properties of received electric field. Finally, we include the effect of directivity of LMS antenna systems, in general, in the 3D scattering models available in literature and formulate the autocovariance function which will be useful for calculation of second order moments and statistics for the channel models proposed in later part of this thesis.

3.1 Statistical Representation of the Fading Effects in Different Propagation Scenario

One of the main objectives of this thesis work is to represent the propagation effects in diverse type of propagational situations. Towards this, one must first sort out the propagation scenarios which exhibit completely different fading effects i.e. signal received in two different propagation scenario should differ widely in average power, fluctuation, and fade durations. After that, the complex envelope of received signal have to be given a mathematical form which will approximately represent the fading processes contributed by different propagation phenomena like scattering, reflection, random attenuation etc. In other words, the mathematical expression for the complex envelope should be able to give an insight into the effect of the actual propagation phenomena in a particular propagation scenario. As propagation scenarios represent variety of geographical areas (urban, rural, jungle etc.), combining several narrowband models by a Markov chain into a finite-state channel model will enable it to represent any kind of propagational situations. Hereby, we are going to elaborate some propagation scenarios that will be considered for modeling in subsequent

chapters and we also try to provide the rationale behind the choice of additive and multiplicative envelope process in connection with actual propagation phenomena.

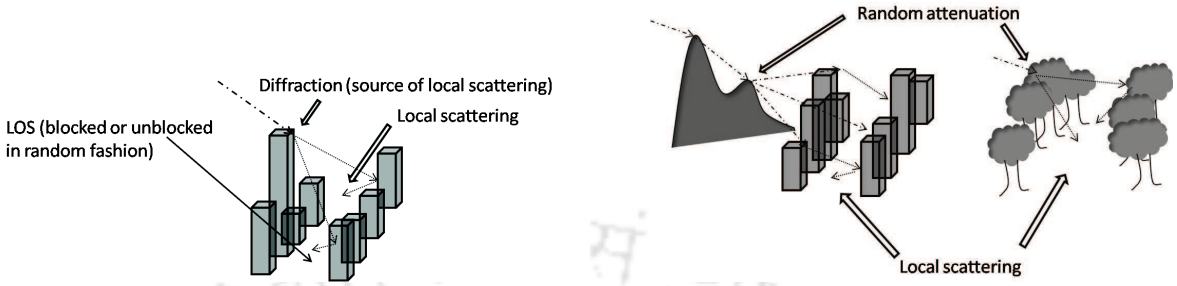

Figure 3.1: Propagation phenomena in (a) flat urban/sub-urban area, (b) non-flat urban and tree-covered area.

3.1.1 Flat areas with low clustering density

An additive envelope process is suitable to depict propagation characteristics in a flat urban or suburban area (without irregular terrain or hills) where there is no kind of interaction (e.g. reflection or scattering) on signal waves before getting scattered by local cluster of scatterers around the receiver. The LOS component is shadow faded and has a random average power because it is available in a random manner due to irregularity in building heights and gaps between them (Fig. 3.1(a)). The scattered components are not under the effect of shadow fading as no random attenuation occurs before diffraction in rooftops and building edges. Thus, the small-scale fading of the scattered components can be represented by a complex envelope process with constant power while a separate random process describes the shadow faded LOS. An additive envelope process turns out eventually,

$$\widetilde{R} = X_1 + jX_2 + Y \tag{3.1}$$

where $\widetilde{R}$ is the low pass complex envelope of received signal, X_1 and X_2 are the inphase and quadrature components of the low pass complex envelope of scattered components, and Y stands for the shadow fading experienced by LOS component.

3.1.2 Non-flat or tree-covered area

When interactions happen before entering into local cluster of scatterers, random attenuation causes slow variation of mean received power of both the LOS and scattered components which

necessitates the exploitation of a multiplicative process. A very irregular terrain around urban or suburban areas (streets shadowed by hills around) or roadside trees forming canopy like structures might lead to this type of situation (Fig. 3.1(b)). Three propagation phenomena happen in this situation in a consecutive manner – first, random attenuation by irregular terrain (hills) and/or trees; second, local scattering around the receiver; third, reception of some dominant and scattered components, all of which has suffered random attenuation in the first place. As the total signal power in a local cluster is random itself, the shadow fading process (Y) should be multiplicative to another random process (denoted here as Z) which represents the small-scale fading caused by the interference of different dominant and non-dominant components. The multiplicative complex envelope process is given by

$$\widetilde{R} = Z \cdot Y. \tag{3.2}$$

3.1.3 High clustering density with LOS blocked

In a dense urban area with high-rise buildings, it is usual that LOS path is blocked especially in case of geosynchronous and LEO satellites with low elevation angle. Only the scattered components are received without any effect of shadow fading. So, the complex envelope in this case can be expressed as

$$\widetilde{R} = X_1 + jX_2. \tag{3.3}$$

The most common statistical distribution in literature for this case is Rayleigh. However, it is shown in [59] that, Nakagami-q is more suitable in a mobile satellite link.

3.1.4 Open area with few obstacles

In areas where LOS path is unblocked (e.g. rural areas, farmland, coasts), there have to be a constant in the complex envelope along with the inphase and quadrature components of the scattered components,

$$\widetilde{R} = X_1 + jX_2 + A(\text{constant}). \tag{3.4}$$

The usual distribution in literature for this case is Rician.

3.2 Effect of Circular Polarization in Small-Scale Fading of Received Electric Field

The resultant electric field at a mobile receiver in a three-dimensional propagation environment is analytically expressed in equation (6) of [19] as,

$$E(t) = T_c(t)\cos\omega_c t - T_s(t)\sin\omega_c t. \tag{3.5}$$

For RHCP plane wave, the expression for in-phase and quadrature components $T_c(t)$ and $T_s(t)$ (given in equation (7) of [19] for vertically polarized plane wave) can be rewritten as

$$\begin{aligned} T_c(t) &= \sum_{n=1}^{N} c_n \left[|\mathrm{AR}|\cos(\omega_n t + \theta_n) + \sin(\omega_n t + \theta_n)\right] \\ T_s(t) &= \sum_{n=1}^{N} c_n \left[|\mathrm{AR}|\sin(\omega_n t + \theta_n) - \cos(\omega_n t + \theta_n)\right] \end{aligned} \tag{3.6}$$

where |AR| is the axial ratio defined as the ratio of amplitudes of axial components of a circularly polarized plane wave. LMS antennas, when used in end-fire mode, have $|\mathrm{AR}| \approx 1$. In that case, it can be shown that the autocorrelation function has analytical expression same as given by equation (10) and (11) of [19]. Therefore, it can be concluded that circular polarization has no extra effect on received signal properties in LMS communication.

3.3 Effect of Antenna Directivity in Three-dimensional Scattering Model

In an LMS communication link, a mobile receiver can be thought of to be in a three-dimensional space where signal waves arrive from several directions. So, with the direction of motion of mobile receiver, each received wave makes an angle which has two components – azimuth angle of arrival (AoA) and elevation angle of arrival (EoA). In [1], a 3D scattering model with the pdf of AoA and EoA was proposed for a terrestrial mobile communication link. The AoA pdf was taken uniform assuming isotropic propagation in horizontal plane, while the EoA pdf was cosine with a mean of 0° and was heavily biased towards small angles. The underlying reason in [1] for high concentration of incoming waves around horizontal plane is given by observing the similarity between measured spectra and spectra of Clarke's 2D scattering model. However, the EoA does not have the same characteristics in LMS systems where antennas are adjusted to have more directivity towards a

positive angle close to satellite elevation angle [20,21] while being omnidirectional in the azimuthal plane. In [20], a crossed-drooping-dipole antenna with a radiation pattern (Fig. 2 of [20]) elevated at 40° was used for the reception of MARECS signal at L-Band. Thus, some of the waves coming from beneath the antenna will be rejected and the EoA pdf must have a non-zero mean. In general, the cosine pdf of [1] can be modified to have a non-zero mean. However, if information is available about the used antenna system, then the radiation pattern itself can be used instead of an EoA pdf. Crossed-drooping-dipole, quadrifilar helix and log-spiral antennas are mostly used due to their capability of generating circular polarization and all have a uniform gain pattern in azimuthal plane and a cosine-like elevation-plane gain pattern though there is no compact mathematical expression for these kind of complex antenna systems.

Keeping the EoA pdf same as [1], the normalized autocovariance or autocorrelation function $r_\rho(\tau)$ of the zero mean complex Gaussian envelope of scattered multipath components thus turns out to be

$$r_\rho(\tau) = \int_\beta J_0(2\pi f_{\max}\tau\cos\beta)p_\beta(\beta)G(\beta)d\beta \tag{3.7}$$

where $f_{\max}$ is the maximum Doppler frequency and $G(\beta)$ is the radiation power pattern of antenna in elevation plane. Hereby, we assume an elevated cosine for the field pattern for mathematical simplicity and thus the elevation-plane power pattern turns out to be

$$G(\beta) = \cos^2\left(\frac{\pi}{2}\frac{\beta-\beta_0}{\beta_{\text{maxG}}}\right)d\beta \tag{3.8}$$

where, $\beta_0(>0)$ is the angle of maximum gain and β_{maxG} is the half of the full beamwidth so that the range is $(\beta_0-\beta_{\text{maxG}}, \beta_0+\beta_{\text{maxG}})$. The expression for $p_\beta(\beta)$ is [1]

$$p_\beta(\beta) = \frac{\pi}{4\beta_{\text{m}}}\cos\left(\frac{\pi}{2}\frac{\beta}{\beta_{\text{m}}}\right) \tag{3.9}$$

where $\beta_{\text{m}}(>0)$ is the maximum value of EoA. Depending upon the relative difference of β_0, β_{maxG}, and β_{m}, there can be three different conditions for intersection of $p_\beta(\beta)$ and $G(\beta)$, and therefore, three different sets of limit for the integration in equation (3.7). The three different pairs of limit are $(\beta_0-\beta_{\text{maxG}}, \beta_0+\beta_{\text{maxG}})$ for $\beta_{\text{m}} > \beta_0+\beta_{\text{maxG}}$ as $\beta_0+\beta_{\text{maxG}}$ is always greater than $|\beta_0-\beta_{\text{maxG}}|$, $(\beta_0-\beta_{\text{maxG}}, \beta_{\text{m}})$ for $|\beta_0-\beta_{\text{maxG}}| < \beta_{\text{m}} \le \beta_0+\beta_{\text{maxG}}$, and $(-\beta_{\text{m}}, \beta_{\text{m}})$ for $\beta_{\text{m}} \le |\beta_0-\beta_{\text{maxG}}|$.

However, the second order moments are actual parameters of importance to be used to calculate

LCR which reflects the fluctuation rate of received signal. The variance of the time derivative around a specified envelope level simply gives an idea about the amount of fluctuation around that level and it is equal to $\left|\frac{d^2}{d\tau^2} r_\rho(\tau) \mid_{\text{at}\tau=0}\right|$ or $|\ddot{r}_\rho(0)|$ multiplied with the variance of in-phase and quadrature components of the received complex envelope.

In general,

$$-\ddot{r}_\rho(0) = (2\pi f_{\max})^2 \times \gamma. \tag{3.10}$$

Without putting the limits of integration in equation (3.7), γ takes the following form,

$$\begin{aligned}\gamma = {} & \frac{p\sin((p-2)\beta)}{32(p-2)} + \frac{\sin(p\beta)}{16} + \frac{p\sin((p+2)\beta)}{32(p+2)} + \frac{p\sin(q(\beta_0-\beta)+p\beta)}{32(p-q)} + \frac{p\sin(q\beta_0+(p+2-q)\beta)}{64(p+2-q)} \\ & + \frac{p\sin(q\beta_0+(p-2-q)\beta)}{64(p-2-q)} + \frac{p\sin(q\beta_0-(p-2+q)\beta)}{64(p-2+q)} + \frac{p\sin(q\beta_0-(p+q)\beta)}{32(p+q)} \\ & + \frac{p\sin((p+2+q)\beta-q\beta_0)}{64(p+2+q)}\end{aligned} \tag{3.11}$$

which after putting the proper limits yield three different expressions. Here, $p = \pi/(2\beta_{\text{m}})$ and $q = \pi/\beta_{\text{maxG}}$. For the first case of intersection i.e. for the range $(\beta_0 - \beta_{\text{maxG}},\ \beta_0 + \beta_{\text{maxG}})$,

$$\begin{aligned}\gamma = {} & \Bigg[\frac{1}{8}\cos(p\beta_0)\sin(p\beta_{\text{maxG}}) + \frac{p\beta_{\text{maxG}}}{16}\cos((p-2)\beta_0)\text{sinc}((p-2)\beta_{\text{maxG}}/\pi) \\ & + \frac{p}{16(p+2)}\cos((p+2)\beta_0)\sin((p+2)\beta_{\text{maxG}}) + \frac{p\beta_{\text{maxG}}}{16}\cos(p\beta_0)\text{sinc}((p-q)\beta_{\text{maxG}}/\pi) \\ & + \frac{p}{16(p+q)}\cos(p\beta_0)\sin((p+q)\beta_{\text{maxG}}) + \frac{p\beta_{\text{maxG}}}{32}\cos((p-2)\beta_0)\text{sinc}((p-2-q)\beta_{\text{maxG}}/\pi) \\ & + \frac{p\cos((p-2)\beta_0)}{32(p-2+q)}\sin((p-2+q)\beta_{\text{maxG}}) + \frac{p\beta_{\text{maxG}}}{32}\cos((p+2)\beta_0)\text{sinc}((p+2-q)\beta_{\text{maxG}}/\pi) \\ & + \frac{p}{32(p+2+q)}\cos((p+2)\beta_0)\sin((p+2+q)\beta_{\text{maxG}})\Bigg]\end{aligned} \tag{3.12}$$

where $\text{Sinc}(x) = \frac{\sin(\pi x)}{\pi x}$. For the second case of intersection i.e. for the range $(\beta_0 - \beta_{\text{maxG}},\ \beta_{\text{m}})$,

$$\begin{aligned}\gamma = {} & \frac{p[\beta_{\text{m}}\text{sinc}((p-2)\beta_{\text{m}}/\pi) - \beta_{\text{l}}\text{sinc}((p-2)\beta_{\text{l}}/\pi)]}{32(p-2)} + \frac{[\sin(p\beta_{\text{m}}) - \sin(p\beta_{\text{l}})]}{16} \\ & + \frac{p[\sin((p+2)\beta_{\text{m}}) - \sin((p+2)\beta_{\text{l}})]}{32(p+2)} + \frac{p[\sin(q(\beta_0-\beta_{\text{m}})+p\beta_{\text{m}}) - \sin(q(\beta_0-\beta_{\text{l}})+p\beta_{\text{l}})]}{32(p-q)} \\ & + \frac{p[\sin(q\beta_0+(p+2-q)\beta_{\text{m}}) - \sin(q\beta_0+(p+2-q)\beta_{\text{l}})]}{64(p+2-q)} \\ & + \frac{p[\sin(q\beta_0+(p-2-q)\beta_{\text{m}}) - \sin(q\beta_0+(p-2-q)\beta_{\text{l}})]}{64(p-2-q)} \\ & + \frac{p[\sin(q\beta_0-(p-2+q)\beta_{\text{m}}) - \sin(q\beta_0-(p-2+q)\beta_{\text{l}})]}{64(p-2+q)}\end{aligned}$$

$$+\frac{p[\sin(q\beta_0-(p+q)\beta_{\rm m})-\sin(q\beta_0-(p+q)\beta_{\rm l})]}{32(p+q)}$$
$$+\frac{p[\sin((p+2+q)\beta_{\rm m}-q\beta_0)-\sin((p+2+q)\beta_{\rm l}-q\beta_0)]}{64(p+2+q)} \quad (3.13)$$

where $\beta_{\rm l}=\beta_0-\beta_{\rm maxG}$.

For the third case of intersection i.e. for the range $(-\beta_{\rm m},\beta_{\rm m})$,

$$\gamma=\left[\frac{p\beta_{\rm m}}{16}{\rm sinc}((p-2)\beta_{\rm maxG}/\pi)+\frac{\sin(p\beta_{\rm m})}{8}+\frac{p\sin((p+2)\beta_{\rm m})}{16(p+2)}\right.$$
$$+\frac{p\beta_{\rm m}}{32}\cos(q\beta_0){\rm sinc}((p-2-q)\beta_{\rm maxG}/\pi)+\frac{p\beta_{\rm m}}{32}\cos(q\beta_0){\rm sinc}((p+2-q)\beta_{\rm maxG}/\pi)$$
$$+\frac{p}{16(p+q)}\cos(q\beta_0)\sin((p+q)\beta_{\rm m})+\frac{p}{32(p-2+q)}\cos(q\beta_0)\sin((p-2+q)\beta_{\rm m})$$
$$\left.+\frac{p}{32(p+2+q)}\cos(q\beta_0)\sin((p+2+q)\beta_{\rm m})+\frac{p\beta_{\rm m}}{16}\cos(q\beta_0){\rm sinc}((p-q)\beta_{\rm maxG}/\pi)\right]. \quad (3.14)$$

The calculated value of $r_\rho''(0)$ from the above group of equations (3.10)–(3.14) will be used in subsequent chapters for calculation of the second order moments. If antenna radiation pattern is not included, like in the scattering model of [1], the value of $|r_\rho''(0)|$ usually goes on decreasing if $\beta_{\rm m}$ (which is fixed in a particular location) is increased. In other words, the fluctuation of received signal and LCR increases if scatterers are located closely around the azimuthal plane. An interesting change happens if antenna system like in [20] is used. Due to high elevation of the main lobe (40° here), the overlapping of the radiation pattern and scattering geometry is almost non-existent if $\beta_{\rm m}$ is low and thus $|r_\rho''(0)|$ and eventually LCR is decreased (shown in Section 4.2) due to non-availability of fluctuating scattered power. As, $\beta_{\rm m}$ is increased (e.g. highly elevated scatterers like tall tree or building), $|r_\rho''(0)|$ gets higher value signifying increased fluctuation in contrast to model proposed in [1]. However, for low antenna elevation, the situation can be different depending upon the spatial distribution of the scatterers.

3.4 Summary

The prerequisite for our approach on narrowband and wideband LMS channel modeling, to be covered in subsequent chapters, has been carried out here by the initial classification of the propagation scenarios and the inclusion of the effects of LMS antenna systems in a 3D scattering model. Some interesting effects of antenna directivity on the second order moments have been

investigated which will be addressed in more detail when calculating second order statistics in upcoming chapters.

4

Narrowband Modeling with Additive Envelope Process

Contents

This chapter proposes and develops a model taking into account the fading process experienced by the different components of the received signal. Here, a narrowband model is introduced using additive complex envelope process with a Doppler PSD generated from a 3D scattering model. The expressions for the pdf of the envelope and phase components are derived first; taking into account appropriate fading process as experienced by the LOS and NLOS components. The mathematical expressions for LCR and AFD are then derived. By comparing with measurement results of LCR and AFD available in literature, it is shown that this model can be used to depict a wide variety of fading situations for flat urban and suburban areas. If LOS component is not included, the model represents the scenario normally encountered in dense urban conditions. With LOS component being present but not experiencing shadow fading, the model represents fading conditions experienced in open areas. For such cases, the proposed model give rise to a new distribution which is termed here as extended Nakagami-q or extended Hoyt fading process.

4.1 The Proposed Model Based on an Additive Envelope Process

In the model proposed here, as discussed in Section 3.1.1, only the LOS component gets effected by shadow fading while the local mean power of scattered components is kept constant. This otherwise means that NLOS components of the transmitted signal are not shadow faded before entering into the local cluster of scatterers in the close vicinity of the receiver. Therefore, this leads to an additive process same as equation (3.1) and has the applicability in flat urban and suburban area as explained in Section 3.1.1. Here, X_1 and X_2 are both low pass Gaussian process with zero mean and unequal variances σ_1^2 and σ_2^2 respectively, leading to Nakagami-q or Hoyt distribution of the envelope of scattered components [52, 53]. Y represents the shadow faded LOS component with lognormal distribution given as

$$p_Y(y) = \frac{1}{\sqrt{2\pi}\sigma_s y} \exp\left[-\frac{(\ln y - \mu_s)^2}{2\sigma_s^2}\right], \quad y \geq 0 \tag{4.1}$$

where σ_s and μ_s are standard deviation and mean of $\ln y$ respectively. The mean signal level in a large area (large enough to experience the slow variation of shadow fading) is denoted here as S_0, which is related to μ_s as $\mu_s = \ln S_0$.

So, the envelope is given by

$$R = |\widetilde{R}| = \sqrt{(X_1 + Y)^2 + X_2^2}. \tag{4.2}$$

4.1.1 First Order Statistics

The probability density function (pdf) of envelope R can be derived with the help of conditional probability. Given the condition $Y = y$, the in-phase component of $\widetilde{R}$ is modified into a non-zero mean Gaussian process $X_1' = X_1 + y$ with mean y. So, the joint pdf of X_1' and X_2 is

$$p_{X_1',X_2}(x_1', x_2) = \frac{1}{2\pi\sigma_1\sigma_2} \exp\left(-\left[\frac{{x_1'}^2}{2\sigma_1^2} + \frac{x_2^2}{2\sigma_2^2}\right]\right). \tag{4.3}$$

Now, by transformation from cartesian to polar coordinates, we get the joint conditional pdf $p_{R,\Theta}(r, \theta|Y = y)$ as [60]

$$p_{R,\Theta}(r, \theta|Y = y) = \frac{r \exp\left(-\left[\frac{(r\cos\theta - y)^2}{2\sigma_1^2} + \frac{r^2\sin^2\theta}{2\sigma_2^2}\right]\right)}{2\pi\sigma_1\sigma_2} \tag{4.4}$$

where $r \geq 0$ and $0 \leq \theta \leq 2\pi$. So, the joint envelope-phase pdf $p_{R,\Theta}(r, \theta)$ can be derived as [61]

$$p_{R,\Theta}(r, \theta) = \int_0^\infty p_{R,\Theta}(r, \theta|Y = y) p_Y(y) dy. \tag{4.5}$$

In light of the technique given in [60] (pp. 128-131), we deduce the individual pdf of envelope and phase as marginal pdf of equation (4.5), as

$$\begin{aligned} p_R(r) = \frac{r}{\sqrt{2\pi}\sigma_1\sigma_2\sigma_s} \exp\left(-\frac{r^2}{4}\left(\frac{1}{\sigma_1^2} + \frac{1}{\sigma_2^2}\right)\right) \int_0^\infty \frac{1}{y} \exp\left[-\frac{(\ln y - \mu_s)^2}{2\sigma_s^2} - \frac{y^2}{2\sigma_1^2}\right] \\ \times \sum_{k=0}^{\infty} (-1)^k \epsilon_k I_k\left(\frac{r^2}{4}\left(\frac{1}{\sigma_1^2} - \frac{1}{\sigma_2^2}\right)\right) I_{2k}\left(\frac{ry}{\sigma_1^2}\right) dy \end{aligned} \tag{4.6}$$

where $\epsilon_k = 2$ for $k \neq 0$ ($\epsilon_0 = 1$), $I_k(\cdot)$ is modified Bessel function of first kind with order k; and

$$\begin{aligned} p_\Theta(\theta) = \frac{1}{(2\pi)^{3/2}\sigma_s} \int_0^\infty \frac{1}{y} \exp\left[-\frac{(\ln y - \mu_s)^2}{2\sigma_s^2}\right] \left[\frac{\sigma_1\sigma_2}{G(\theta)} \exp\left(-\frac{y^2}{2\sigma_1^2}\right)\right. \\ \left. + \frac{\sqrt{2\pi}\sigma_2^2 y\cos\theta}{G^{3/2}(\theta)} \exp\left(-\frac{y^2\sin^2\theta}{2G(\theta)}\right) Q\left(-\frac{\sigma_2 y\cos\theta}{\sigma_1\sqrt{G(\theta)}}\right)\right] dy \end{aligned} \tag{4.7}$$

where $G(\theta) = \sigma_2^2\cos^2\theta + \sigma_1^2\sin^2\theta$ and $Q(\cdot)$ is the Q-function which is related with error function as $Q(x) = \frac{1}{2}\left[1 - \text{erf}\left(\frac{x}{\sqrt{2}}\right)\right]$.

Under certain conditions, if the shadow fading is absent, the joint envelope-phase distribution in equation (4.4) denotes a new distribution. We, hereby, name it as extended Nakagami-q or extended Hoyt distribution and describe its statistics in Section 4.3.2.

4.1.2 Second Order Statistics

4.1.2.1 LCR and AFD

Level Crossing Rate (LCR) is the rate at which envelope of received signal crosses a specified threshold. In analytical representation, it is expressed as

$$N_R(r) = \int_0^\infty \dot{r} p_{R\dot{R}}(r, \dot{r}) d\dot{r} \tag{4.8}$$

where R and $\dot{R}$ are received signal envelope and its time derivative, respectively, and $p_{R,\dot{R}}(r, \dot{r})$ is the joint pdf of R and $\dot{R}$. $p_{R,\dot{R}}(r, \dot{r})$ can be derived with the use of conditional probability in a similar way as in Section 4.1.1.

$$p_{R,\dot{R}}(r, \dot{r}) = \int_{-\infty}^{\infty} \int_0^\infty p_{R,\dot{R}}(r, \dot{r}|Y = y, \dot{Y} = \dot{y}) p_{Y,\dot{Y}}(y, \dot{y}) dy d\dot{y} \tag{4.9}$$

where $r \geq 0$, $-\infty < \dot{r} < \infty$, $0 \leq \theta \leq 2\pi$ and $-\infty < \dot{\theta} < \infty$ and $p_{Y,\dot{Y}}(y, \dot{y})$ is the joint pdf of Y and $\dot{Y}$ given as [62]

$$p_{Y\dot{Y}}(y, \dot{y}) = \frac{1}{2\pi\sigma_s\sigma_{s'}y^2} \exp\left[-\frac{(\ln y - \mu_s)^2}{2\sigma_s^2} - \frac{\left(\dot{y}/y\right)^2}{2\sigma_{s'}^2}\right] \tag{4.10}$$

where $y \geq 0$, $-\infty < \dot{y} < \infty$ and $\sigma_{s'}$ is the standard deviation of time derivative of the normal or Gaussian variate associated with $\dot{Y}$.

Given the condition $Y = y$, the in-phase component of $\widetilde{R}$ is a Gaussian process $X_1' = X_1 + y$, as shown in Section 4.1.1. So, its derivative, $\dot{X}_1' = \dot{X}_1 + \dot{y}$, is also a Gaussian process with non-zero mean $\dot{y}$ while $\dot{X}_2$ is zero mean Gaussian distributed. The joint pdf $p_{X_1',X_2,\dot{X}_1',\dot{X}_2}(x_1', x_2, \dot{x}_1', \dot{x}_2)$ comes out to be a four variable joint Gaussian distribution as

$$p_{X_1',X_2,\dot{X}_1',\dot{X}_2}(x_1', x_2, \dot{x}_1', \dot{x}_2) = \frac{1}{(2\pi)^2\sigma_1\sigma_2\sqrt{\beta_1\beta_2}} \exp\left(-\frac{1}{2}\left[\frac{(x_1' - y)^2}{\sigma_1^2} + \frac{x_2^2}{\sigma_2^2} + \frac{(\dot{x}_1' - \dot{y})^2}{\beta_1} + \frac{\dot{x}_2^2}{\beta_2}\right]\right) \tag{4.11}$$

where β_1 and β_2 are variances of $\dot{X}_1'$ and $\dot{X}_2$ respectively and can be related with σ_1 and σ_2 by method shown in Section 4.1.2.2.

Now, by transformation from cartesian to polar coordinates, we get the joint conditional pdf as

$$p_{R,\dot{R},\Theta,\dot{\Theta}}(r, \dot{r}, \theta, \dot{\theta}|Y = y, \dot{Y} = \dot{y}) = \frac{r^2}{(2\pi)^2\sigma_1\sigma_2\sqrt{\beta_1\beta_2}} \exp\left[-\frac{(r\cos\theta - y)^2}{2\sigma_1^2} - \frac{r^2\sin^2\theta}{2\sigma_2^2}\right.$$

$$- \frac{(\dot{r}\cos\theta - r\dot{\theta}\sin\theta - \dot{y})^2}{2\beta_1} - \frac{(\dot{r}\sin\theta + r\dot{\theta}\cos\theta)^2}{2\beta_2}\Bigg]. \quad (4.12)$$

Equation (4.12) is integrated with respect to θ and $\dot{\theta}$ to derive $p_{R,\dot{R}}(r,\dot{r}|Y=y,\dot{Y}=\dot{y})$.

$$p_{R,\dot{R}}(r,\dot{r}|Y=y,\dot{Y}=\dot{y}) = \frac{r}{(2\pi)^{3/2}\sigma_1\sigma_2}\int_0^{2\pi}\exp\left(-\frac{(r\cos\theta - y)^2}{2\sigma_1^2} - \frac{r^2\sin^2\theta}{2\sigma_2^2}\right) \times \frac{1}{\sqrt{\beta_2 + (\beta_1-\beta_2)\cos^2\theta}}\exp\left(-\frac{(\dot{r}-\dot{y}\cos\theta)^2}{2\left[\beta_2 + (\beta_1-\beta_2)\cos^2\theta\right]}\right)d\theta. \quad (4.13)$$

Then using equation (4.9), expression for $p_{R,\dot{R}}(r,\dot{r})$ is derived as

$$p_{R,\dot{R}}(r,\dot{r}) = \frac{r}{(2\pi)^2\sigma_1\sigma_2\sigma_s}\int_0^{\infty}\frac{1}{y}\exp\left[-\frac{(\ln y - \mu_s)^2}{2\sigma_s^2}\right]\int_0^{2\pi}\exp\left(-\frac{(r\cos\theta - y)^2}{2\sigma_1^2} - \frac{r^2\sin^2\theta}{2\sigma_2^2}\right) \times \frac{1}{\sqrt{\beta_2 + \left(\beta_1 - \beta_2 + \sigma_{s'}^2 y^2\right)\cos^2\theta}} \times \exp\left(-\frac{\dot{r}^2}{2\left[\sqrt{\beta_2 + \left(\beta_1 - \beta_2 + \sigma_{s'}^2 y^2\right)\cos^2\theta}\right]}\right)d\theta dy. \quad (4.14)$$

Finally, using equation (4.8), expression for LCR is derived.

$$N_R(r) = \frac{r}{(2\pi)^2\sigma_1\sigma_2\sigma_s}\int_0^{\infty}\frac{1}{y}\exp\left[-\frac{(\ln y - \mu_s)^2}{2\sigma_s^2}\right]\int_0^{2\pi}\sqrt{\beta_2 + \left(\beta_1 - \beta_2 + \sigma_{s'}^2 y^2\right)\cos^2\theta} \times \exp\left(-\frac{(r\cos\theta - y)^2}{2\sigma_1^2} - \frac{r^2\sin^2\theta}{2\sigma_2^2}\right)d\theta dy. \quad (4.15)$$

Using the knowledge of computed LCR, average fade duration (AFD), which is defined as the average period of time for which the received signal is below a specified threshold level R, can be computed as

$$T_R(R) = \frac{\int_0^R p_R(r)}{N_R(R)}. \quad (4.16)$$

In other words, it is the ratio of cumulative distribution function to LCR at a particular signal level.

4.1.2.2 Normalization with respect to Maximum Doppler Frequency Using 3D Scattering Model

Different maximum doppler frequency $f_{\max_i}$ $(i = 1, 2)$ has been assumed for the Gaussian processes X_i $(i = 1, 2)$, as was done in [59]. Using equations (3.10), (3.12), (3.13), and (3.14), the quantities β_i $(i = 1, 2)$ can be expressed in terms of $f_{\max_i}$ as

$$\beta_i = \sigma_i^2 \times (2\pi f_{\max_i})^2 \times \gamma. \tag{4.17}$$

If antenna effects are not included (recommended only if omnidirectional pattern in elevation plane), then value of γ is given by [1],

$$\gamma = \left[\frac{1}{4} + \frac{1}{8}\left(\frac{\pi}{\pi + 4\beta_{\mathrm{m}}}\cos(2\beta_{\mathrm{m}}) + \frac{\pi}{2}\mathrm{Sinc}\left(\frac{1}{2} - \frac{2\beta_{\mathrm{m}}}{\pi}\right)\right)\right]. \tag{4.18}$$

However, instead of taking individual values for $f_{\max_i}$ (as done in [59]), the ratio $f_{\max_2}/f_{\max_1} = k$ is used here as a normalization factor while the assumption $f_{\max} = f_{\max_1}$ is kept same as [59].

Due to slowly time-varying nature of shadow fading, power spectral density (PSD) of it is usually assumed as low-pass functions like Gaussian, R-C low pass or 3-pole butterworth filters. With this low-pass PSD assumption, it can be shown that $\frac{\sigma_{s'}}{\sigma_s} = \frac{\sqrt{n}}{f_{\mathrm{ratio}}} 2\pi f_{\max}$; where the constant n depends on the filter assumed and f_{ratio} is the ratio between $f_{\max}$ and 3-dB cut-off frequency of the filter. As time variation of shadow fading is very small compared to the frequently changing small-scale fading, high value of f_{ratio} is considered here.

Taking into account all these assumptions, equation (4.15) can be normalized with respect to maximum doppler frequency as

$$\frac{N_R(r)}{f_{\max}} = \frac{r}{2\pi\sigma_1\sigma_2\sigma_s}\int_0^{\infty}\frac{1}{y}\exp\left[-\frac{(\ln y - \mu_s)^2}{2\sigma_s^2}\right]\int_0^{2\pi}\sqrt{\gamma k^2\sigma_2^2 + \left(\gamma\sigma_1^2 - \gamma k^2\sigma_2^2 + k_1^2\sigma_s^2 y^2\right)\cos^2\theta}$$
$$\times \exp\left(-\frac{(r\cos\theta - y)^2}{2\sigma_1^2} - \frac{r^2\sin^2\theta}{2\sigma_2^2}\right)d\theta dy \tag{4.19}$$

where $k_1 = \frac{\sqrt{n}}{f_{\mathrm{ratio}}}$.

4.2 Results and Discussions

In Figure 4.1(a) and 4.1(b), effect of important parameters of Hoyt/Nakagami-q and lognormal distribution, i.e. σ_1, σ_2 and σ_s, and also parameters of 3D scattering model namely β_{m}, β_0,

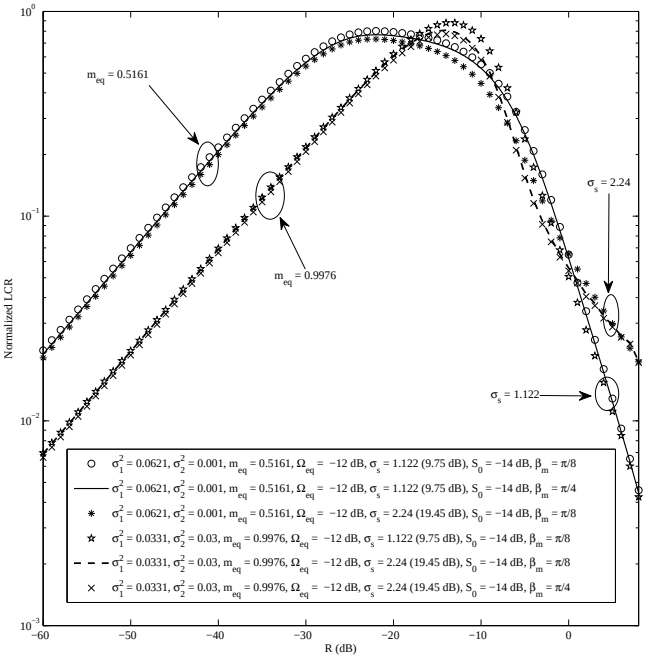

(a)

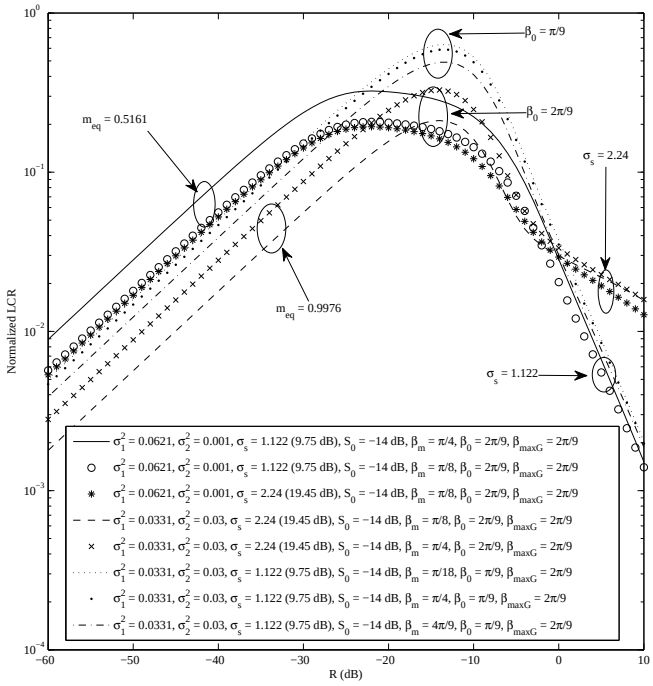

(b)

Figure 4.1: Effect of σ_1^2, σ_2^2, σ_s, and 3D scattering model parameters on LCR, (a) without and (b) with antenna effect.

β_{maxG} on LCR curves are shown. In both of these figures, LCR curves have a maximum around $S_0 = -14$ dB as signal envelope crosses the area mean signal level most of the time. Fig. 4.1(a) shows LCR, at a particular threshold, decreases for increasing β_{m} which is possible if the mobile receiver is moving around in an area with variation in height and concentration of building, trees and other obstacles. An increasing β_{m} signifies sparse distribution of scatterers in the elevation plane, and longer difference in path length traversed and in time of arrival causing interference of waves spread over time and eventually less fluctuation rate. The opposite trend is observed in Fig. 4.1(b) due to antenna directivity at a high angle (40°) as said earlier in Section 3.3. The overall LCR values are also less compared to Fig. 4.1(a) due to rejection of a lot of fluctuating scattered power. Variation among the curves is also very high for a change in β_{m} with other parameters kept constant. However, for small β_0 (20°), LCR values change like Fig. 4.1(a) because of increased intersection of the radiation pattern and scattering geometry if β_{m} is low. It is also observed that small-scale fading parameters σ_1, σ_2 have more influence on the LCR curves at $R < S_0$ and shadow fading parameter σ_{s} at $R > S_0$ (which accords with observation in [63] and complies with equation (4.5-18) in [60]). This is the reason why LCR curves suddenly go up from the earlier curvature and tend to flatten out for $R > S_0$ at very high values of shadow fading variance such as σ_{s} =2.24 (19.45 dB).

However, the quantities m_{eq} and Ω_{eq} should not be mistaken same as equation (4.27) and (4.28). Ω_{eq} is total power of the scattered components only and m_{eq} is the fading severity parameter as though any LOS path is blocked to the receiver. Hence, m_{eq} and Ω_{eq} here stand for equivalent Nakagami-m parameters for Nakagami-q alone. So, the relation between m_{eq}, Ω_{eq} and σ_1, σ_2 are [52]

$$m_{\text{eq}} = \frac{(\sigma_1^2 + \sigma_2^2)^2}{(\sigma_1^2 + \sigma_2^2)^2 + (\sigma_1^2 - \sigma_2^2)^2} \tag{4.20}$$

and

$$\Omega_{\text{eq}} = \sigma_1^2 + \sigma_2^2. \tag{4.21}$$

We, hereby, present a comparison of LCR derived from our proposed model with the same given in [22,23] along with the same parameters and show this result in Figure 4.2(a) and 4.2(b). LCR of the proposed model based on 2D scattering is zero when effect of highly elevated antenna system (Fig. 2 of [20]) is included. Since Nakagami-q is a generalized distribution, our proposed model provides several LCR curves for different fading situations which can be obtained by changing σ_1

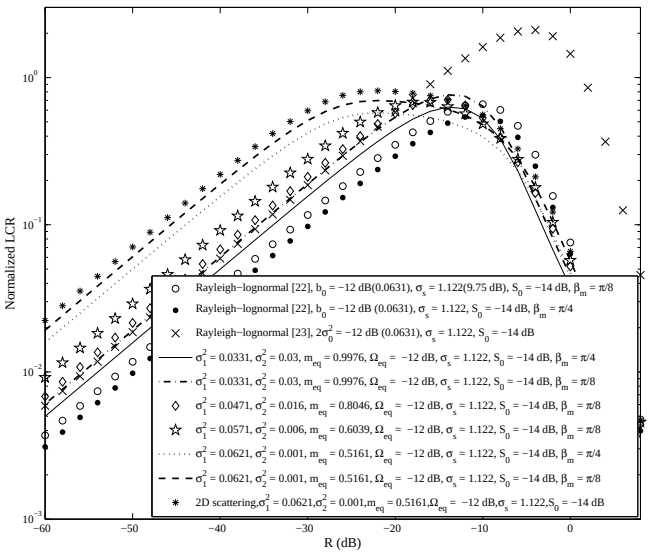

(a)

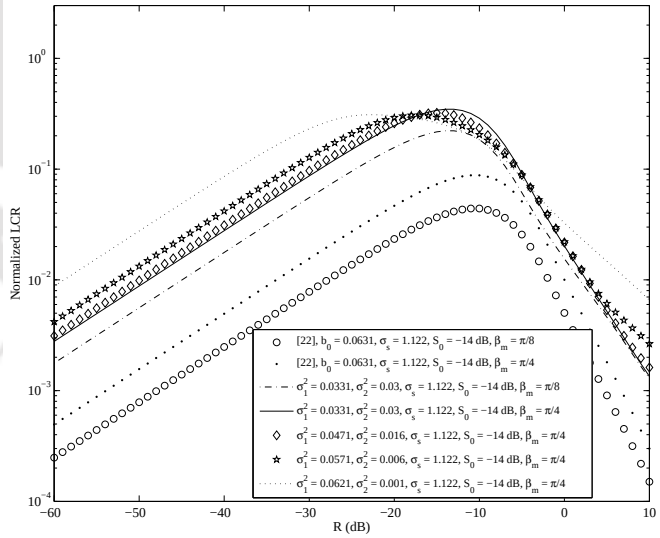

(b)

Figure 4.2: Comparison of LCR obtained from proposed model with existing models for same multipath power and shadow fading for (a) without and (b) with antenna effect.

and σ_2 (i.e. changing m_{eq}).

As can be observed from Figure 4.2(a) and 4.2(b), the LCR curves obtained from our proposed model have not only good correlation with the existing additive Rayleigh-lognormal models [22,23] when $m_{\text{eq}} = 1$; but are also at higher values compared to the curves of the existing models for $0.5161 \leq m_{\text{eq}} \leq 0.8046$, denoting worse fading situations. In 4.2(a) and 4.2(b), we have depicted the lower and upper limit of this wide range of m_{eq} by the 'dashed' and the 'diamond' curves, respectively, as well as one intermediate point $m_{\text{eq}} = 0.6039$ is also shown by the 'star' curve to show that increment of m_{eq} gradually decreases LCR at a particular value of R. Hence it can be broadly concluded that for $m_{\text{eq}} \in (0.5, 0.8]$, the proposed model in this chapter can represent worse fading situations which other existing additive models are unable to depict.

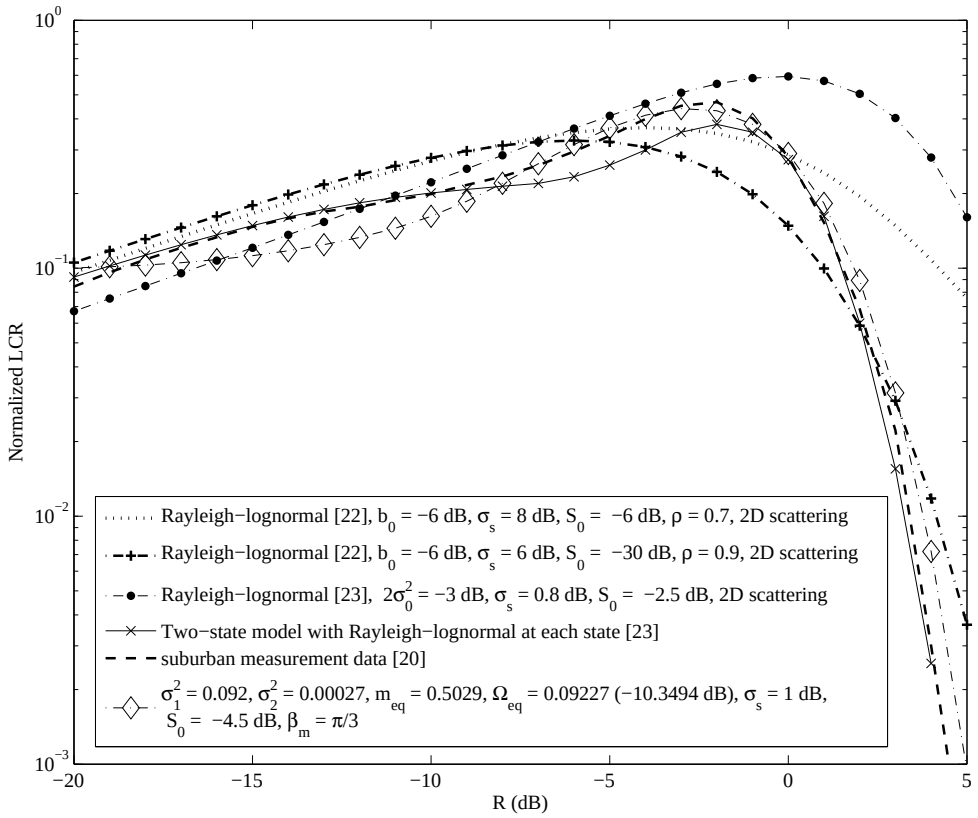

Figure 4.3: Comparison of computed LCR with measurement data and with other models.

In Figure 4.3, the analytically computed LCR is compared with LCR curve of suburban measurement data reproduced from [20]. It is reported in [20] that this suburban data were collected

at a satellite elevation angle of 19° on streets within a residential area of Ottawa with one and two storey homes. LCR curve obtained from equation (4.19) at $\beta_m = \pi/3$ and at values of β_0, β_{maxG} taken from Fig. 2 of [20] is in good match with the suburban measurement LCR curve justifying the claim made at the beginning of Section 4.1. Good match is also achieved by a two-state model proposed in [23] with Rayleigh-lognormal distribution in both states and with parameters given in Section IV-B and Table II of the same paper. However, the increased number of states gives rise to more rigorous analytical computation as in the two-state model in [23]. Our model being a single state model, is devoid of such computational hazards while still capable of adaptation to measurement data. However, the analytical curves of the other established single state additive models [22, 23] do not show a good degree of match with the measurement result beyond a certain range of threshold level. Since the propagation characteristics of a flat urban area with low density of obstacles is not significantly different than that of a flat suburban area, as explained in Section 3.1.1, it is expected that LCR/AFD measurement of a flat urban area would also yield a good degree of accuracy with respect to our proposed model similar to that reported in Figure 4.3 in the context of a flat suburban area.

Dependence of AFD on the parameters are shown in Figure 4.4. Like Figure 4.1(a) and 4.1(b), similar grouping is also possible here depicting the dominance of small-scale fading for $R \ll S_0$ and of shadow fading in reverse case. It is also observed that long duration fades occur either in case of severe fading condition (i.e. low m_{eq}) or infrequent shadow fading (i.e. low σ_{s}). In similarity with Figure 4.2(a) and 4.2(b), AFD curves obtained from the proposed model are in accordance with the curves of existing additive Rayleigh-lognormal model [22] when $m_{\text{eq}} = 1$ and showing higher fade durations for $m_{\text{eq}} < 1$, thus reflecting the ability of the proposed model to epitomize worse fading conditions.

It is shown in Figure 4.5 that the AFD curve of our model is in good match with suburban measurement curve of AFD reproduced from [20] and also outperforms other related models [22,23] in the aspect of matching with measurement curve.

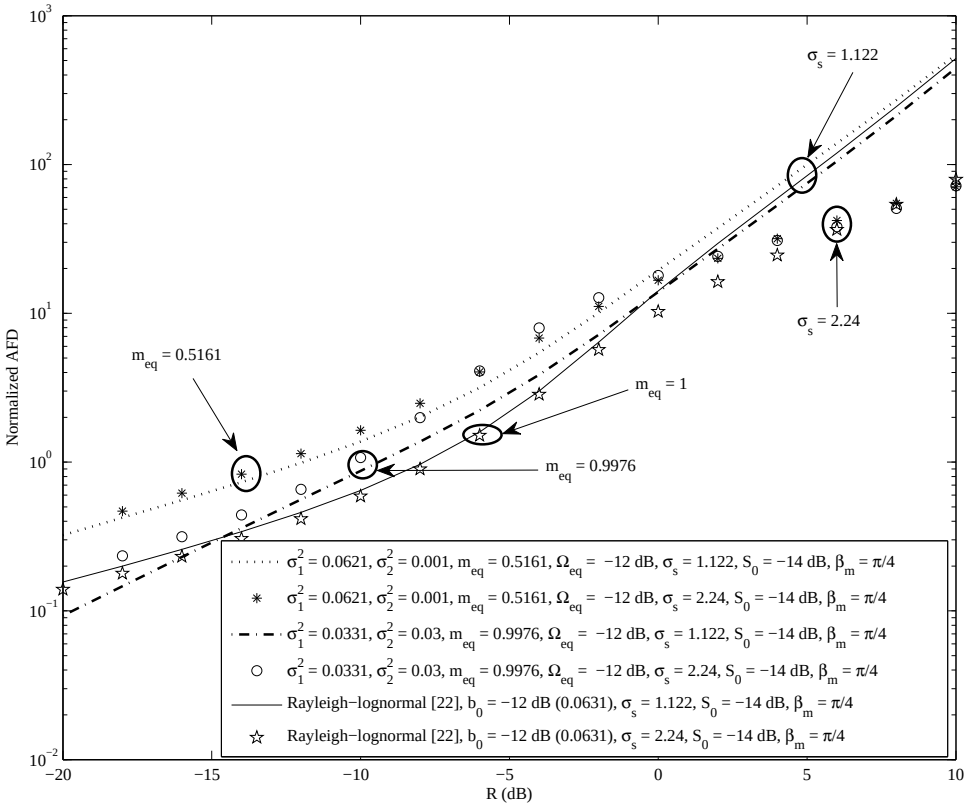

Figure 4.4: Effect of σ_1^2, σ_2^2, and σ_s on AFD and comparison with existing models for same multipath power and S_0.

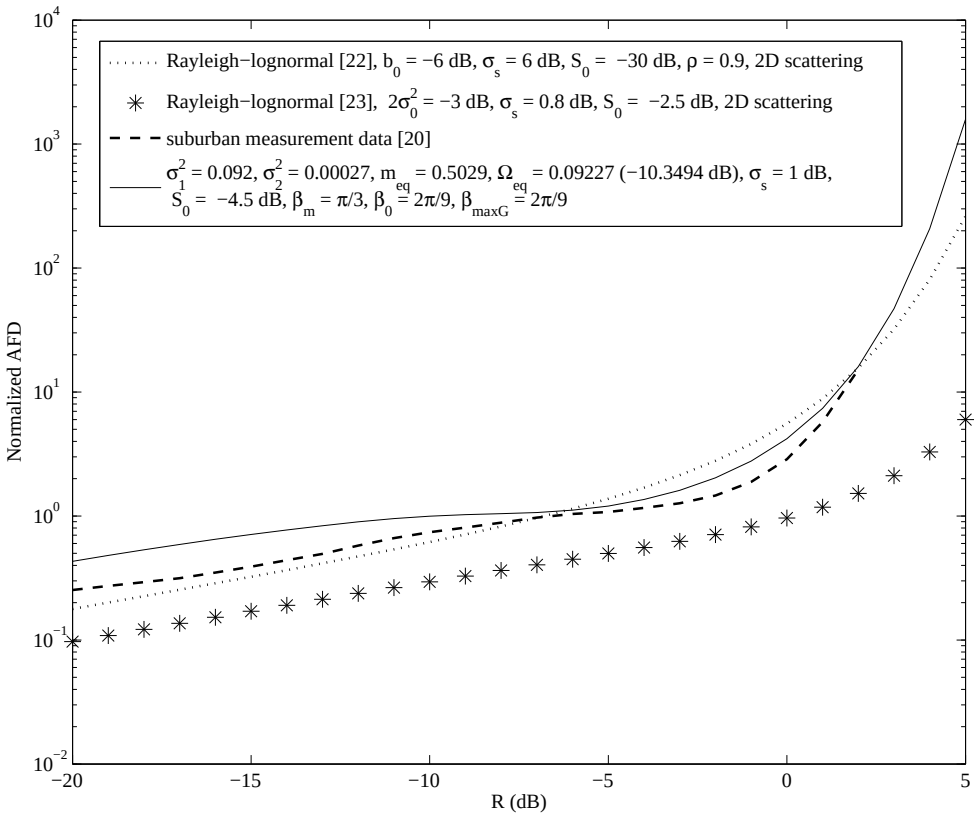

Figure 4.5: Comparison of computed AFD with measurement data and with other models.

4.3 Special Cases

4.3.1 Absence of LOS: Nakagami-q envelope process

In absence of LOS component, equation (4.2) turns out to be the envelope of Nakagami-q by putting $Y = 0$. The expressions of its first and second order statistics can be formulated by putting $p_Y(y) = \delta(y)$ in the equations given in Section 4.1.1 and 4.1.2 and they will be same as derived in [59]. The only modification will be introduced by the 3D scattering model proposed in Section 3.3. Some results on this is shown later in Section 6.2.2.3.

4.3.2 Absence of Shadow Fading: Extended Nakagami-q Distribution

When shadow fading is absent, the LOS component can be represented by a constant equal to area mean signal level S_0. So, the low-pass complex envelope (let now be denoted by $\widetilde{R_1}$) is modified as

$$\widetilde{R_1} = X_1 + jX_2 + S_0. \tag{4.22}$$

This complex envelope is different from the additive envelope expressed in equation (3.1) in the sense that, here the LOS component is unfaded and thus is not a random process. Therefore, this distribution has practical utility when the receiver does not move a considerable distance (over few tens of meters) so that the effect of shadow fading can be neglected (which includes indoor environment too). This distribution can also be used instead of Rician to represent channel conditions in open areas due to LOS availability. Thus, it is implied that by a little modification, the narrowband model in Section 4.1 can be used for both the scenarios described in Section 3.1.2 and 3.1.3.

Let us denote the modified envelope and phase as R_1 and Θ_1. The modified envelope is now

$$R_1 = |\widetilde{R_1}| = \sqrt{(X_1 + S_0)^2 + X_2^2}. \tag{4.23}$$

Following equation (4.4), the joint envelope-phase pdf $p_{R_1,\Theta_1}(r_1, \theta_1)$ in this special case is given by

$$p_{R_1,\Theta_1}(r_1, \theta_1) = \frac{r_1 \exp\left(-\left[\frac{(r_1\cos\theta_1 - S_0)^2}{2\sigma_1^2} + \frac{r_1^2 \sin^2\theta_1}{2\sigma_2^2}\right]\right)}{2\pi\sigma_1\sigma_2} \tag{4.24}$$

where $r_1 \geq 0$ and $0 \leq \theta_1 \leq 2\pi$. With $S_0 = 0$, equation (4.24) is marginalized to the joint envelope-phase pdf of Nakagami-q distribution and all other statistics of $\widetilde{R_1}$ becomes same as of a Nakagami-q process. This promotes us to employ the term extended Nakagami-q distribution.

Following the procedure of equation (4.6) and (4.7), the envelope and phase pdfs ($p_{R_1}(r_1)$ and $p_{\Theta_1}(\theta_1)$) can be deduced as

$$p_{R_1}(r_1) = \frac{r_1}{\sigma_1\sigma_2}\exp\left(-\frac{r_1^2}{4}\left(\frac{1}{\sigma_1^2}+\frac{1}{\sigma_2^2}\right)\right)\exp\left[-\frac{S_0^2}{2\sigma_1^2}\right]\sum_{k=0}^{\infty}(-1)^k\epsilon_k I_k\left(\frac{r_1^2}{4}\left(\frac{1}{\sigma_1^2}-\frac{1}{\sigma_2^2}\right)\right)I_{2k}\left(\frac{r_1 S_0}{\sigma_1^2}\right) \tag{4.25}$$

and

$$p_{\Theta_1}(\theta_1) = \frac{1}{2\pi}\left[\frac{\sigma_1\sigma_2}{G(\theta_1)}\exp\left(-\frac{S_0^2}{2\sigma_1^2}\right)+\frac{\sqrt{2\pi}\sigma_2^2 S_0\cos\theta_1}{G^{3/2}(\theta_1)}\exp\left(-\frac{S_0^2\sin^2\theta_1}{2G(\theta_1)}\right)Q\left(-\frac{\sigma_2 S_0\cos\theta_1}{\sigma_1\sqrt{G(\theta_1)}}\right)\right] \tag{4.26}$$

where $G(\theta_1) = \sigma_2^2\cos^2\theta_1 + \sigma_1^2\sin^2\theta_1$. $p_{R_1}(r_1)$ is plotted in Figure 4.6 for different values of the parameters. It is observed from this figure that the pdf approaches to Gaussian pdf at higher value of S_0 as it signifies a corresponding increase in m (equation (4.28)). Lower value of S_0 is required to reach the Gaussian shape when $\sigma_1 \approx \sigma_2$, as it denotes larger m (e.g. $m = 2.64$ for $\sigma_1^2 = 0.0331$, $\sigma_2^2 = 0.03$, $S_0 = 0.5$ and $m = 1.4$ for $\sigma_1^2 = 0.0621$, $\sigma_2^2 = 0.001$, $S_0 = 0.5$).

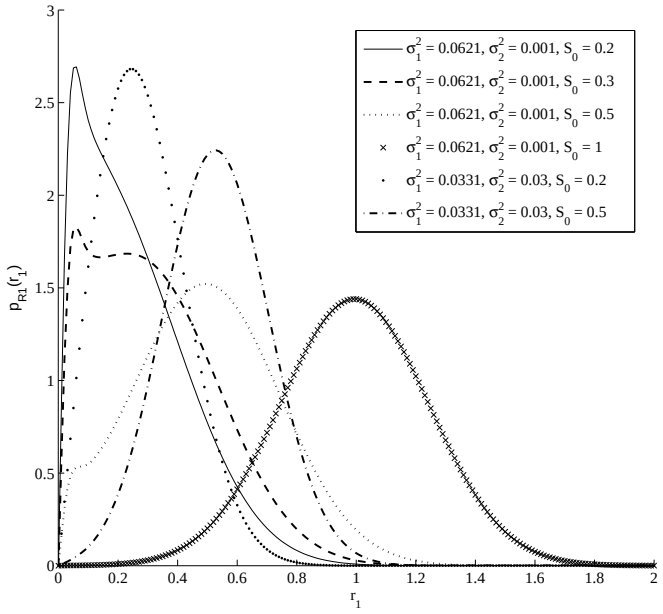

Figure 4.6: pdf of envelope of extended Nakagami-q distribution.

4.3.2.1 Relation with Nakagami-m, Rician and Rayleigh Distribution

The relation between the parameters of Nakagami-m (m and Ω) and Nakagami-q (σ_1 and σ_2) distribution are also modified in this special case. Following [52], the relations are

$$\Omega = E\left[R_1^2\right] = E\left[(X_1 + S_0)^2 + X_2^2\right] = S_0^2 + \sigma_1^2 + \sigma_2^2 \tag{4.27}$$

and

$$m = \frac{\Omega^2}{E[(R_1^2 - \Omega)^2]} = \frac{\left(S_0^2 + \sigma_1^2 + \sigma_2^2\right)^2}{2\left(\sigma_1^4 + \sigma_2^4\right) + 4\sigma_1^2 S_0^2}. \tag{4.28}$$

When $\sigma_1 = \sigma_2 = \sigma$, it becomes Rician distribution. In that case, the relation between m, Ω and σ is

$$\Omega = S_0^2 + 2\sigma^2 \tag{4.29}$$

and

$$m = \frac{\left(S_0^2 + 2\sigma^2\right)^2}{4\sigma^4 + 4\sigma^2 S_0^2} = \frac{\left(S_0^2 + 2\sigma^2\right)^2}{\left(S_0^2 + 2\sigma^2\right)^2 - S_0^4} = \frac{(1+K)^2}{1+2K} \tag{4.30}$$

where K is the Rician factor given by $K = S_0^2/2\sigma^2$. When S_0 assumes a high value, the corresponding value of K (and m) also becomes large and thus the extended Nakagami-q distribution tends to Gaussian distribution like the marginal case of Rician distribution with a high LOS component power.

A more special case of Rayleigh distribution turns out when the LOS path is absent i.e. $S_0 = 0$ along with $\sigma_1 = \sigma_2 = \sigma$. In this case, $\Omega = 2\sigma^2$ and $m = 1$.

4.4 Summary

Analytical expressions for first and second order statistics along with simulation results have been given for a new additive channel model proposed in this chapter. This narrowband model has its applicability in flat urban and suburban area for practical reasons already explained and it has been proved to be superior than other single state LMS models in case of suburban scenario by comparison with measurement data. The model can also be used to depict a wide variety of fading situations including the marginal cases covered by some other models (e.g. [22, 23]). It is also shown that when LOS component is either absent or present without shadow fading, this model can represent two other channel conditions – LOS non-availability in dense urban areas and LOS availability in open areas respectively. In the later case, a new distribution, termed here as

'extended Nakagami-q' or 'extended Hoyt', turns out from our proposed model as a special case. Relation of this distribution with Nakagami-m, Rician, and Rayleigh distribution have also been discussed.

5

Narrowband Modeling with Multiplicative Envelope Process

Contents

In this chapter, we propose a narrowband model based on a multiplicative envelope process which is targeted to capture fading mechanism in a propagation scenario described in Section 3.1.2. To represent the unfaded LOS component and small-scale faded scattered components in a combined process, we, hereby, consider Nakagami-m distribution. This distribution can epitomize a wide range of fading situations, by simply changing the parameter $m \in [0.5, \infty)$, including the LOS availability condition described by Rician distribution ($m \gg 1$), non-LOS condition of Rayleigh ($m = 1$) and the worst condition of Nakagami-q ($0.5 < m \leq 1$). Multiplicative to this Nakagami-m process is the shadow fading which is taken as lognormally distributed.

5.1 Statistics of the Proposed Envelope Process

As per the discussion above, the overall signal envelope (R) of received signal is represented as a multiplication of a Nakagami-m (Z) and a lognormal (Y) process; i.e.

$$R = Z \cdot Y. \tag{5.1}$$

Starting with a Gaussian random process X with mean $\mu_{\rm s}$ and standard deviation $\sigma_{\rm s}$, the lognormal process Y can be written as $Y = e^X$. The time derivative of X and Z, $\dot{X}$ and $\dot{Z}$ are Gaussian with zero mean [16]. As X, $\dot{X}$, and $\dot{Z}$ are all Gaussian, we have opportunity to examine the first and second order statistics of envelope R under the assumption that X, $\dot{X}$, and $\dot{Z}$ are jointly correlated.

5.1.1 First and Second Order Statistics

We start with the multivariate Gaussian density function ($p_{X,\dot{X},\dot{Z}}(x, \dot{x}, \dot{z})$) of X, $\dot{X}$, and $\dot{Z}$ given as

$$p_{X,\dot{X},\dot{Z}}(x, \dot{x}, \dot{z}) = \frac{\exp\left(-\frac{1}{2}(\mathbf{x}-\mathbf{m})^T\mathbf{K}^{-1}(\mathbf{x}-\mathbf{m})\right)}{(2\pi)^{3/2}\sqrt{|\mathbf{K}|}} \tag{5.2}$$

where T indicates the transpose of a vector or matrix, $\mathbf{x} = [x\ \dot{x}\ \dot{z}]^T$, $\mathbf{m} = [\mu_{\rm s}\ 0\ 0]^T$, and $\mathbf{K}^{-1}$ denotes the inverse ($|\mathbf{K}|$ is determinant) of the covariance matrix

$$\mathbf{K} = \begin{pmatrix} \sigma_{\rm s}^2 & R_{X,\dot{X}}(\tau) & R_{X,\dot{Z}}(\tau) \\ R_{X,\dot{X}}(\tau) & \sigma_{\rm s'}^2 & R_{\dot{X},\dot{Z}}(\tau) \\ R_{X,\dot{Z}}(\tau) & R_{\dot{X},\dot{Z}}(\tau) & \sigma_{\rm z'}^2 \end{pmatrix} \tag{5.3}$$

where $\sigma_{s'}$ and $\sigma_{z'}$ are the standard deviation of $\dot{X}$ and$\dot{Z}$ respectively. $\sigma_{z'}^2 = \frac{\Omega|\ddot{r}_z(0)|}{4m}$, where $r_z(\tau)$ is the normalized autocorrelation function of the process Z^2 and $\ddot{r}_z(0)$ is the second derivative of $r_z(\tau)$ at $\tau = 0$ [16]. $R_{X,\dot{X}}(\tau)$, $R_{X,\dot{Z}}(\tau)$, and $R_{\dot{X},\dot{Z}}(\tau)$ are crosscorrelation functions of pairs out of X, $\dot{X}$, and $\dot{Z}$. As both $\dot{X}$ and $\dot{Z}$ are zero mean processes, the crosscovariance functions in covariance matrix K are replaced with the corresponding crosscorrelation functions. To calculate second order statistics like LCR and AFD, the observation time instant for all the processes should be same, implying that $\tau = 0$ should be set for all the crosscorrelation functions in K. As a matter of fact, the crosscorrelation functions can be replaced with correlation coefficients, e.g. $\rho_{X,\dot{X}} = R_{X,\dot{X}}(0)/(\sigma_s\sigma_{s'})$.

Next, to transform the variables from $X, \dot{X}$ to $Y, \dot{Y}$ ($\dot{Y}$ is the time derivative of Y), we use the relations $Y = e^X$, $x = \ln y$, $\dot{Y} = \dot{X}e^X$ and $\dot{x} = \dot{y}/y$ to get the Jacobian of transformation as $1/y^2$. As Z is assumed independent of X, $\dot{X}$, $Y, \dot{Y}$ and $\dot{Z}$, $p_{Y,\dot{Y},Z,\dot{Z}}(y, \dot{y}, z, \dot{z})$ turns out as $p_{Y,\dot{Y},Z,\dot{Z}}(y, \dot{y}, z, \dot{z})$ $= p_Z(z) \cdot p_{X,\dot{X},\dot{Z}}(\ln y, \dot{y}/y, \dot{z})/y^2$, where $p_Z(z)$ is the pdf of Z given by

$$p_Z(z) = \frac{2}{\Gamma(m)}\left(\frac{m}{\Omega}\right)^m z^{2m-1}\exp\left(-\frac{mz^2}{\Omega}\right), \quad z \geq 0 \tag{5.4}$$

with $\Omega = E[Z^2]$, $m = \Omega^2/E[(Z^2 - \Omega)^2]$. Using the relations $y = r/z$, $\dot{y} = \frac{\dot{r}}{z} - \frac{\dot{z}r}{z^2}$, $\frac{\dot{y}}{y} = \frac{\dot{r}}{r} - \frac{\dot{z}}{z}$, and the Jacobian of transformation as $1/z^2$, $p_{R,\dot{R},Z,\dot{Z}}(r, \dot{r}, z, \dot{z})$ is obtained after transformation of variables. Integrating for z and $\dot{z}$, we get the expression for the joint pdf $p_{R\dot{R}}(r, \dot{r})$ of signal envelope (R) and its time derivative ($\dot{R}$) as

$$p_{R,\dot{R}}(r, \dot{r}) = \int_0^\infty \frac{\left(\frac{mz^2}{\Omega}\right)^m}{\pi\Gamma(m)\sigma_s\sqrt{P(z)}r^2}\exp\Bigg(-\frac{\left(\ln\frac{r}{z} - \mu_s\right)^2}{2R_\rho\sigma_s^2} \cdot \left[1 - \rho_{\dot{X},\dot{Z}}^2 - \frac{\sigma_{z'}^2(1 + \rho_{\dot{X},\dot{Z}})^2(\rho_{X,\dot{X}} - \rho_{X,\dot{Z}})^2}{P(z)}\right] - \frac{mz^2}{\Omega} - \frac{z^2\dot{r}^2}{P(z)r^2}\Bigg)dz \tag{5.5}$$

where $P(z) = \sigma_{z'}^2(1 - \rho_{X,\dot{Z}}^2) + \sigma_{s'}^2 z^2(1 - \rho_{X,\dot{X}}^2) + 2\sigma_{s'}\sigma_{z'}z(\rho_{\dot{X},\dot{Z}} - \rho_{X,\dot{X}}\rho_{X,\dot{Z}})$ and $R_\rho = 1 - \rho_{X,\dot{X}}^2 - \rho_{X,\dot{Z}}^2 - \rho_{\dot{X},\dot{Z}}^2 + 2\rho_{X,\dot{X}}\rho_{X,\dot{Z}}\rho_{\dot{X},\dot{Z}}$. Integrating $p_{R\dot{R}}(r, \dot{r})$ with respect to $\dot{r}$, the expression for pdf is derived as

$$p_R(r) = \int_0^\infty \frac{\sqrt{2}z^{2m-1}}{\sqrt{\pi}\Gamma(m)\sigma_s r}\left(\frac{m}{\Omega}\right)^m \exp\Bigg(-\frac{\left(\ln\frac{r}{z} - \mu_s\right)^2}{2R_\rho\sigma_s^2}\left[1 - \rho_{\dot{X},\dot{Z}}^2 - \frac{\sigma_{z'}^2(1 + \rho_{\dot{X},\dot{Z}})^2(\rho_{X,\dot{X}} - \rho_{X,\dot{Z}})^2}{P(z)}\right] - \frac{mz^2}{\Omega}\Bigg)dz. \tag{5.6}$$

Table 5.1: Parameters for the analytical models

Channel Model	infrequent light shadowing	frequent heavy shadowing
Proposed	$m = 2, \Omega = -2.7dB, \mu_s = 2dB, \sigma_s = 0.3dB$	$m = 1.2, \Omega = -8dB, \mu_s = -5dB, \sigma_s = 3dB$
[63]		$m = 1.4, \Omega = -8dB, \mu_s = -5dB, \sigma_s = 7dB$
[10]		$\sigma_s = 2dB, \mu_s = -2dB, 2\sigma_0^2 = -10dB$
[24]	$\sigma_s = 0.4dB, \mu_s = 2dB, K = 5.35, 2\sigma_0^2 = -2dB$	$\sigma_s = 12dB, \mu_s = -5dB, K = 1, 2\sigma_0^2 = -8dB$
[22]	$\sigma_s = 1dB, \mu_s = 1dB, b_0 = -8dB, \rho = 0.9$	$\sigma_s = 7dB, \mu_s = -34dB, b_0 = -12dB, \rho = 0.6$

The final expression of LCR using $N_R(r) = \int_0^\infty \dot{r} p_{R,\dot{R}}(r, \dot{r}) d\dot{r}$ is

$$N_R(r) = \frac{\left(\frac{m}{\Omega}\right)^m}{\pi \Gamma(m) \sigma_s} \int_0^\infty \sqrt{P(z)} z^{2m-2} \times \exp\left(-\frac{mz^2}{\Omega} - \frac{\left(\ln \frac{r}{z} - \mu_s\right)^2}{2R_\rho \sigma_s^2} \left[1 - \rho_{\dot{X},\dot{Z}}^2 - \frac{\sigma_{z'}^2 (1 + \rho_{\dot{X},\dot{Z}})^2 (\rho_{X,\dot{X}} - \rho_{X,\dot{Z}})^2}{P(z)} \right] \right) dz. \quad (5.7)$$

The AFD can then be computed as $T_R(R) = \frac{\int_0^R p_R(r)}{N_R(R)}$.

5.1.2 Effect of 3D Scattering Model on the Derived Statistics

For the purpose of normalization of LCR and AFD, the autocorrelation function $r_z(\tau)$ must be related with the maximum doppler frequency $f_{\max}$. According to [16], $r_z(\tau)$ is related with the normalized autocorrelation function $r_\rho(\tau)$ of independent Gaussian processes of complex envelope of scattered multipath components as $r_z(\tau) = 1 + r_\rho^2(\tau)$. That implies $\ddot{r}_z(0) = 2\ddot{r}_\rho(0) = -2 \times (2\pi f_{\max})^2 \times \gamma$. γ is calculated using equations (3.12), (3.13), and (3.14).

Considering all the aforementioned assumption, equation (5.7) can now be normalized with respect to $f_{\max}$. The modified expression is

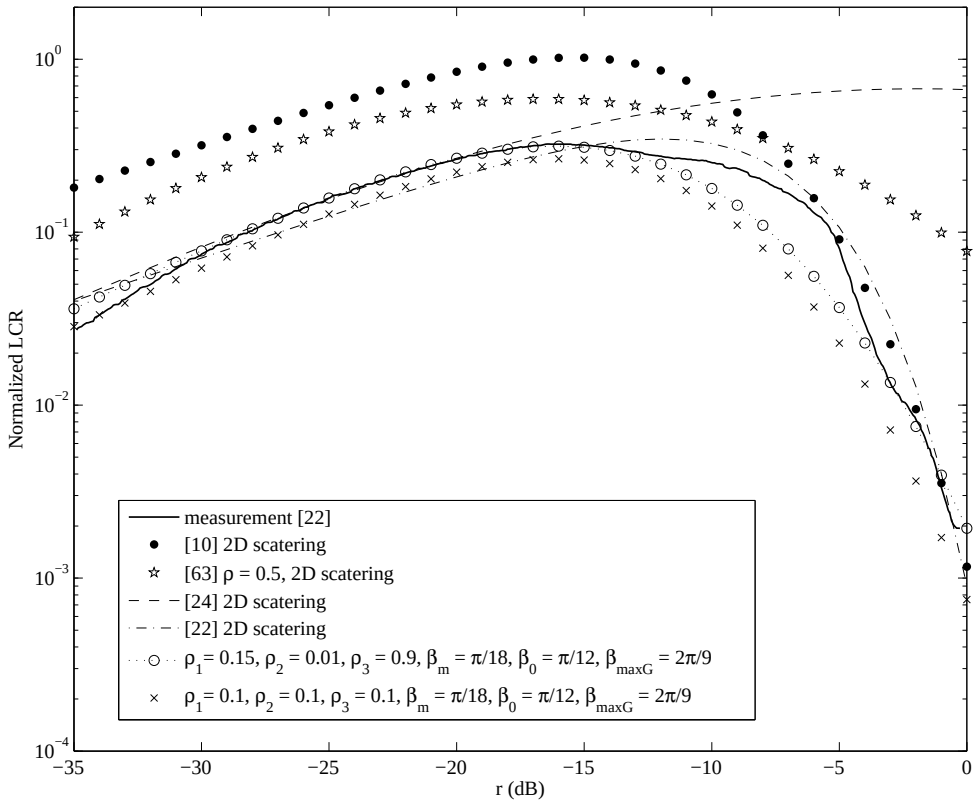

Figure 5.1: Comparison of computed LCR with measurement data and with other models in case of frequent heavy shadowing; ρ_1, ρ_2 and ρ_3 stands for $\rho_{X,\dot{X}}$, $\rho_{X,\dot{Z}}$ and $\rho_{\dot{X},\dot{Z}}$ respectively.

$$\frac{N_R(r)}{f_{\max}} = \frac{\left(\frac{m}{\Omega}\right)^m}{\Gamma(m)\sigma_s} \int_0^\infty \sqrt{P'(z)} z^{2m-2} \times \exp\left(-\frac{mz^2}{\Omega} - \frac{\left(\ln\frac{r}{z} - \mu_s\right)^2}{2R_\rho \sigma_s^2}\left[1 - \rho_{\dot{X},\dot{Z}}^2 - \frac{[k_1(1+\rho_{\dot{X},\dot{Z}})(\rho_{X,\dot{X}} - \rho_{X,\dot{Z}})]^2}{P'(z)}\right]\right) dz. \quad (5.8)$$

where $k_1 = \sqrt{\frac{2\gamma\Omega}{m}}$, $k_2 = \frac{2\sqrt{n}}{f_{\text{ratio}}}$, and $P'(z) = k_1^2(1-\rho_{X,\dot{Z}}^2) + k_2^2\sigma_s^2 z^2(1-\rho_{X,\dot{X}}^2) + 2k_1k_2\sigma_s z(\rho_{\dot{X},\dot{Z}} - \rho_{X,\dot{X}}\rho_{X,\dot{Z}})$.

5.2 Analysis of Results

LCR and AFD curves obtained from measured data in [22] are reproduced for comparison with the same quantities obtained from the model proposed in Section 5.1 and other existing models. The measurement was taken at an elevation angle of 15° in a rural site with 35% tree cover. The value of the parameters used for the analytical models for the two cases of infrequent light shadowing

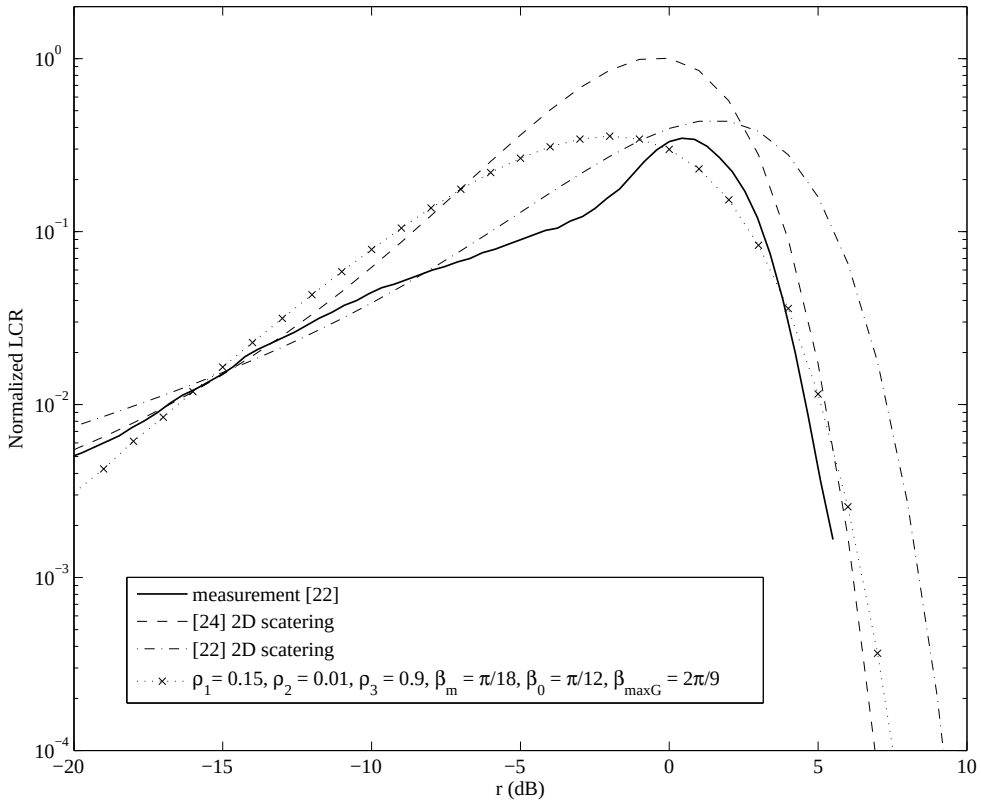

Figure 5.2: Comparison of computed LCR with measurement data and with other models in case of infrequent light shadowing; ρ_1, ρ_2 and ρ_3 stands for $\rho_{X,\dot{X}}$, $\rho_{X,\dot{Z}}$ and $\rho_{\dot{X},\dot{Z}}$ respectively.

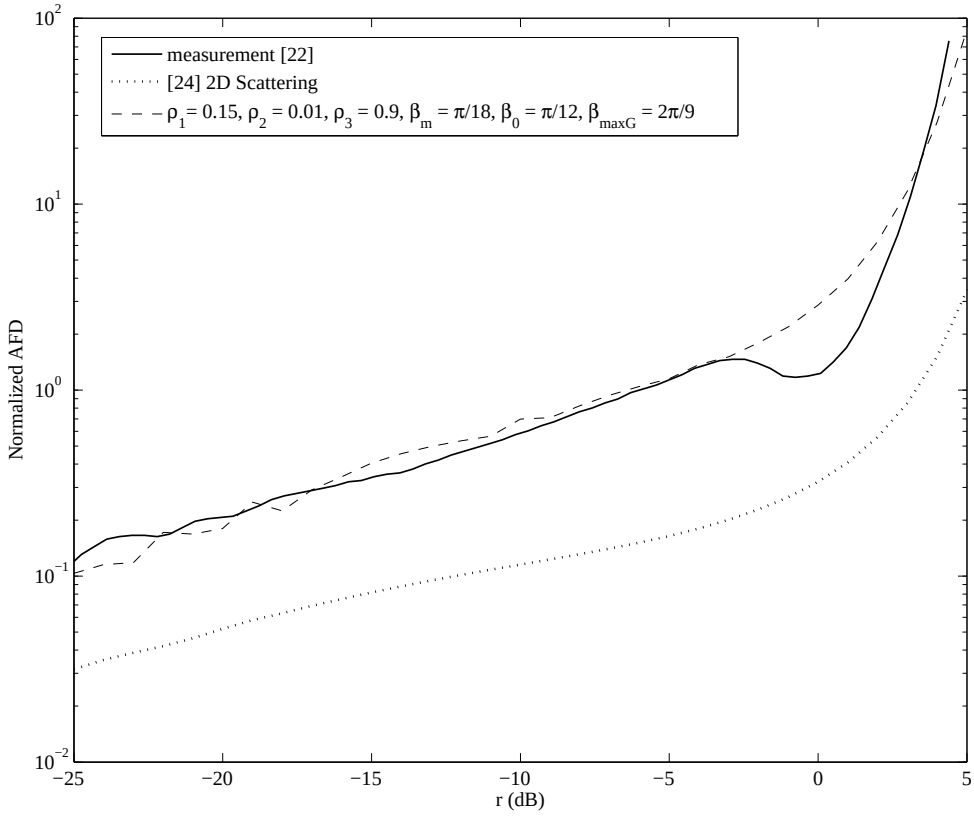

Figure 5.3: Comparison of computed AFD with measurement data and with other models in case of infrequent light shadowing; ρ_1, ρ_2 and ρ_3 stands for $\rho_{X,\dot{X}}$, $\rho_{X,\dot{Z}}$ and $\rho_{\dot{X},\dot{Z}}$ respectively.

and frequent heavy shadowing are shown in Table 5.1.

The multiplicative Rayleigh-lognormal distribution in [10] was first proposed in [64] for propagation in cellular urban scenario and later used several times in different terrestrial wireless systems. As the expressions of LCR were not given in [10, 24], we hereby deduce those for the sake of comparison. The expressions of LCR for the models in [10, 24] are deduced respectively as

$$N_R(r) = \int_0^\infty \frac{\sqrt{\sigma'^2 + z^2\sigma_{s'}^2}}{2\pi\sigma_0^2\sigma_s} \exp\left(-\frac{z^2}{2\sigma_0^2} - \frac{\left(\ln\frac{r}{z} - \mu_s\right)^2}{2\sigma_s^2}\right) dz \tag{5.9}$$

and

$$N_R(r) = \sqrt{\sigma'^2 + z^2\sigma_{s'}^2}\frac{(K+1)}{\pi\sigma_s} \int_0^\infty \exp\left(-z^2(K+1) - K\right) \times I_0\left(2z\sqrt{K(K+1)}\right) \exp\left(-\frac{\left(\ln\frac{r}{z} - \mu_s\right)^2}{2\sigma_s^2}\right) dz \tag{5.10}$$

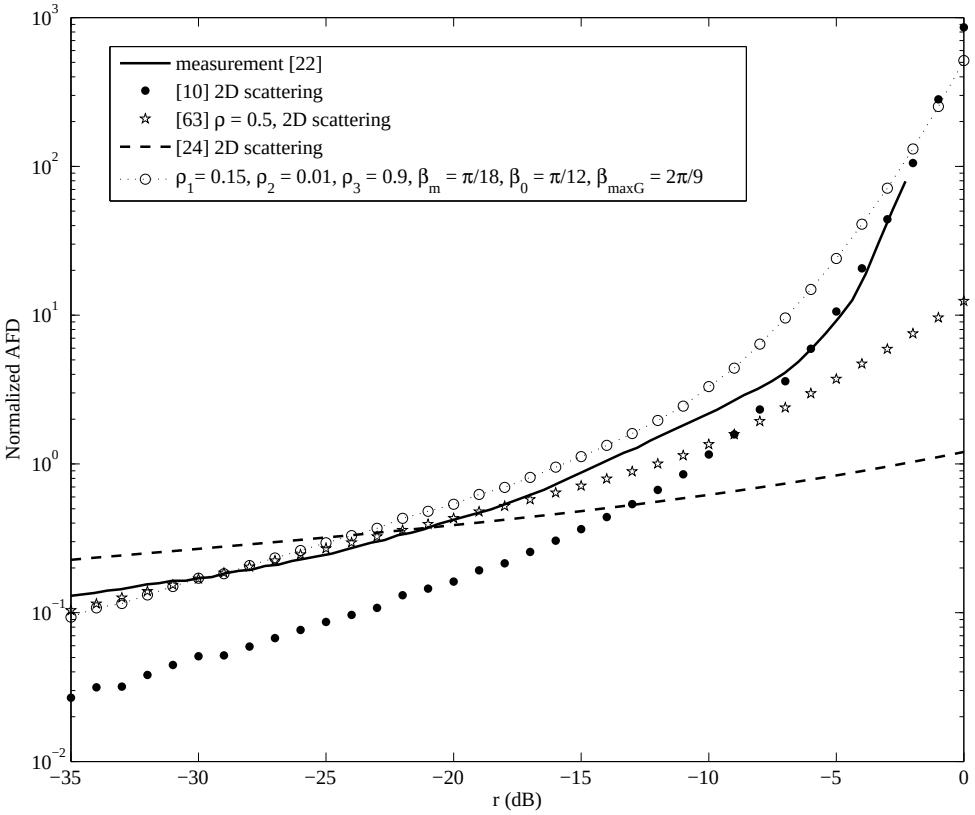

Figure 5.4: Comparison of computed AFD with measurement data and with other models in case of frequent heavy shadowing; ρ_1, ρ_2 and ρ_3 stands for $\rho_{X,\dot{X}}$, $\rho_{X,\dot{Z}}$ and $\rho_{\dot{X},\dot{Z}}$ respectively.

where σ_0^2 is the variance of in-phase and quadrature components of a complex Gaussian process associated with Rayleigh or Rician distributed signal envelope, σ'^2 denotes variance of the time derivative of the same two components, and K is the Rician K-factor.

In case of frequent heavy shadowing in Figure 5.1, LCR of our model is matching nicely with the measurement at $\rho_{X,\dot{X}} = 0.15, \rho_{X,\dot{Z}} = 0.01, \rho_{\dot{X},\dot{Z}} = 0.9, \beta_{\rm m} = \pi/18$. In accord with the measurement elevation angle, radiation pattern parameters are set at $\beta_0 = \pi/12, \beta_{\rm maxG} = 2\pi/9$. The mean square of absolute error for fitting is 0.0023 in this case. The mean square of fractional or relative error is 0.0935 although its only 0.0128 for thresholds in the range of -35 to -13 dB which is significant range of interest in heavy shadowing conditions. The employment of increased number of correlation coefficients and 3D scattering effect provides better adaptability of our model to measurement results by giving the choice of multiple curves than other existing models [10, 22, 24, 63].

The LCR curves obtained from our model shows a partial match with LCR obtained from measurement in case of infrequent light shadowing (Fig. 5.2) with mean square of absolute error and fractional error turning out to be 0.009 and 0.1012, respectively. But in case of AFD with both parameter sets, we got very good match, shown in Fig. 5.3 and 5.4. Mean square of fractional or relative errors are 0.011 and 0.0242 respectively. As results for infrequent light shadowing obtained from [10, 63] are far away from matching with measurement, those curves are not shown in Figure 5.2 and 5.3.

5.3 Summary

Analytical expressions have been derived for a generalized Nakagami-lognormal multiplicative model affected by 3D propagation environment in an LMS link. The analytically obtained curves match closely with the ones obtained from measurement data collected in a rural tree-shadowed area. This model provides more degrees of freedom due to the joint correlation between various processes. However, for Rician like situations ($m \gg 1$ e.g. when satellite elevation angle is high and the obstacles are not so high), such a multiplicative model is not recommended since Nakagami-m process alone can represent those situations almost clearly.

6

Wideband Modeling for Land Mobile Satellite Channel

Contents

In the earlier chapters, we concentrated mainly on modeling of narrowband LMS channel conditions. In this chapter we extend the modeling for wideband scenarios. In continuation of the discussion in Section 2.3.3, the multipaths in a channel impulse response have different fading statistics along with different distributions in some cases like the presence of dominant components and shadow fading. The statistics of the received signal is completely that of the first path in the first delay bin (interval between consecutive multipath arrivals). But from the second delay bin onwards, the effect of a new multipath arrival contributes to the statistics of the received signal. Given this situation, it is not worthwhile to attempt to deriving analytical expressions for CDF, LCR, AFD from the envelope pdf as it changes over time. Statistical distributions can only be proposed for individual path envelopes or tap gains, which is actually done in existing wideband models. If steady state values are taken for CDF, LCR, AFD, then it becomes same as narrowband.

6.1 Formulation of Statistical Parameters in Linearly Time-Varying Channel

The time-varying impulse response of a multipath propagation channel with N number of multipaths at some observation time t is written as

$$h(t,\tau) = \sum_{i=0}^{N-1} A_i(t) e^{j\theta_i(t)} \delta(t - \tau_i(t)). \tag{6.1}$$

where $A_i(t)$, $\theta_i(t)$ and $\tau_i(t)$ are time-varying random amplitude, phase and delay in arrival respectively.

For a unit amplitude signal (like BPSK or MSK) with envelope $u(t)$ (unit step function), from equation (6.1) the processed signal is $y(t) = \sum_{i=0}^{N-1} A_i(\tau_i(t)) e^{j\theta_i(\tau_i(t))} u(t - \tau_i(t))$. In inphase-quadrature form it can be expressed as,

$$\begin{aligned} y(t) = \quad & \underbrace{Y_0(t)}_{\text{1st multipath}} \quad + \underbrace{[X_{1I}(t-\tau_1(t)) + jX_{1Q}(t-\tau_1(t))]}_{\text{2nd multipath}} \\ & + \underbrace{[X_{2I}(t-\tau_2(t)) + jX_{2Q}(t-\tau_2(t))]}_{\text{3rd multipath}} \cdots \end{aligned} \tag{6.2}$$

The first path is assumed a real dominant component, may or may not be shadow faded, without any scattered multipath component. So, the envelope of $y(t)$ is $R_{\Delta\tau_0} = Y_0$ at delay bin 0, $R_{\Delta\tau_1} = \sqrt{(X_{1I} + Y_0)^2 + X_{1Q}^2}$ at delay bin 1, $R_{\Delta\tau_2} = \sqrt{(X_{1I} + X_{2I} + Y_0)^2 + (X_{1Q} + X_{2Q})^2}$ at delay bin 2 (henceforth we are omitting the time variable t for convenience) and so on (Fig. 6.1).

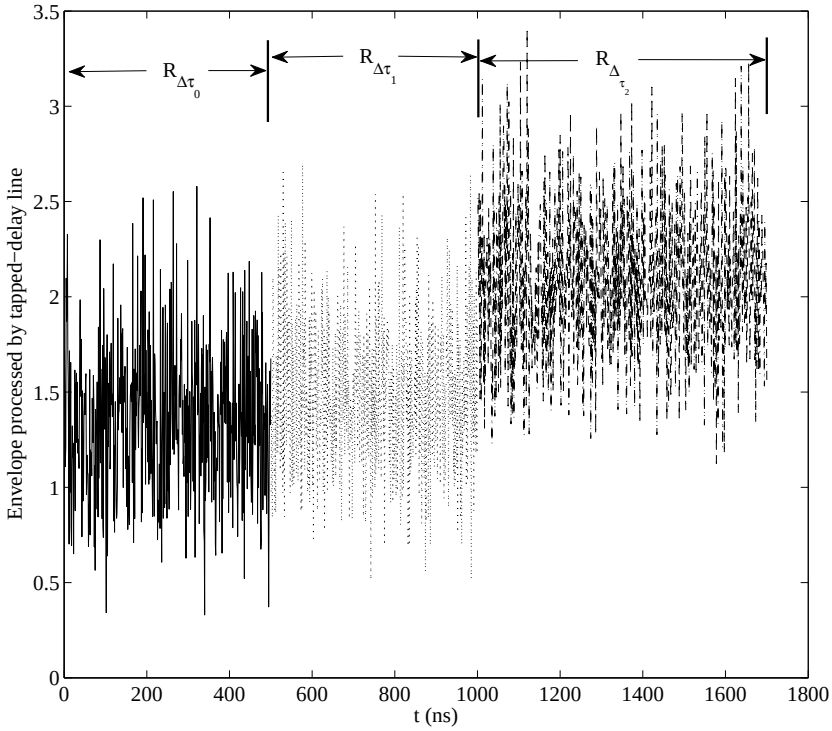

Figure 6.1: Change of statistics in each delay bin of received signal.

The CDF and mean LCR at a particular delay bin can be calculated using standard formulae: $\text{CDF}_{R_{th}}|_{\Delta\tau_i} = P[R_{\Delta\tau_i} < R_{th}]$ and $\text{LCR}_{R_{th}}|_{\Delta\tau_i} = \int_0^\infty \dot{r} p_{R_{\Delta\tau_i},\dot{R}}(R_{th}, \dot{r}) d\dot{r}$. Knowledge of these quantities at individual delay bins is not sufficient for design and control of transmission and reception techniques because frequent modification of these is not feasible and especially when the delays are random e.g. changing the parameters of an error control coding scheme by knowing the mean LCR at all the delay bins is only possible if the delays are deterministic.

As the pdf and joint pdf of whole received signal $p_R(r)$ and $p_{R,\dot{R}}(r, \dot{r})$ are changing over time in a random fashion, the overall CDF and mean level crossing rate cannot be derived using conventional formulas. Thus, a quite different approach based on sample counting has been introduced by us. If we count the number of samples with envelope below the specified threshold (R_{th}) or the number of envelope crossings with respect to that threshold for a ceratin period of time, then we can get the CDF or LCR at a particular delay bin by dividing the count by total number of samples at that bin. For three delay bins, as shown in Fig. 6.1, the overall CDF can be related with CDF at particular delay bins as, $P[y(t) < R_{th}] = (\Delta\tau_0 \times P[R_{\Delta\tau_0} < R_{th}] + \Delta\tau_1 \times P[R_{\Delta\tau_1} < R_{th}] +$

$\Delta\tau_2 \times P[R_{\Delta\tau_2} < R_{th}])/\ (\Delta\tau_0 + \Delta\tau_1 + \Delta\tau_2)$. However, this is impulse response specific and a random instantaneous value. To remove the randomness, some sort of averaging is needed which can be accomplished in two ways. One is using some available power delay profile which stands for temporal and spatial averaging of the instantaneous CIR measured at a geographical area. Another one is statistical averaging which requires *a priory* assumption about distribution of the excess delays (duration of delay bins) and the corresponding multipath power.

For a power delay profile, CDF and LCR of received signal $y(t)$ for a threshold R_{th} can be analytically expressed as,

$$P[y(t) < R_{th}] = \sum_{i=0}^{N-2} (\Delta\tau_i/\tau_{\max}) \times P[R_{\Delta\tau_i} < R_{th}] + (1 - (\Delta\tau_{N-1}/\tau_{\max})) \times P[R_{\Delta\tau_{N-1}} < R_{th}] \quad (6.3)$$

and

$$\begin{aligned} E[N_{R_{th}}(y(t))] = &\sum_{i=0}^{N-2} (\Delta\tau_i/\tau_{\max}) \times \mathrm{LCR}_{R_{th}}|_{\Delta\tau_i} \\ &+ (1-(\Delta\tau_{N-1}/\tau_{\max}))\times \mathrm{LCR}_{R_{th}}|_{\Delta\tau_{N-1}}. \end{aligned} \quad (6.4)$$

And for statistical averaging, there will be an expectation operation for the $\Delta\tau_i$s. The expression of LCR in this case can be expressed as,

$$\begin{aligned} E[N_{R_{th}}(y(t))] = &\sum_{i=0}^{N-2} E[\Delta\tau_i/\tau_{\max}] \times \mathrm{LCR}_{R_{th}}|_{\Delta\tau_i} \\ &+ (1-E[\Delta\tau_{N-1}/\tau_{\max}])\times \mathrm{LCR}_{R_{th}}|_{\Delta\tau_{N-1}} \end{aligned} \quad (6.5)$$

where $\Delta\tau_i$ is excess delay for ith delay bin, $\tau_{\max}$ is the maximum excess delay, and $P[y(t)_{\Delta\tau_i} < R_{th}]$ and $\mathrm{LCR}_{R_{th}}|_{\Delta\tau_i}$ are the analytically calculated CDF and LCR at ith delay bin. The $N-1$th term is given a different time share. It stands for a practical situation where last few multipaths are ignored for insignificant received power.

6.2 First and Second-Order Statistics in Wideband LMS Channel Model

6.2.1 Initial Considerations

We, hereby, consider four different propagation scenarios discussed in Section 3.1 for wideband LMS channel modeling.

As discussed in Section 2.3.3, the suitable distributions for the CIR in the wideband models

are achieved by splitting the distributions that has been used for narrowband modeling in the aforementioned scenarios:

1. flat areas with low clustering density: first path – lognormal, second onwards – Nakagami-q.
2. non-flat or tree-covered area: Multiplicative lognormal-Rayleigh for all paths; first path can be just lognormal if any dominant component exists.
3. High clustering density with LOS blocked: Nakagami-q for all paths.
4. Open area with few obstacles: first path – constant or no fading, second onwards – Rayleigh.

The number of paths or taps (in the consequent tapped-delay line) is kept variable and have to be changed accordingly to match the analytical results with measurement and simulation results for a particular scenario.

6.2.2 Calculation of CDF, LCR and AFD

The distribution of the excess delays $\Delta\tau_i$ is taken here as exponential distribution,

$$p(\Delta\tau_i) = \lambda \exp(-\lambda\Delta\tau_i). \tag{6.6}$$

where λ is the multipath arrival rate. The mean power of the multipaths are taken to be exponentially decreasing [29].

Thus, the mean of the excess delays from statistical averaging turns out as, $E[\Delta\tau_i/\tau_{\max}] = \frac{1}{\lambda\tau_{\max}}$. Therefore, the CDF of the received wideband signal can be calculated as

$$\begin{aligned} P[y(t) < R_{th}] = \frac{1}{\lambda\tau_{\max}} &\left(P[R|_{\Delta\tau_0} < R_{th}] + P[R|_{\Delta\tau_1} < R_{th}] + \cdots\right) \\ &+ \left(1 - \frac{1}{\lambda\tau_{\max}}\right) \times P[R|_{\Delta\tau_{N-1}} < R_{th}]. \end{aligned} \tag{6.7}$$

In similar way, the LCR can be calculated as

$$\begin{aligned} E[N_{R_{th}}(y(t))] = \frac{1}{\lambda\tau_{\max}} &\left(\mathrm{LCR}_{R_{th}}|_{\Delta\tau_0} + \mathrm{LCR}_{R_{th}}|_{\Delta\tau_1} + \cdots\right) \\ &+ \left(1 - \frac{1}{\lambda\tau_{\max}}\right) \times \mathrm{LCR}_{R_{th}}|_{\Delta\tau_{N-1}}. \end{aligned} \tag{6.8}$$

So, once we have the analytical expressions for CDF and LCR at individual delay bins i.e. $P[R_{\Delta\tau_i} <$

R_{th}] and $\text{LCR}_{R_{th}}|_{\Delta\tau_i}$, we can calculate the overall CDF and LCR from equations (6.7) and (6.8). Then we can calculate AFD which is the ratio of CDF and LCR.

6.2.2.1 Propagation scenario – flat areas with low clustering density

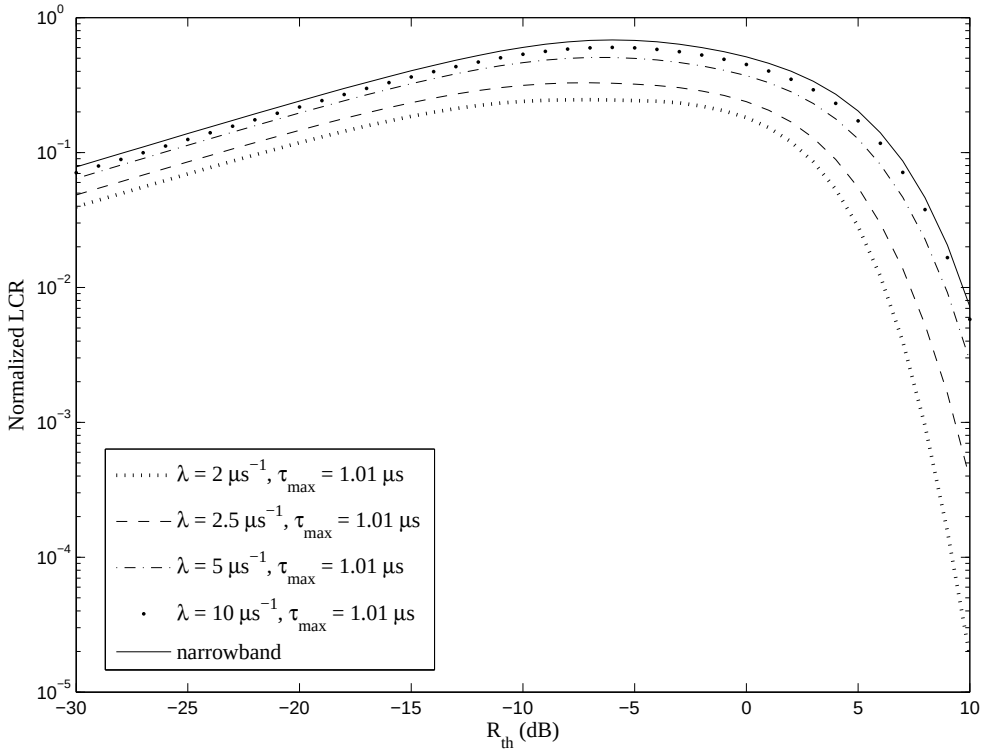

Figure 6.2: LCR calculated for different multipath arrival rate and a channel impulse response with distributions – [lognormal Nakagami-q Nakagami-q].

The statistical distribution for delay bin 0 is same as that of first dominant path – lognormal in this case. For subsequent bins, its additive lognormal-Nakagami-q as the complex envelope takes a form $X_I + jX_Q + Y_0$. The variance of Nakagami-q goes on increasing from one delay bin to the next as the variance at a particular delay bin is the addition of variance of signal at previous bin to the variance of the newly arrived multipath.

The CDF of a lognormally distributed envelope process is given by,

$$F_Y(y) = \frac{1}{2}\text{erfc}\left[-\frac{\ln y - \mu_s}{\sqrt{2}\sigma_s}\right] \tag{6.9}$$

and LCR as [65],

$$N_Y(y) = \frac{\sigma_{s'}}{2\pi\sigma_s}\exp\left[-\frac{(\ln y - \mu_s)^2}{2\sigma_s^2}\right] \tag{6.10}$$

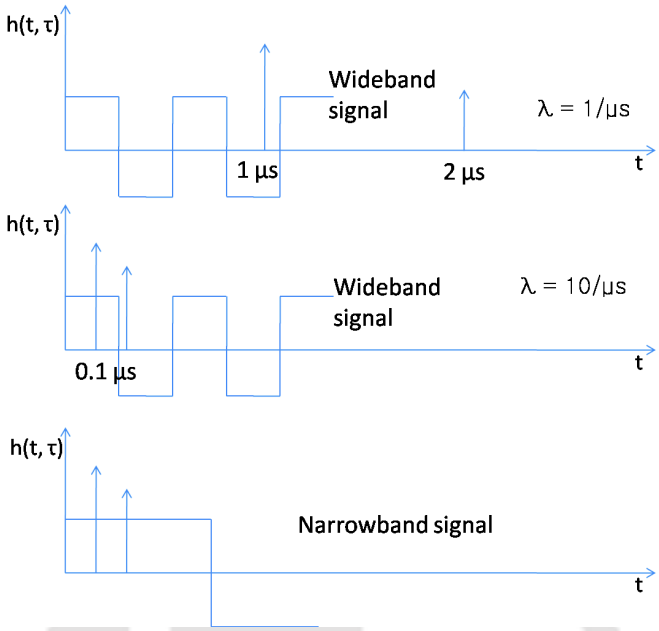

Figure 6.3: Channel impulse response for different multipath arrival rate.

The CDF of additive lognormal-Nakagami-q process can be derived by integrating its pdf from 0 to R_{th}. The expression of the pdf at a particular delay bin (other than 0th bin) is (equation 4.6)

$$p_R(r) = \frac{r}{\sqrt{2\pi}\sigma_{1_i}\sigma_{2_i}\sigma_s} \exp\left(-\frac{r^2}{4}\left(\frac{1}{\sigma_{1_i}^2}+\frac{1}{\sigma_{2_i}^2}\right)\right) \int_0^\infty \frac{1}{y} \exp\left[-\frac{(\ln y-\mu_s)^2}{2\sigma_s^2} - \frac{y^2}{2\sigma_{1_i}^2}\right] \times \sum_{k=0}^{\infty}(-1)^k \epsilon_k I_k\left(\frac{r^2}{4}\left(\frac{1}{\sigma_{1_i}^2}-\frac{1}{\sigma_{2_i}^2}\right)\right) I_{2k}\left(\frac{ry}{\sigma_{1_i}^2}\right) dy \tag{6.11}$$

where $\sigma_{1_i}^2$ and $\sigma_{2_i}^2$ in a particular delay bin is the cumulative sum of all σ^2 up to that particular bin i.e. here, $\sigma_{1_2}^2 = \sigma_1^2|_{\Delta\tau_0} + \sigma_1^2|_{\Delta\tau_1} + \sigma_1^2|_{\Delta\tau_2}$.

The expression of LCR at a particular delay bin (other than 0th bin) is (equation 4.15)

$$\mathrm{LCR}_{R_{th}}|_{\Delta\tau_i} = \frac{R_{th}}{(2\pi)^2\sigma_{1_i}\sigma_{2_i}\sigma_s} \int_0^\infty \frac{1}{y} \exp\left[-\frac{(\ln y-\mu_s)^2}{2\sigma_s^2}\right] \int_0^{2\pi} \sqrt{\beta_2 + (\beta_1-\beta_2+\sigma_s^2 y^2)\cos^2\theta} \times \exp\left(-\frac{(R_{th}\cos\theta - y)^2}{2\sigma_{1_i}^2} - \frac{R_{th}^2\sin^2\theta}{2\sigma_{2_i}^2}\right) d\theta dy. \tag{6.12}$$

The normalization with respect to maximum Doppler frequency is done here like Section 4.1.2.2.

Using equations (6.7), (6.8), (6.9), (6.10), (6.11), and (6.12), we calculate CDF, LCR and AFD for the received wideband signal in this propagation scenario.

LCR calculated for different multipath arrival rate λ are plotted in Fig. 6.2. As multipath

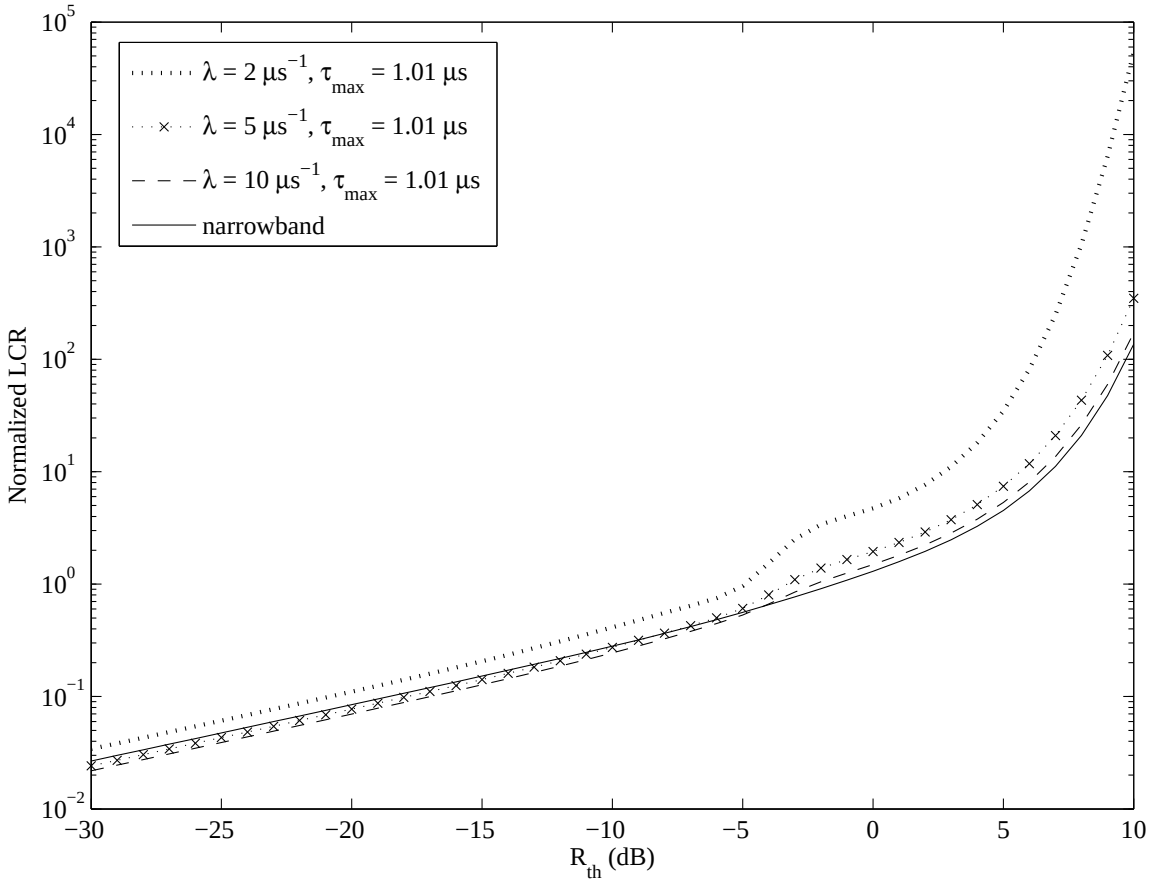

Figure 6.4: AFD calculated for different multipath arrival rate and a channel impulse response with distributions – [lognormal Nakagami-q Nakagami-q].

arrival rate is increased, the LCR curves move up to the upper limit of narrowband. The reason is explained in Fig. 6.3. For increased λ, with same number of significant multipaths, more replicas of the transmitted signal arrive within a shorter period of time thus creating more interference and consequent fluctuation of received signal. In the limiting case, all significant multipaths arrive within a symbol period and yields LCR values close to that of narrowband. In case of AFD too, shown in Fig. 6.4, the curves are close to that of narrowband for an increased λ.

For calculation based on a power-delay-profile, we used the SUI-2 channel model given in [66]. We compared the result calculated using this model and equation (6.4) with the LCR obtained from equations (6.8), (6.10), and (6.12) in Fig. 6.5. The good match between the two curves prove that an exponential delay model can represent a propagation scenario well for wideband transmission.

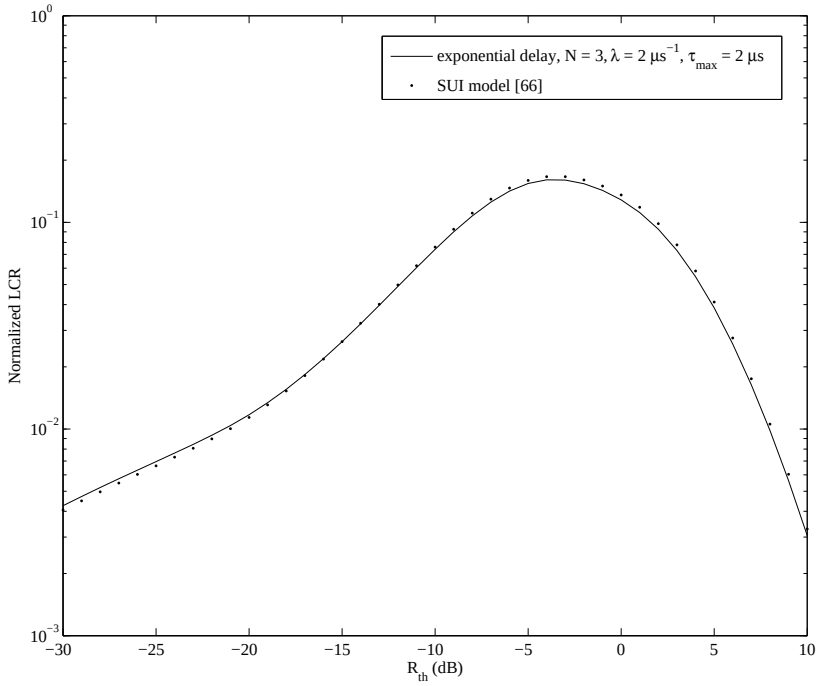

Figure 6.5: Comparison of LCR calculated from exponential delay model (equations (6.8), (6.10), and (6.12)) and SUI tap-delay line model.

6.2.2.2 Propagation scenario – non-flat or tree-covered area

Here, we are considering multiplicative lognormal-Rayleigh envelope pdf for all taps. The expression of LCR, as given in section 5.2 and replicated here, for a particular delay bin,

$$\mathrm{LCR}_{R_{th}}|_{\Delta\tau_i} = \int_0^\infty \frac{\sqrt{\sigma_i'^2 + z^2\sigma_{s'}^2}}{2\pi\sigma^2\sigma_s} \exp\left(-\frac{z^2}{2\sigma_i^2} - \frac{\left(\ln\frac{R_{th}}{z} - \mu_s\right)^2}{2\sigma_s^2}\right) dz \tag{6.13}$$

where σ_i^2 in a particular delay bin is the cumulative sum of all σ^2 up to that particular bin i.e. here, $\sigma_2^2 = \sigma^2|_{\Delta\tau_0} + \sigma^2|_{\Delta\tau_1} + \sigma^2|_{\Delta\tau_2}$. Same is true for $\sigma_i'^2$ which denotes variance of the time derivative of in-phase and quadrature components of a complex Gaussian process in ith bin.

LCR calculated for different multipath arrival rate λ are plotted in Fig. 6.6. Unlike Fig. 6.2, LCR curves does not move up as multipath arrival rate is increased. This is because all the paths are not devoid of small-scale fading and the first path have comparatively high LCR unlike the case of Fig. 6.2. The initial LCR is thus not too different from overall LCR. Due to the dominance of shadow fading for threshold values greater than area mean signal level, LCR of narrowband signal

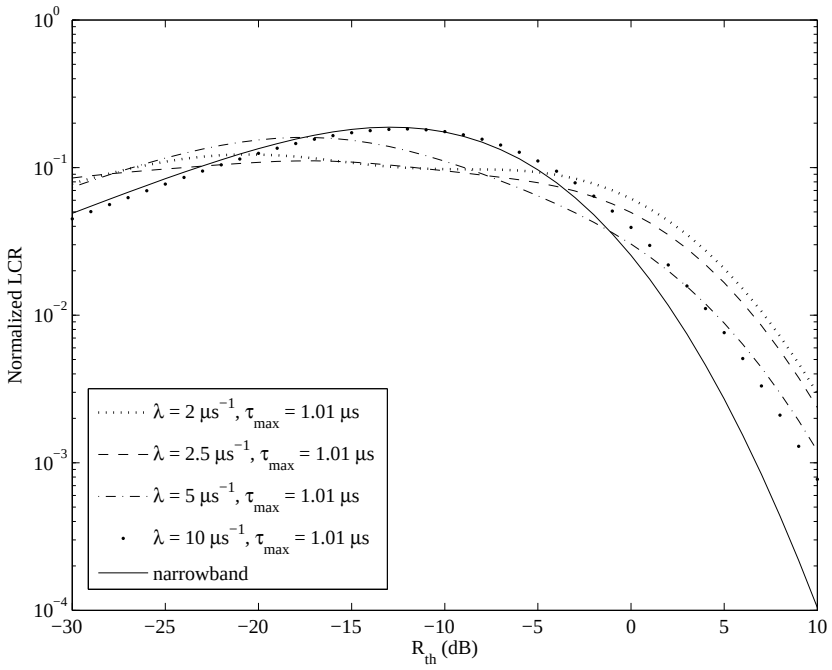

Figure 6.6: LCR calculated for different multipath arrival rate and a channel impulse response with lognormal-Rayleigh distribution for all paths.

is significantly less at $R_{th} > 0$ dB.

6.2.2.3 Propagation scenario – High clustering density with LOS blocked

Here, we are considering Nakagami-q distribution for all taps. The expression of LCR, given in [59] and replicated here, for a particular delay bin,

$$\mathrm{LCR}_{R_{th}}|_{\Delta\tau_i} = \frac{R_{th}}{(2\pi)^{3/2}\sigma_{1_i}\sigma_{2_i}} \int_0^{2\pi} \sqrt{\beta_2 + (\beta_1 - \beta_2)\cos^2\theta}\, \exp\left(-\frac{R_{th}^2\cos^2\theta}{2\sigma_{1_i}^2} - \frac{R_{th}^2\sin^2\theta}{2\sigma_{2_i}^2}\right) d\theta. \quad (6.14)$$

LCR calculated for different multipath arrival rate are plotted in Fig. 6.7. At initial values of threshold, the curves show exactly opposite nature of Fig. 6.2 for dependence on λ. This is due to large variance of first multipath and consequent high initial LCR. If the variance of initial path is kept smaller than others, then there will not be any crossover and the curves will be similar to Fig. 6.2.

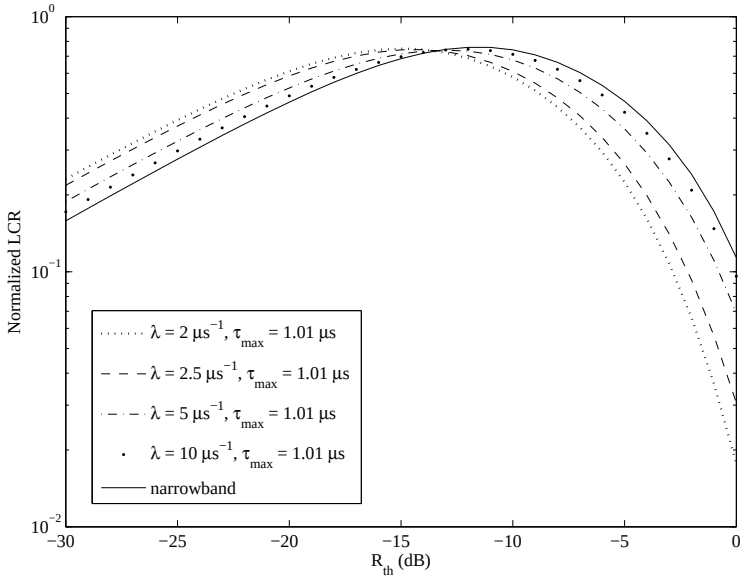

Figure 6.7: LCR calculated for different multipath arrival rate and a channel impulse response with Nakagami-q distribution for all paths.

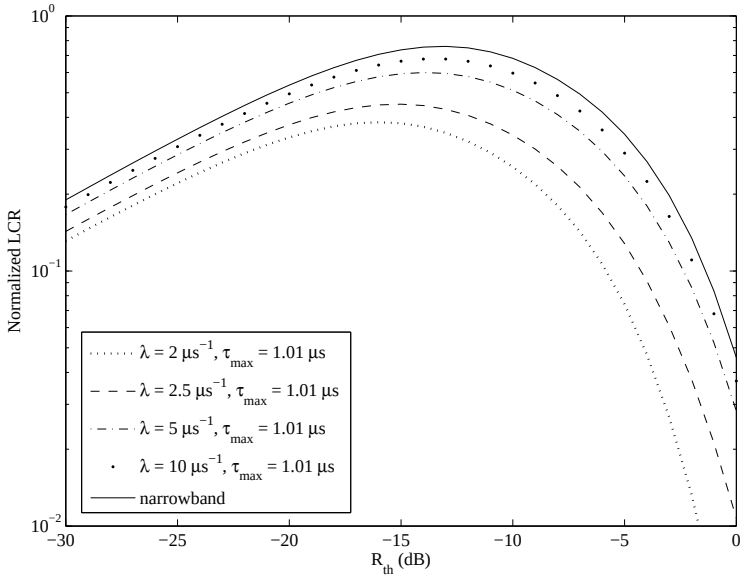

Figure 6.8: LCR calculated for different multipath arrival rate and a channel impulse response with distributions – [constant Rayleigh Rayleigh].

6.2.2.4 Propagation scenario – Open area

Based on the assumption made, the received signal in first delay bin is without any randomness and fluctuation meaning LCR is zero in first delay bin. Envelope of subsequent paths are considered Rayleigh distributed. According to equation (6.2), envelope of subsequent delay bins are Rician

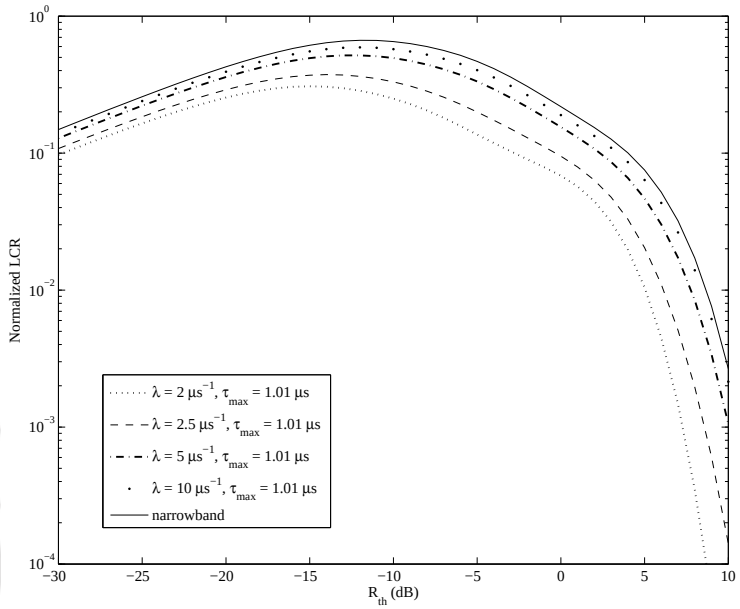

Figure 6.9: LCR calculated for a 4-state model using narrowband and wideband models of Section 4.1, 6.2.2.1, and 6.2.2.4.

distributed. The expression of LCR, in this condition, for a particular delay bin (other than 0th) is given by [51]

$$\mathrm{LCR}_{R_{th}}|_{\Delta\tau_i} = \frac{\sigma' R_{th}}{\sqrt{2\pi\sigma_i^2}} \exp\left(-\frac{R_{th}^2 + A_c^2}{2\sigma_i^2}\right) I_0\left(\frac{R_{th} A_c}{\sigma_i^2}\right). \tag{6.15}$$

LCR calculated for different multipath arrival rate are plotted in Fig. 6.8. As initial LCR is zero, the nature of the curves are similar to Fig. 6.2.

6.3 Calculation of Statistics in a State-based Model

In calculation of envelope pdf in a state-based model, the overall pdf is generally expressed as the linear combination of pdfs in individual channel states with state probabilities as weightages [9, 21, 27, 28, 67]. A simple integration will show that the overall CDF can be expressed in the same way. For calculation of LCR, the approach demonstrated in Section 6.2 can be extended to state-based models whether narrowband or wideband. The overall LCR for an M-state channel model, thus can be expressed as,

$$\mathrm{LCR}_{R_{th}} = \sum_{i=1}^{M} P_i \times \mathrm{LCR}_{R_{th}}|_i \tag{6.16}$$

where P_i and $\text{LCR}_{R_{th}}|_i$ are the state probability and LCR at ith channel state. As each one of the four propagation scenarios considered earlier can be considered as individual channel states, the overall statistics (CDF, LCR or AFD) can be calculated using equation like above for a mobile receiver traveling through different type of areas (urban, suburban, rural, forested). Hereby, we calculate overall LCR for a 4-state model [67] based on a measurement campaign reported in [56] and plot it in Fig. 6.9. We use the parameters of shadowing and multipath fading reported in [67]. The state probability matrix is $P = [0.169, 0.461, 0.312, 0.058]$. The first two states are reported to be in open areas and Rician-like with 14 dB and 18 dB value for Rice K-factor, while other two are shadowed states represented by additive Rayleigh-lognormal distribution in [67]. Therefore, we, use channel models already proposed in this thesis for open areas and flat urban/suburban areas with low clustering density.

6.4 Summary

First and second order statistics of a wideband LMS channel has been formulated. The statistics has been formulated and calculated for the four different propagation scenarios considered in this thesis along with various aspects on the results. The relation between the results of narrowband and wideband statistics have been explained clearly. Finally, results have been shown for LCR, formulated and calculated for a state-based model with both narrowband and wideband condition, which concludes our work on various aspects of LMS channel modeling.

7

Capacity Issues for Land Mobile Satellite Channel

Contents

In this chapter, we put our effort into calculating the capacity of the channels proposed in earlier chapters, both in ergodic and non-ergodic condition. Depending on the signal bandwidth and channel parameters, the channel can be ergodic or non-ergodic. If the transmission time T is very large compared to the coherence time (T_{coh}), the fading effects on received signal can be considered ergodic because the signal is expected to encounter all possible channel realizations. In this case, the channel capacity is calculated by taking statistical average over all possible fading situations. In cellular communications, T cannot be very large, particularly for delay-sensitive applications like speech or video transmission. However, in LMS communications, T has relatively large value due to very large distance between satellite and earth. Even if T does not exceed T_{coh}, the transmission bandwidth (W) can be large enough (Ku-, K-, Ka-bands) so that $WT \gg 1$; thus the ergodic assumption will still be valid [68] in wideband LMS channel. For lower bands (L, S), the LMS channel might be non-ergodic when $T < T_{\text{coh}}$ and the capacity-versus-outage performance have to be determined instead of ergodic capacity.

7.1 Ergodic Capacity with Frequency-Selective Fading

Calculation of ergodic capacity for frequency-selective fading channel usually involves the random channel matrix with the fading coefficients of the channel impulse response as its elements. The discrete-time frequency-selective channel model is

$$y_i = \sqrt{\gamma} \sum_{l=0}^{L} h_l x_{i-l} + z_i, \qquad i = 1, \ldots, n \tag{7.1}$$

or, in matrix form

$$\mathbf{y} = \sqrt{\gamma}\mathbf{H}\mathbf{x} + \mathbf{n} \tag{7.2}$$

Ergodic capacity of this model:

$$C_{\text{erg}}(\gamma) = \lim_{n\to\infty} \sup_{\Sigma_x \geq 0 : \text{tr}(\Sigma_x) \leq n} \frac{1}{n} E\left[\log\det\left(\mathbf{I} + \gamma \mathbf{H}\Sigma_x \mathbf{H}^T\right)\right] \tag{7.3}$$

To the best of our knowledge, there is no closed-form expression for this equation available in literature. Simplification has been attempted by researchers mostly by avoiding direct involvement of the channel matrix. In [69], the channel capacity is expressed as an integral with respect to the eigenvalues of a matrix dependent upon the channel matrix. A more straightforward and statistical formulation is given in [70] where the channel matrix $\mathbf{H}$ is transformed into a diagonal matrix $\mathbf{G}$ as

$\mathbf{H} = \mathbf{F}\mathbf{G}\mathbf{F}^T$. Here, $\mathbf{H}$ is a circulant matrix formed by the fading coefficients h_l, $l = 0, 1, \ldots, L$. The product $\mathbf{FG}$ stands for Fourier transform of the diagonal coefficients (G_i) in $\mathbf{G}$ and $\mathbf{Fx}$ denotes the Fourier transform of the transmitted symbols. So, the elements of $\mathbf{G}$ are transformed version of the exact channel coefficients. In [70], G_is are considered as original fading coefficients represented by i.i.d. Rayleigh variables. Rayleigh distribution should have been assigned for the elements of $\mathbf{H}$ and then the distribution of G_is have to be determined through matrix transformation. $\mathbf{G}$ is obtained from $\mathbf{H}$ by,

$$\mathbf{G} = \mathbf{F}^{-1}\mathbf{H}(\mathbf{F}^T)^{-1}. \tag{7.4}$$

As $\mathbf{F}$ is unitary matrix, $\mathbf{F}^{-1} = (\mathbf{F}^*)^T$. So, $\mathbf{G} = (\mathbf{F}^*)^T\mathbf{H}\mathbf{F}^*$.

With the assumption of unavailability of LOS or any other dominant path and shadow fading, if the fading envelope of the multipaths or the elements of $\mathbf{H}$ are represented with complex Gaussian distribution with equal variance (i.e. the absolute values are Rayleigh), then G_i is a sequence of complex Gaussian variables too. This can be shown easily by matrix multiplication as elements of $\mathbf{F}$ are complex with unit magnitude. But it would be different for other scenario with the presence of dominant LOS component and/or shadow fading. In these cases, the complex G_is have a dominant part both in in-phase and quadrature component along with a Gaussian part. The dominant part is deterministic if the original one is unfaded LOS and then both the in-phase and quadrature components turn out to be Gaussian with non-zero mean. So, $|\mathrm{G}_i|^2$ is a sequence of non-central chi-square random variable with two degrees of freedom and the pdf is

$$p(r) = \frac{1}{2\sigma^2} e^{-(s^2+r)/2\pi\sigma^2} I_0\left(\sqrt{r}\frac{s}{\sigma^2}\right), \quad r \geq 0 \tag{7.5}$$

where σ is the standard deviation of the complex Gaussian variable and s is the non-centrality parameter related to the non-zero means m_1 and m_2 as $s^2 = m_1^2 + m_2^2$.

In case of LOS path under lognormal shadow fading, the dominant part in G_i is lognormal. If the non-dominant paths are considered Rayleigh faded (i.e. complex Gaussian with equal variance), then the pdf of $|\mathrm{G}|^2$ is

$$p(r) = \frac{1}{2\sqrt{2\pi}\sigma^2\sigma_\mathrm{s}} \int_0^\infty e^{-(s^2y^2+r)/2\pi\sigma^2} I_0\left(\sqrt{r}\frac{sy}{\sigma^2}\right) \frac{1}{y} \exp\left[-\frac{(\ln y - \mu_\mathrm{s})^2}{2\sigma_\mathrm{s}^2}\right] dy, \quad r \geq 0 \tag{7.6}$$

and if the fading envelope of the non-dominant paths are considered Nakagami-q (Hoyt) distributed

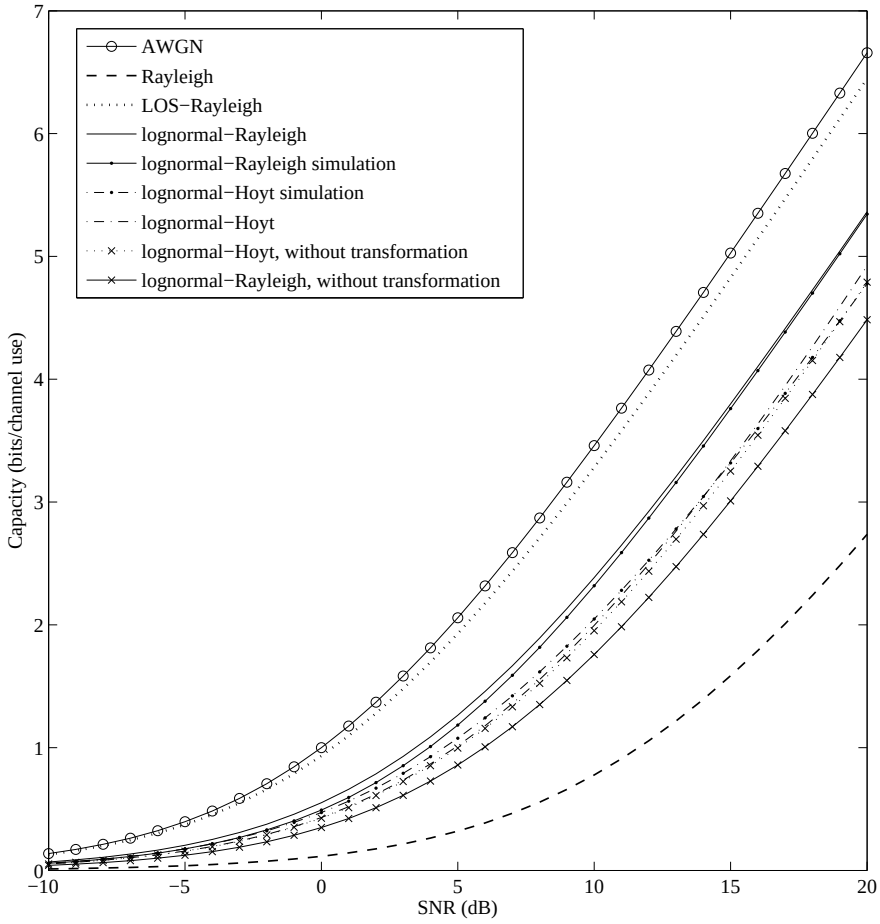

Figure 7.1: Capacity for different channel impulse response for same multipath power = 0.0862 (-10.645 dB) with respect to LOS. Also shown is Monte Carlo simulation of the finite-dimensional mutual information formula $\frac{1}{n}E\left[\log\det\left(\mathbf{I}+\gamma\mathbf{F}\mathbf{G}\mathbf{G}^T\mathbf{F}^T\right)\right]$ for $n=64$.

(i.e. complex Gaussian with unequal variance), then the pdf of $|\mathrm{G}|^2$ is

$$p(r)=\frac{1}{2\sqrt{2\pi}\sigma_1\sigma_2\sigma_\mathrm{s}}\int_0^\infty\frac{1}{y}\int_0^{2\pi}\exp\left(-\left[\frac{(\sqrt{r}\cos\theta-m_1y)^2}{2\sigma_1^2}+\frac{(\sqrt{r}\sin\theta-m_2y)^2}{2\sigma_2^2}\right]-\frac{(\ln y-\mu_\mathrm{s})^2}{2\sigma_\mathrm{s}^2}\right)d\theta dy,\ r\geq 0 \tag{7.7}$$

where σ_1 and σ_2 are the standard deviation of the inphase and quadrature components of Nakagami-q process.

Thus, the expression for channel capacity is given by (with the assumption that the channel

state information or knowledge of **G** is only available at the receiver)

$$C_{\text{erg}}(\gamma) = E[\log(1+\gamma|\text{G}|^2)] = \int_0^\infty \log(1+\gamma r)p(r)dr \tag{7.8}$$

where γ is the signal-to-noise ratio (SNR) defined as the ratio of signal power to noise power.

$C_{\text{erg}}(\gamma)$ is calculated for different CIRs mentioned in Section 6.2.1 and compared in Fig. 7.1 for same multipath power ($2\sigma^2$ or $\sigma_1^2 + \sigma_2^2$). The ratio of s^2 and total multipath power $2\sigma^2$ or the ratio of m_1^2 and σ_1^2, and m_2^2 and σ_2^2 are set to a value (here, 10) and this ratio is equivalent to the Rician K-factor. Here, we name the distributions of the channel impulse response h_l as Rayleigh, LOS-Rayleigh (first path - unfaded LOS), lognormal-Rayleigh (first path lognormal) and lognormal-Hoyt. For different values of SNR, the curves go up in the order – Rayleigh, lognormal-Hoyt, lognormal-Rayleigh, LOS-Rayleigh, as the fading severity becomes less or channel conditions get better.

7.2 Capacity versus outage

If transmission bandwidth is not very high and delay constraints are imposed, the ergodicity assumption is not satisfied in LMS channels with fading effects. The idea of classical Shannon capacity cannot be applied in this situation as the channel variation is negligible during the transmission interval. The probability of transmission rate being greater than the instantaneous mutual information may not be negligible in this case. The capacities for all possible channel realizations cannot be averaged out as is done when calculating ergodic capacity and the channel capacity is considered a random quantity [33]. The evaluation of the capacity-versus-outage performance is done by determining the probability that reliable communication is not possible at a given rate or in other words, an outage probability is associated to any given rate. In mathematical form, the outage probability for a given rate R is given by

$$P_{\text{out}}(R) = P[C_{\text{out}} < R] \tag{7.9}$$

where C_{out} is the random channel capacity dependent upon the fading gain as

$$C_{\text{out}} = \log(1+\rho \times \text{SNR}) \tag{7.10}$$

where ρ is the square of the absolute of the complex fading gain.

One very important metric related to outage is the outage ϵ-capacity which is defined as the maximum transmission rate that can be supported by the channel for a given outage probability ϵ i.e.

$$C_\epsilon = \max\{R : P_{\text{out}}(R) \leq \epsilon\} \tag{7.11}$$

We have calculated C_ϵ for $\epsilon = 0.1$ and $\epsilon = 0.01$ for different distributions used in narrowband models and the curves are shown in Fig. 7.2 for different values of SNR.

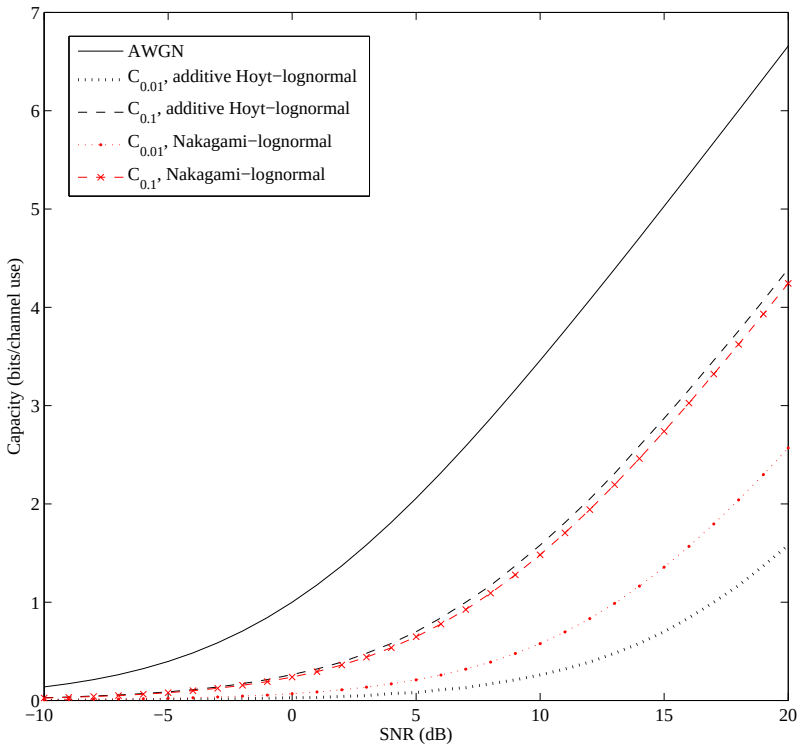

Figure 7.2: Outage Capacity for $\epsilon = 0.1$ and $\epsilon = 0.01$.

7.3 An example of calculating capacity in state-based channel model

Let's consider a three-state model with the states representing open, shadowed and blocked areas. Suppose from a measurement campaign, we get the state duration probabilities of these states, respectively, as: $p_{\text{open}} = 0.6$, $p_{\text{shadowed}} = 0.1$, and $p_{\text{blocked}} = 0.3$. As the channel conditions in these states are independent to each other, the overall capacity is the weighted average of capacity

of individual channel states, in light of the theory in [33]. In [33], this theory was developed for independent block transmissions.

So, the overall capacity of the three-state model considered here is $C = p_{\text{open}} C_{\text{LOS-Rayleigh}} + p_{\text{shadowed}} C_{\text{lognormal-Hoyt}} + p_{\text{blocked}} C_{\text{Rayleigh}}$.

From Fig. 7.1, at 10 dB SNR, $C_{\text{LOS-Rayleigh}} = 3.282$, $C_{\text{lognormal-Hoyt}} = 2$, and $C_{\text{Rayleigh}} = 0.7769$. So, the overall capacity at 10 dB SNR is $C = 1.92$ bits/channel use.

7.4 Summary

The channel capacity for the narrowband and wideband channels considered in earlier chapters has been computed and compared along with simulation results which match well with the analytical ones. Examples has also been given to compute the overall channel capacity for the Markov/semi-Markov chain used in combining the channels respective to specific propagation scenario, so that cut-offs for transmission rate in different satellite bands can be recommended.

8

Summary and Future Work

Contents

In this thesis, we propose several narrowband and wideband channel models based on some newly identified complex envelope process and a modified 3D scattering model for LMS communications. We also combine these models into state-based model to calculate the overall statistics for signal received by an LMS receiver traveling through a wide variety of propagation scenarios. In this chapter, we summarize the contributions made in this thesis work and also provide some future directions extending this research.

8.1 Summary of Contributions

In this section, we briefly summarize and discuss our contributions and findings during this thesis work.

A. Identification of proper envelope process for different propagation scenarios

We choose different propagation scenarios and analyzed the underlying propagation mechanism involved. More specifically, we investigated that, in which sequence, the different propagation phenomena (diffraction, scattering, reflection, random attenuation etc.) affected the signal waves. After finding out the proper sequence of phenomena specific to a propagation scenario, we were able to give the justification for the use of additive or multiplicative interaction of the small-scale fading and shadow fading process. Then we proposed mathematical expressions for the complex envelope which should be able to give an insight into the effect of the actual propagation phenomena in a particular propagation scenario.

B. Investigation and inclusion of antenna effects in a 3D scattering model

We formulated the effect of circular polarization on the received electric field and found out that it has no extra effect on received signal attributes in a LMS system. Finally, we included the effect of directivity of LMS antenna systems, in general, in the 3D scattering models available in literature and formulated the autocovariance function. This can be useful for calculation of second order moments and statistics for channel modeling in any wireless communication system including LMSC.

C. Narrowband models based on additive and multiplicative envelope process

We proposed two narrowband models using both additive and multiplicative complex envelope process with a Doppler PSD generated from the 3D scattering model introduced in previous

chapter. The expressions for the first and second order statistics are derived for these models. By comparing with measurement results of LCR and AFD available in literature, it has been shown that the additive model can be used to depict a wide variety of fading situations for flat urban and suburban areas while the model based on multiplicative process is applicable to areas shadowed by irregular terrain and trees.

D. New mathematical framework for calculation of statistics in wideband models

In this part of work, a new technique to derive statistics in a wideband wireless communication channel is proposed. The analytical formulation of CDF, LCR, and AFD is based upon the channel impulse response. As the statistics of the received multipath signal changes from one delay bin to another, statistical quantities like CDF and LCR are calculated separately at each delay bin and then they are combined by proper weights to obtain the overall LCR and AFD of the signal. It has been also shown, that LCR for a state-based model can be calculated using similar approach.

E. Computation of channel capacity

We computed capacity of the LMS narrowband and wideband channels considered in earlier chapters. We also gave example to compute the overall channel capacity for a state-based model.

8.2 Suggestions for Future Work

Some possible directions in which the present work can be extended are outlined below:

i) A simulation set-up can be designed following the analytical framework in the wideband model to calculate CDF and LCR.

ii) It has been shown that, by changing the elevation angle of the antenna system, LCR of received signal can be controlled. This can have an impact on crosscorrelation between two antenna elements and thus in the diversity techniques used. Investigation on diversity improvement, controlled by antenna elevation plane pattern, can be carried out in future.

iii) Improvement of channel capacity for aforementioned effect of antenna directivity on diversity schemes can be investigated.

Bibliography

[1] J. D. Parsons and A. M. D. Turkmani, "Characterisation of mobile radio signals: model description," *Communications, Speech and Vision, IEE Proceedings I*, vol. 138, no. 6, pp. 549–556, Dec. 1991.

[2] F. Nagase, J. Mitsugi, M. Nakayama, and M. Ueba, "Ku band mobile multimedia satellite communications system for trains," in *Proc. 21st AIAA ICSSC*, Yokohama, Japan, Apr. 2003.

[3] Y. Song, P. Kim, D. Oh, S. Jeon, and H. Lee, "Development of mobile broadband interactive satellite access system for Ku/Ka band," *International Journal of Satellite Communications and Networking*, vol. 24, no. 2, pp. 101–117, 2006.

[4] P. Kim, D.-I. Chang, and H.-J. Lee, "The development of broadband satellite interactive access system based on DVB-S2 and mobile DVB-RCS standard," *Space Commun.*, vol. 21, no. 1-2, pp. 19–30, Jan. 2007.

[5] M. Rieche, D. Arndt, A. Ihlow, and G. Del Galdo, "State modeling of the land mobile satellite channel by an image-based approach," in *7th European Conference on Antennas and Propagation (EuCAP)*, 2013, pp. 672–676.

[6] A. Jarndal, M. Salameh, A. Alsaqaf, and Y. Hulba, "Wideband modeling of land-mobile-satellite channel in built-up environment," *Journal of Electromagnetic Analysis and Applications*, vol. 4, no. 3, pp. 101–107, 2012.

[7] M. Z. H. Bhuiyan, J. Zhang, E.-S. Lohan, W. Wang, and S. Sand, "Analysis of multipath mitigation techniques with land mobile satellite channel model," *Radioengineering*, vol. 21, no. 4, pp. 1067–1077, Dec. 2012.

[8] X. Li, R. Vauzelle, Y. Pousset, and P. Combeau, "Hybrid propagation channel modelling for city area land mobile satellite communications," *EURASIP Journal on Wireless Communications and Networking*, vol. 2012, no. 1, p. 139, 2012.

[9] M. Milojević, M. Haardt, E. Eberlein, and A. Heuberger, "Channel modeling for multiple satellite broadcasting systems," *IEEE Trans. Broadcast.*, vol. 55, no. 4, pp. 705–718, Dec. 2009.

[10] S. Scalise, H. Ernst, and G. Harles, "Measurement and modeling of the land mobile satellite channel at Ku-band," *IEEE Trans. Veh. Technol.*, vol. 57, no. 2, pp. 693–703, Mar. 2008.

[11] R. Steele and L. Hanzo, Eds., *Mobile Radio Communications*, 2nd ed. Chicheste, England: John Wiley and Sons, 2000.

[12] A. G. Kanatas and P. Constantinou, "Narrowband characterisation of the land mobile satellite channel: A comparison of empirical models," *Eur. Trans. Telecomm.*, vol. 7, no. 4, pp. 315–321, 1996.

[13] R. Vaughan and J. B. Andersen, Eds., *Channels, Propagation and Antennas for Mobile Communications*. Institution of Electrical Engineers, 2003.

[14] H.-J. Li, C.-C. Chen, T.-Y. Liu, and H.-C. Lin, "Applicability of ray-tracing technique for the prediction of outdoor channel characteristics," *IEEE Trans. Veh. Technol.*, vol. 49, no. 6, pp. 2336–2349, 2000.

[15] J. Morris and J.-L. Chang, "Burst error statistics of simulated Viterbi decoded BFSK and high-rate punctured codes on fading and scintillating channels," *IEEE Trans. Commun.*, vol. 43, no. 234, pp. 695–700, 1995.

[16] N. Youssef, T. Munakata, and M. Takeda, "Fade statistics in Nakagami fading environments," in *Proc. IEEE 4th Int. Symp. Spread Spectrum Techniques and Applications*, vol. 3, Mainz, Germany, Sep. 1996, pp. 1244–1247.

[17] E. N. Gilbert, "Energy reception for mobile radio," *Bell Syst. Tech. J.*, vol. 44, no. 8, pp. 1779–1803, 1965.

[18] R. H. Clarke, "A statistical theory of mobile-radio reception," *Bell Syst. Tech. J.*, vol. 47, pp. 957–1000, 1968.

[19] T. Aulin, "A modified model for the fading signal at a mobile radio channel," *IEEE Trans. Veh. Technol.*, vol. 28, no. 3, pp. 182–203, Aug. 1979.

[20] R. W. Huck, J. S. Butterworth, and E. E. Matt, "Propagation measurements for land mobile satellite services," in *33rd IEEE Vehicular Technology Conference*, vol. 33, May 1983, pp. 265–268.

[21] Y. Karasawa, K. Kimura, and K. Minamisono, "Analysis of availability improvement in LMSS by means of satellite diversity based on three-state propagation channel model," *IEEE Trans. Veh. Technol.*, vol. 46, no. 4, pp. 1047–1056, Nov. 1997.

[22] C. Loo, "A statistical model for a land mobile satellite link," *IEEE Trans. Veh. Technol.*, vol. 34, no. 3, pp. 122–127, Aug. 1985.

[23] M. Pätzold, Y. Li, and F. Laue, "A study of a land mobile satellite channel model with asymmetrical Doppler power spectrum and lognormally distributed line-of-sight component," *IEEE Trans. Veh. Technol.*, vol. 47, no. 1, pp. 297–310, Feb. 1998.

[24] G. E. Corazza and F. Vatalaro, "A statistical model for land mobile satellite channels and its application to nongeostationary orbit systems," *IEEE Trans. Veh. Technol.*, vol. 43, no. 3, pp. 738–742, Aug. 1994.

[25] F. Vatalaro, "Generalised Rice-lognormal channel model for wireless communications," *Electron. Lett.*, vol. 31, no. 22, pp. 1899–1900, Oct. 1995.

[26] S.-H. Hwang, K.-J. Kim, J.-Y. Ahn, and K.-C. Whang, "A channel model for nongeostationary orbiting satellite system," in *Proc. IEEE Veh. Technol. Conf.*, vol. 1, May 4-7 1997, pp. 41–45.

[27] E. Lutz, D. Cygan, M. Dippold, F. Dolainsky, and W. Papke, "The land mobile satellite communication channel-recording, statistics, and channel model," *IEEE Trans. Veh. Technol.*, vol. 40, no. 2, pp. 375–386, May 1991.

[28] F. P. Fontán, M. V. Castro, C. E. Cabado, J. P. Garcia, and E. Kubista, "Statistical modeling of the LMS channel," *IEEE Trans. Veh. Technol.*, vol. 50, no. 6, pp. 1549–1567, Nov. 2001.

[29] A. Jahn, H. Bischl, and G. Heib, "Channel characterisation for spread spectrum satellite communications," in *Spread Spectrum Techniques and Applications Proceedings, 1996., IEEE 4th International Symposium on*, vol. 3, Sep. 1996, pp. 1221–1226.

[30] M. A. N. Parks, S. R. Saunders, and B. G. Evans, "Wideband measurements and modeling at L- and S-bands of the mobile satellite propagation channel," in *COST 252 TD*, 1997.

[31] C. Tzaras, S. R. Saunders, and B. G. Evans, "A tap-gain process for wideband mobile satellite PCN channels," in *Proc. COST 252/259 Joint Workshop*, Bradford, UK, Apr. 21-22 1998, pp. 156–161.

[32] S. Scalise, M. A. V. Castro, A. Jahn, and H. Ernst, "A comparison of the statistical properties of the land mobile satellite channel at Ku, Ka and EHF bands," in *IEEE Veh. Technol. Conf.*, vol. 4, 2005, pp. 2687–2691.

[33] L. Ozarow, S. Shamai, and A. Wyner, "Information theoretic considerations for cellular mobile radio," *IEEE Trans. Veh. Technol.*, vol. 43, no. 2, pp. 359–378, May 1994.

[34] R. S. Lawrence, C. G. Little, and H. J. A. Chivers, "A survey of ionospheric effects upon earth-space radio propagation," *Proc. IEEE*, vol. 52, no. 1, pp. 4–27, Jan. 1964.

[35] T. S. Rappaport, *Wireless Communications*, 2nd ed. NJ, USA: Prentice-Hall, 2002.

[36] J. Salo, L. Vuokko, H. M. El-Sallabi, and P. Vainikainen, "An additive model as a physical basis for shadow fading," *IEEE Trans. Veh. Technol.*, vol. 56, no. 1, pp. 13–26, Jan. 2007.

[37] M. A. Weissberger, "An initial critical summary of models for predicting the attenuation of radio waves by foliage," Electromagnetic Compatibility Center, Annapolis, Md., USA, ECAC-TR-81-101, Aug. 1981.

[38] "Influence of terrain irregularities and vegetation on tropospheric propagation," ITU, CCIR Report 236-6, vol. XIII-3, 1986.

[39] W. T. Smith and W. L. Stutzman, "Statistical modeling for land mobile satellite communications," Virginia, Tech. Rep. EE Satcom 86-3, Aug. 1986.

[40] R. M. Barts and W. L. Stutzman, "Modeling and simulation of mobile satellite propagation," *IEEE Trans. Antennas Propag.*, vol. 40, no. 4, pp. 375–382, Apr. 1992.

[41] W. J. Vogel and J. Goldhirsh, "Tree attenuation at 869 MHz derived from remotely piloted aircraft measurements," *IEEE Trans. Antennas Propag.*, vol. 34, no. 12, pp. 1460–1464, 1986.

[42] J. Goldhirsh and W. J. Vogel, "Roadside tree attenuation measurements at UHF for land mobile satellite systems," *IEEE Trans. Antennas Propag.*, vol. 35, no. 5, pp. 589–596, 1987.

[43] ——, "Mobile satellite system fade statistics for shadowing and multipath from roadside trees at UHF and L-band," *IEEE Trans. Antennas Propag.*, vol. 37, no. 4, pp. 489–498, Apr. 1989.

[44] ——, "An overview of results derived from mobile-satellite propagation experiments," in *Inter. Mobile Satellite Conf.*, Ottawa, Canada, 1990.

[45] "Factors affecting the choice of antennas for mobile stations of the land mobile-satellite service," ITU, CCIR Report 925-1, vol. VIII, 1986.

[46] W. J. Vogel and J. Goldhirsh, "Mobile satellite system propagation measurements at L-band using MARECS-B2," *IEEE Trans. Antennas Propag.*, vol. 38, no. 2, pp. 259–264, 1990.

[47] M. Sforza, S. Buonomo, and A. Martini, "ESA research activities in the field of channel modelling nnd simulation for land mobile satellite systems," in *COST 227 TD*, 1993.

[48] M. A. N. Parks, B. G. Evans, and G. Butt, "High elevation angle propagation results, applied to a statistical model and an enhanced empirical model," in *COST 227 TD*, 1993.

[49] J. F. Ossanna, "A model for mobile radio fading due to building reflections: Theoretical and experimental waveform power spectra," *Bell Syst. Tech. J.*, vol. 43, pp. 2935–2971, 1964.

[50] W. R. Young, "Comparison of mobile radio transmission at 150, 450, 900 and 3700 MC," *Bell Syst. Tech. J.*, vol. 31, no. 6, pp. 1068–1085, 1952.

[51] S. O. Rice, "Statistical properties of a sine wave plus random noise," *Bell Syst. Tech. J.*, vol. 27, pp. 109–157, Jan. 1948.

[52] M. Nakagami, "The m-distribution - a general formula of intensity distribution of rapid fading," in *Statistical methods in radio wave propagation*, W. G. Hoffman, Ed. Oxford, U.K.: Pergamon press, 1960, pp. 3–36.

[53] R. S. Hoyt, "Probability functions for the modulus and angle of the normal complex variate," *Bell Syst. Tech. J.*, vol. 26, pp. 318–359, 1947.

[54] J. J. Egli, "Radio propagation above 40 MC over irregular terrain," *Proc. IRE*, vol. 45, no. 10, pp. 1383–1391, Oct. 1957.

[55] D. C. Cox, R. R. Murray, and A. W. Norris, "800 MHz attenuation measured in and around suburban houses," *Bell Syst. Tech. J.*, vol. 63, no. 6, pp. 921–954, July-Aug. 1984.

[56] Y. Hase, W. J. Vogel, and J. Goldhirsh, "Fade-durations derived from land-mobile-satellite measurements in Australia," *IEEE Trans. Commun.*, vol. 39, no. 5, pp. 664–668, May 1991.

[57] *Propagation Data Required for the Design of Earth Space Land Mobile Telecommunication Systems*, ITU-R Recommendation P.681-5, 1999.

[58] L. E. Bråten and T. Tjelta, "Semi-markov multistate modeling of the land mobile propagation channel for geostationary satellites," *IEEE Trans. Antennas Propag.*, vol. 50, no. 12, pp. 1795–1802, Dec. 2002.

[59] N. Youssef, C. X. Wang, and M. Patzold, "A study on the second order statistics of Nakagami-Hoyt mobile fading channels," *IEEE Trans. Veh. Technol.*, vol. 54, no. 4, pp. 1259–1265, July 2005.

[60] P. Beckmann, *Probability in Communication Engineering.* New York: Harcourt, Brace and World, 1967.

[61] A. Leon-Garcia, *Probability and Random Processes for Electrical Engineering*, 2nd ed. New Jersey: Pearson Education, 2007.

[62] M. Pätzold, U. Killat, and F. Laue, "An extended Suzuki model for land mobile satellite channels and its statistical properties," *IEEE Trans. Veh. Technol.*, vol. 47, no. 2, pp. 617–630, May 1998.

[63] S. Hazra and A. Mitra, "Level crossing rate in land mobile satellite channel with a modified Nakagami-lognormal distribution," in *Advances in Computing and Communications, Kochi, India*, ser. Communications in Computer and Information Science. Springer Berlin Heidelberg, 2011, vol. 192, pp. 601–608.

[64] H. Suzuki, "A statistical model for urban radio propogation," *IEEE Trans. Commun.*, vol. 25, no. 7, pp. 673–680, July 1977.

[65] W. C. Y. Lee, *Mobile Communications Engineering*, 2nd ed. NY, USA: McGraw-Hill, 1998.

[66] V. Erceg, K. S. Hari, M. Smith, D. Baum, K. Sheikh, C. Tappenden, J. Costa, C. Bushue, A. Sarajedini, R. Schwartz, D. Branlund, T. Kaitz, and D. Trinkwon, *Channel Models for Fixed Wireless Applications*, IEEE 802.16.3c-01/29r4, Jul. 2001. [Online]. Available: http://www.ieee802.org/16/tg3/contrib/802163c-01_29r4.pdf

[67] B. Vucetic and J. Du, "Channel modeling and simulation in satellite mobile communication systems," *IEEE J. Sel. Areas Commun.*, vol. 10, no. 8, pp. 1209–1218, Oct. 1992.

[68] E. Biglieri, J. Proakis, and S. Shamai, "Fading channels: information-theoretic and communications aspects," *IEEE Trans. Inf. Theory*, vol. 44, no. 6, pp. 2619–2692, Oct. 1998.

[69] V. Kafedziski, "Capacity of frequency selective fading channels with side information," in *Signals, Systems amp; Computers, 1998. Conference Record of the Thirty-Second Asilomar Conference on*, vol. 2, 1998, pp. 1758–1762.

[70] A. M. Tulino, G. Caire, S. Shamai, and S. Verdu, "Capacity of channels with frequency-selective and time-selective fading," *IEEE Trans. Inf. Theory*, vol. 56, no. 3, pp. 1187–1215, 2010.